Engineering Bicycle Stability:

A Study of Control Strategies for Crash Prevention on Icy and Normal Terrain

Mechanical Engineering Thesis Report Sara A. Youngblood





Engineering Bicycle Stability:

A Study of Control Strategies for Crash Prevention on Icy and Normal Terrain

by

Sara A. Youngblood

Instructor: Dr. J.K. Moore

Faculty: Faculty of Mechanical Engineering, Delft

Cover: *Realistic Al-generated image of icy road conditions* (created by

the author using OpenAl's tools)



Acknowledgements

I would like to express my sincere gratitude to Dr. Jason Moore for his continued support and clear explanations of bicycle dynamics. At the beginning of this project, I had minimal experience in coding, dynamics, controls, and even biking. I am truly grateful that you took the time to help me change that. It has been a long and sometimes frustrating journey with several road blocks, but I am thankful you were there to help me navigate them.

As someone who had not ridden a bicycle for ten years before moving here, getting back on two wheels was definitely an adjustment. I would like to thank everyone in the bicycle lab for showing me that bicycles are not only less intimidating than I remembered, but can actually be fun.

Thank you to the many minor cycling crashes I experienced during my first year for inspiring the development of a traction control system that might prevent a few of those graceful wipe outs. Thank you to those I have hit, almost hit, or convinced to walk alongside me instead.

Finally, Thank you to my laptop for being the backbone of my project, I couldn't have done it without you.

Sara A. Youngblood Delft, May 2025

AI Usage Statement

Declaration of Generative AI and AI-assisted technologies in the writing process, and cover page generation. During the preparation of this work, the author utilized ChatGPT to enhance English grammar and format in Latex. After using this tool, the author reviewed and edited the content as needed and takes full responsibility for the content of the publication.

The use of Al adhered to ethical academic standards and university guidelines. No generative tools were used to fabricate data, plagiarize content, or bypass the author's responsibility in conducting and documenting the research.

Abstract

Bicycles have seen relatively few safety features added since their invention, especially in comparison to the numerous advancements in automotive safety. This thesis investigates the use of simulation to model bicycle dynamics, progressing from a no-slip model to a more complex model incorporating slip, and finally to a model that simulates the interaction of a bicycle with an unexpected patch of ice. Tire slip on ice was estimated using car tire slip data combined with bicycle measurements taken on dry asphalt. The study evaluates the effectiveness of two control strategies, Proportional-Derivative (PD) control, and Linear Quadratic Regulator (LQR) control, through these simulations. The PD controller was tested with gain values ranging from 0 to 20 at regular intervals, while the LQR controller's weightings were selected through a process of trial and error. The analysis focuses on how variations in PD gains and LQR weightings affect the bicycle's stability and ability to traverse icy terrain. Results indicate that the LQR controller consistently stabilized the bicycle at an 8° lean angle across all tested speeds and maintained stability at a 12.5° lean angle at higher speeds when crossing ice. Ultimately, the selected LQR controller used diagonal values of 50 and 5 in the state weighting matrix Q, and a value of 1 in the control weighting matrix R. These findings suggest that advanced control strategies, particularly LQR, can enhance bicycle stability in adverse conditions.

Contents

Pr	reface	i
Αb	ostract	iii
No	omenclature	vii
1	Introduction 1.1 Background	1 1 3
2	Modeling a bicycle 2.1 Model setup	4 5 7 8 10
3	Linearization 3.1 Equilibrium 3.2 Taylor series 3.3 State-space 3.4 Controllability 3.5 System type Controllers	15 15 16 17 18 18
4	4.1 Simulating	21 23 25
5	Results5.1 Models5.2 PD Controllers5.3 Linear Quadratic Regulator Control on Asphalt	31 31 33 35
6	Discussion 6.1 Models 6.2 PD performance 6.3 LQR performance 6.4 Comparison of PD and LQR 6.5 Research Outcome 6.6 Limitation and Future work	41 42 42 43 43 44
7	Conclusion	46
Re	eferences	48
Α	Source code	50
В	LQR and PD on ice	51
С	Ice vs no ice	52
D	PD graphs	53
Ε	LQR graphs	56
F	Literature Search	58

List of Figures

	A Visual Comparison of Integrated Safety Features in Cars and Bicycles:	2
2.1 2.2	Diagram of Bicycle	5
2.3	sus slip angle	11 12
3.1 3.2 3.3 3.4	Bicycle in static equilibrium—upright and stationary on a flat surface	16 16 18 19
4.9 4.10 4.11	Time evolution of the generalized coordinates in the absence of feedback control System without Feedback Control with a Roll Event PD Control Block Diagram Emulating Rider Feedback System response under PD control emulating rider behavior Block diagram showing LQR feedback Closed-Loop System Eigenvalues Plotted in the Complex Plane LQR increasing balanced weight on states LQR different state weights LQR different control input PD controller block diagram with ice-triggered gain switching LQR controller block diagram with ice-triggered gain switching Flowchart of ice detection and controller switching logic based on simulation time and surface conditions	22 23 24 25 26 27 27 28 29 29
	PD control at various velocities	32 33 34 36 36 37 37 38 38 39 40
B.1	Side-by-side LQR vs PD control of all variables	51
	Path of bike on ice and not	52 52
D.2	PD at various gains	53 54 55
	LQR at various velocities with all variables	56 57

List of Tables

	Constant parameters	
4.1	Initial conditions for state variables used in system simulation	21
	PD Gains and Stability on Asphalt and Ice Patch at 4 m/s and 7 m/s at 5° roll PD stability ice patch at 4 m/s and 7 m/s at various roll angles	

Nomenclature

Abbreviations

Abbreviation	Definition
COM	Center of Mass
IVP	Initial Value Problem
LQR	Linear Quadratic Regulator
PD	Proportional Derivative
IMU	Inertial Measurement Unit

Symbols

Symbol	Definition	Unit
x	Position in the x-direction (ground frame)	[m]
y	Position in the y-direction (ground frame)	[m]
\dot{x}	Velocity in the x-direction (ground frame)	[m/s]
\dot{y}	Velocity in the y-direction (ground frame)	[m/s]
\ddot{q} , \dot{u}	Generalized accelerations	$[m/s^2]$
a	Acceleration	$[m/s^2]$
I	Inertia	$[kg \cdot m^2]$
g	Acceleration due to gravity	$[m/s^2]$
F	Force	[N]
R	Resultant force	[N]
T	Torque	[N·m]
m	Mass	[kg]
l	Wheelbase	[m]
ω	Angular velocity	[rad/s]
α	Angular acceleration	$[rad/s^2]$
α_f	Front slip angle	[rad]
α_b	Rear slip angle	[rad]
C_{α}	Cornering stiffness	[N/rad]
θ	Roll angle	[rad]
ψ	Yaw angle	[rad]
δ	Steering angle	[rad]
q	Generalized coordinates	-
u	Generalized speeds	-
A	Reference frame A (Yaw)	-
B	Reference frame B (Yaw and Roll)	-
C	Reference frame C (Delta)	-
N	Ground reference frame	-
W_f	Front wheel point of contact	-
W_b	Rear wheel point of contact	-
O	Point of reference	-

1

Introduction

1.1. Background

Bicycling is a low-cost, environmentally friendly mode of transportation that has existed since 1817 [1]. However, despite its long history, the fundamental design of the bicycle has remained largely unchanged. In contrast, the automotive industry has seen continuous advancements in safety technologies over the years. For example, a comparative study of car safety between 1980 and 2018 reported an 88% reduction in fatalities and a 58% reduction in serious injuries, highlighting the impact of safety features [2].

Various studies on cycling safety have been conducted, providing valuable insight into potential safety enhancements for bicycles. Much of this research focuses on cycling infrastructure, particularly how the placement and design of bike paths can improve rider safety [3]. While infrastructure and path planning are important considerations, this work will instead focus on modifications to the bicycle itself aimed at improving its safety.

Bicycle crashes are typically classified as either single-vehicle or multi-vehicle incidents. Single-bicycle crashes involve only the cyclist and are caused by factors unrelated to other road users, such as loss of balance, fixed obstacles, or adverse road conditions. These incidents explicitly exclude collisions with other vehicles or pedestrians and are often under reported [4]. A literature review investigating the causes of bicycle accidents found that approximately 30% of all crashes fall into the single-bicycle category [5]. A crash is classified as a fall if no other road users are involved, indicating that nearly one-third of reported cycling accidents involve only a single road user [6].

After conducting a literature review on the common causes of single-cyclist crashes, these incidents can be categorized into four main types: loss of control, collisions, skidding, and others, as shown in Appendix F. A review of relevant literature on these incidents found that loss of control accounted for approximately 21%, skidding for 32%, and collisions with non-vehicle obstacles for 18% of cases shown in Figure 1.1. It is important to note that there is some overlap between the categories of loss of control and skidding, particularly in scenarios where sudden changes in traction result in instability.

1.1. Background 2

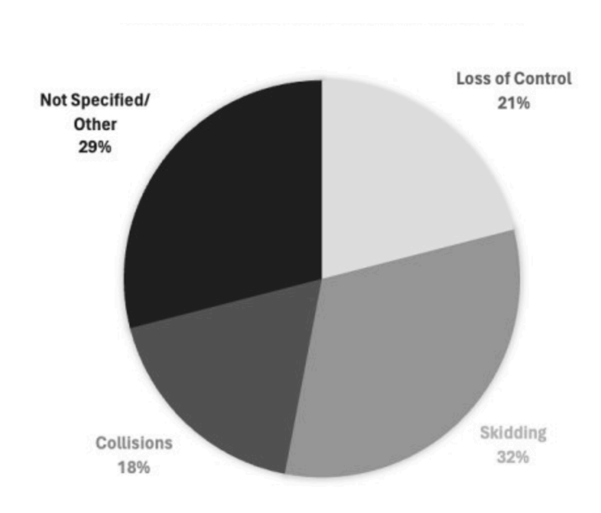


Figure 1.1: Breakdown of Single Cyclist Bicycle Crashes by Cause

Research also shows that, 47% of cyclists involved in a fall reported that the incident could have been avoided had they reacted differently or more quickly [7]. This highlights the potential impact of safety systems designed to assist cyclists in responding to unexpected changes in road surface. This thesis investigates bicycle stability control mechanisms aimed at enhancing rider responsiveness and reducing the likelihood of single-cyclist crashes.

To better understand this need, existing safety features in automobiles were compared to those available for bicycles.

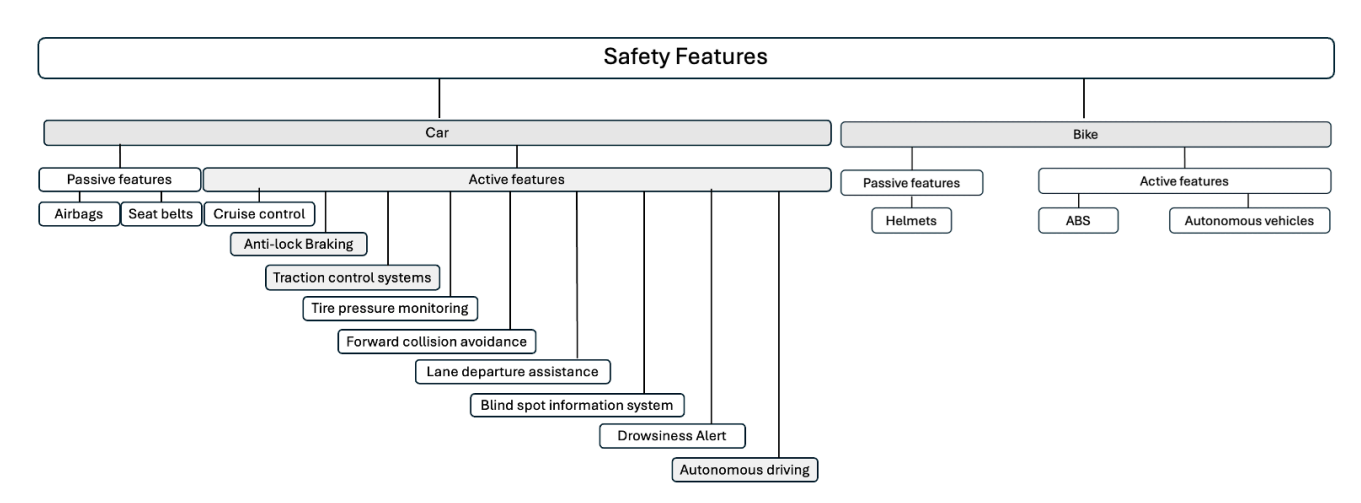


Figure 1.2: A Visual Comparison of Integrated Safety Features in Cars and Bicycles:

Figure 1.2 presents a graphical comparison of safety features found in cars and bicycles. It is evident that cars are equipped with significantly more integrated safety features, highlighting a gap in cyclists safety.

While both cars and bicycles may feature anti-lock braking systems, the similarities largely end there. The safety features of cars shown in Figure 1.2 are listed in chronological order. This progression also aligns with increased complexity of systems, as many technologies build upon earlier innovations. Following this pattern, traction control emerges as the next logical safety feature to explore for bicycles, particularly due to its potential to enhance stability and reduce crashes related to loss of control or skidding.

1.2. Research objective

The previous section outlined common causes of cycling accidents and reviewed existing bicycle safety features. One important but often overlooked area is traction control. A traction control system can detect and respond to changes in surface conditions before loss of control or skidding occurs. By adapting to varying terrain in real time, these systems enhance rider stability and reduce the risk of falls. This improvement increases safety and rider confidence, particularly in challenging conditions, and helps make cycling a more accessible mode of transportation. As electric bicycles become more common and reach higher speeds, the absence of advanced safety features such as traction control presents a growing concern that must be addressed.

Bicycle dynamics and control are important areas of research, due to the increasing use of bicycles as transportation. Maintaining stability and control under unexpected changes in terrain or obstacles remains a significant challenge. Most bicycles do not include active systems to monitor and regulate traction in real time. Without these systems, sudden changes in surface conditions can lead to a loss of grip, increasing the likelihood of falls and instability. This issue poses a heightened risk during commuting, especially in adverse weather. Although prior research has explored balance control and steering automation, relatively few studies have focused on implementing traction control for bicycles. This thesis aims to address this gap by simulating and developing a traction control system that actively detects and responds to changes in surface conditions to enhance rider stability and safety.

This gap in available safety features for reducing avoidable crashes leads to the central question of this thesis:

How do surface conditions affect the dynamic stability of a bicycle and how can control strategies be used to stabilize the bicycle on normal and icy terrain to prevent single-cyclist crashes?

To address the central research question, several supporting topics are explored throughout this work. The investigation begins with the development of a no-slip bicycle model to accurately capture the baseline dynamics on high-friction surfaces. A simplified model will be used to capture the bicycle dynamics needed to evaluate stability.

The effects of slip on the nonlinear dynamics of the bicycle are then examined, specifically how transitions between high-friction and low-friction surfaces influence system behavior. In this stage, the no-slip assumption is removed, and slip dynamics are incorporated to yield a more realistic representation of bicycle behavior. An ice patch is simulated by changing the tires coefficient of slip.

To facilitate controller design, the nonlinear slip-inclusive model is linearized around an equilibrium point. This linearization allows for the design of Linear Quadratic Regulator (LQR) controllers optimized for both asphalt and icy surface conditions. The linearized formulation also significantly reduces computational load, enabling real-time control implementation.

The performance of the LQR controllers, along with a Proportional-Derivative (PD) controller, is then evaluated against an uncontrolled bicycle model across varying surface conditions. Lastly, the integration of a real-time surface condition detection system is explored to enable automatic switching between terrain-specific LQR controllers, with the objective of improving bicycle stability during sudden or gradual changes in road surface conditions.

This study addresses a gap in cyclist safety by exploring how traction control systems, commonly used in automobiles, can be adapted for bicycles. By focusing on real-time lateral stability control in varying surface conditions, the research contributes to the development of smarter, safer bicycles that can reduce the number of single-cyclist crashes, particularly in challenging conditions such as icy or uneven surfaces, where cyclists are at greater risk of falling. This work aims to investigate the influence of encountering an ice patch on bicycle dynamics to develop a simulation-based approach for designing adaptive control systems enhancing rider stability and safety under varying conditions.

2

Modeling a bicycle

This chapter presents the progression of bicycle dynamic models used to explore control strategies under varying traction conditions. The Whipple-Carvallo model is a well-known and commonly used way to describe how bicycles move. For this study, a further simplified model is employed on a flat surface. In this approach, the bicycle is represented as a single rigid body with a pin-jointed steering mechanism [8]. Using a rigid body accounts for moment of inertia and rotational dynamics while using essentially an inverted pendulum on massless skates. It serves as a foundation for developing both linear and non-linear dynamic equations. Deriving the equations of motion using Kanes method [9] shows behaviors such as balance, trajectory deviations, and response to steering actions. These relationships are critical when designing controllers. The model will be used to maintain balance and improve handing on unpredictable road conditions, therefore it must contain rotational dynamics but can omit more complicated bicycle dynamics.

To illustrate the development of the model and its increasing complexity, this chapter is divided into three subsections: a no-slip model, a slip model, and a slip model adapted for low-traction surfaces such as ice.

The contact points between the bicycle and the ground are modeled as skates when constructing the no-slip model. Modeling the contact points as skates treats the wheels as frictionless, non-rolling elements that permit motion only along their direction of travel. Unlike real bicycle tires, which experience deformation, rolling resistance, and lateral slip, skate-like contacts impose a non-holonomic constraint that restricts lateral movement without introducing the complexities associated with tire-ground interaction dynamics.

While modeling the tires as skates simplifies the dynamics of the bicycle, it limits the model's ability to capture key behaviors necessary for developing a traction controller. Accurate tire-ground interaction modeling is essential for assessing lateral stability. To address this limitation, a model incorporating slip was developed by introducing the linear Pacejka tire model [10]. This addition allows the generation of lateral forces as a function of slip angle and slip coefficient. As a result, the model provides a more realistic representation of bicycle dynamics, particularly in scenarios involving cornering or riding over surfaces with varying traction, where tire slip plays a critical role in maintaining stability and control.

Finally, the slip model, using a single rigid body with pin-jointed steering and lateral tire forces, was modified to simulate low-traction conditions such as ice. This was done by reducing the slip coefficient, which limits the amount of lateral force the tires can produce. This modified model will be used to test the controller described in later sections. This section will provide a detailed breakdown of how each model, including the no-slip model, slip model, and slip with ice model, was constructed, the assumptions made, and how the resulting dynamics inform the development of the control strategy.

2.1. Model setup 5

2.1. Model setup

Parameter

A comprehensive bicycle model is complex because of the system's multiple degrees of freedom and many geometries. The Whipple-Carvallo model uses four interconnected frames to represent a bicycle and contains twenty seven parameters that can be reduced to four degrees of freedom. Not all parameters in Whipple-Carvallo are necessary for my analysis. Successful control and maneuverability of a bicycle are primarily governed by the interaction forces between the wheels and the ground, while balance and turning are influenced by lateral forces and steering dynamics [11].

Reducing the number of parameters simplifies the equations of motion and lowers computational costs when implementing controllers. This reduction comes at the expense of model accuracy [12]. Achieving the optimal balance is essential for computational efficiency and accurate system representation [11]. To achieve a more computationally efficient yet sufficiently accurate representation, my model will be based on a model in Karnopp's *Vehicle Dynamics control and stability* [8], which reduces the system to a minimal set of essential parameters for using steer to control roll.

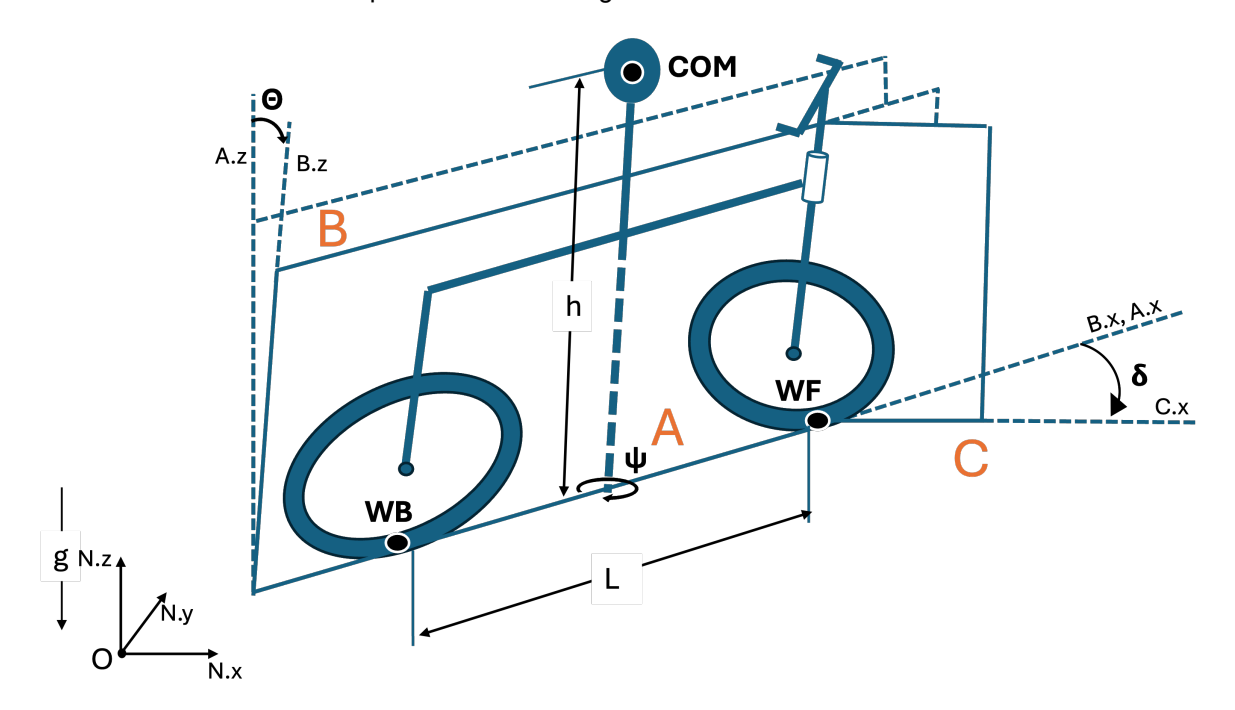


Figure 2.1: Diagram of Bicycle

The numerical values for the constant bicycle parameters used in this study are listed in Table 2.1 and are based on real bicycle parameters [13].

Parameters	Symbols	Values
Mass	m	$87\mathrm{kg}$
Height	h	1 m
Wheelbase	L	1 m
Gravity	g	$9.81 {\rm m/s^2}$
Inertia about B_x	I_{xx}	$9.2\mathrm{kg\cdot m^2}$
Inertia about B_y	I_{yy}	$11\mathrm{kg}\cdot\mathrm{m}^2$
Inertia about B_z	I_{zz}	$2.8\mathrm{kg\cdot m^2}$

Table 2.1: Constant parameters

2.1. Model setup 6

Kinematics

Simplifying the bicycle as a single rigid body with skate-like points of contact results in a system with one degree of freedom. The motion of the bicycle is analyzed with respect to a ground-fixed inertial reference frame, denoted as N. This frame consists of three mutually perpendicular axes, $\hat{\bf n}_x$, $\hat{\bf n}_y$, and $\hat{\bf n}_z$, which intersect at an inertial origin. The orientation of the frame is such that the positive $\hat{\bf n}_z$ axis points upward, opposing the gravitational field.

The orientation of the bicycle is described by a body-fixed reference frame, denoted as B, which is obtained from frame N using successive Euler angle rotations. Specifically, the first rotation is by the yaw angle, ψ , about $\hat{\bf n}_z$ resulting in an intermediate reference frame, denoted as A. This intermediate frame remains aligned with the ground plane but shares the bicycle's yaw orientation, making it useful for constraining the velocity of the system, and setting the steer. The bicycle frame B is built by adding lean rotation, θ , about $\hat{\bf a}_x$. This sequence of rotations ensures that frame B aligns with the bicycle's yaw and lean. Once these rotations are applied, frame B is aligned with the bicycle such that the $\hat{\bf b}_x$ axis points longitudinally along the bicycle's frame, the $\hat{\bf b}_y$ axis points laterally, and $\hat{\bf b}_z$ points upward, aligned with the lean direction. To account for steering dynamics, an additional reference frame, denoted as C, is introduced. Frame C is obtained through right hand rotation steer angle, δ about $\hat{\bf a}_z$. Using notation s_i for sin(i) and sin(i) and sin(i) the three direction cosine matrices are shown in Table 2.2.

Table 2.2: Direction Cosine Matrices of Bicycle, Yaw and Steer frames

The bicycle will be defined using one mass with three points of interest, a contact point at the front, rear and a center of mass. Motion of the front and rear contact points is restricted to the ground frame $\hat{\bf n}_x$ $\hat{\bf n}_y$. Enforcing this constraint eliminates pitch and velocity in the vertical direction, thereby reducing the system from six degrees of freedom to four. Choosing the fewest possible generalized coordinates to describe the system is beneficial, as it minimizes the number of configuration constraints required. Selecting appropriate generalized coordinates also leads to a minimal and independent set of generalized speeds, avoiding the need for additional velocity constraints [9].

The location of the rear contact point in the ground frame N is defined by coordinates (x_B,y_B) , measured from the inertial origin O along $\hat{\mathbf{n}}_x$ and $\hat{\mathbf{n}}_y$. The front contact point is positioned a distance equal to the wheelbase, L, along $\hat{\mathbf{b}}_x$ from the rear contact point. The center of mass of the bicycle is located at a height h along $\hat{\mathbf{b}}_z$ axis, measured from the midpoint of the wheelbase, L/2 in $\hat{\mathbf{b}}_x$ from the rear point of contact.

The position vectors of the rear contact point W_b , the front contact point W_f , and the center of mass COM are given by the following equations:

$${}^{W_b}\mathbf{r}^O = x_B\hat{\mathbf{n}}_x + y_B\hat{\mathbf{n}}_y \tag{2.1}$$

$$W_f \mathbf{r}^{W_b} = L \hat{\mathbf{b}}_x \tag{2.2}$$

$$^{COM}\mathbf{r}^{W_b} = \frac{L}{2}\hat{\mathbf{b}}_x + h\hat{\mathbf{b}}_z \tag{2.3}$$

Velocity

The angular velocity of the rigid body can be found using the rotation of frame B when observed from frame N. The angular velocity of body B is:

$${}^{N}\boldsymbol{\omega}^{B} = \dot{\theta}\hat{\mathbf{a}}_{x} + \dot{\psi}\hat{\mathbf{n}}_{z} \tag{2.4}$$

2.2. No slip 7

This angular velocity will be essential in the next section for determining the translational velocities of each point. The rear contact point, W_b , moves with respect to O in the reference frame N. Point W_b has velocity relative to O expressed by the time derivative of the position vector given in Equation (2.1).

$${}^{N}\mathbf{v}^{W_{b}} = \frac{{}^{N}d^{W_{b}}\mathbf{r}^{O}}{dt}$$
 (2.5)

The velocity of W_b in N is

$${}^{N}\mathbf{v}^{W_b} = \dot{x}_B \hat{\mathbf{n}}_x + \dot{y}_B \hat{\mathbf{n}}_y \tag{2.6}$$

The two-point velocity theorem states that if the velocity at one point on a rigid body is known, and the body's angular velocity and the position vector from that point to another fixed point on the body are also known, then the velocity at the second point can be determined [9]. All points, W_b, W_f , and COM, are fixed within the reference frame B, which has a known angular velocity expressed in Equation (2.4). The velocity of the points are influenced by the bicycle's linear motion and its angular motion. The front contact point, W_f , experiences angular rotation in yaw ψ relative to the rear contact point W_b because both points lie in the ground plane and are rigidly linked. In contrast, the center of mass COM experience angular rotation relative to W_b in yaw ψ and roll θ , because it is located at a height h above the ground plane and L/2 in $\hat{\mathbf{b}}_x$. Position vectors describing the location of each point relative to the others have been defines in Equations 2.2, and 2.3. By applying the two-point velocity theorem, the velocities of points W_f and COM are determined.

$${}^{N}\mathbf{v}^{W_f} = {}^{N}\mathbf{v}^{W_b} + {}^{N}\boldsymbol{\omega}^{B} \times {}^{W_f}\mathbf{r}^{W_b}$$
(2.7)

$${}^{N}\mathbf{v}^{COM} = {}^{N}\mathbf{v}^{W_b} + {}^{N}\boldsymbol{\omega}^{B} \times {}^{COM}\mathbf{r}^{W_b}$$
 (2.8)

At this point, the unconstrained system is fully defined using generalized coordinates. This foundational system will be the basis for both a no slip model using non-holonomic constraints in section 2.2 and a model allowing lateral slip in section 2.4.

2.2. No slip

Nonholonomic constraint

A common simplifying assumption when modeling wheels in dynamics is that wheels spin without slip. The no-slip model uses skates to represent wheels, the longitudinal slip is therefore absent. To further simplify the system, lateral slip is constrained, ensuring the motion at each contact point is purely longitudinal. To enforce this no-slip condition, non-holonomic constraints are introduced. Unlike holonomic constraints, configuration constraints, non-holonomic constraints impose restrictions on the velocities. These constraints do not limit the possible positions configuration of the system but constrain the instantaneous trajectory [9].

For the bicycle model, enforcing a purely longitudinal motion, at the contact points requires constraining the front and rear wheel velocities preventing lateral motion. The constraint for the rear contact point is relatively straightforward. Using the velocity expression derived in Equation (2.6), the lateral velocity component is set to zero. The goal is to constrain motion in the ground frame N, rather than in the bicycle frame B, therefore it is more appropriate to use the lateral axis of frame A, denoted as $\hat{\mathbf{a}}_y$.

The front contact point, on the other hand, follows a different constraint. It is assumed to move in the direction dictated by the steering angle δ , aligning with the orientation of the steer frame F. The velocity of the front contact point W_f , as given in Equation 2.7, is therefore constrained in the lateral direction of the steer frame, $\hat{\mathbf{c}}_y$. This ensures that the motion of the front contact point remains consistent with the direction of steering while still adhering to the no-slip condition. The two constraint equations are:

$${}^{N}\bar{\mathbf{v}}^{W_{b}}\cdot\hat{\mathbf{a}}_{y}=0\tag{2.9}$$

$${}^{N}\bar{\mathbf{v}}^{W_f}\cdot\hat{\mathbf{c}}_{v}=0 \tag{2.10}$$

Generalized speeds

By enforcing these non-holonomic constraints at both the front and rear contact points, the bicycle is restricted from having any lateral velocity at the contact points. The two scalar equations governing this constraint are linear in the generalized velocities and will be used to express the independent velocities in terms of the dependent velocities.

Equations of motion are second order differential equations, which can be equivalently written as two first order differential equations. This transformation is achieved by introducing new variables, known as generalized speeds, which replace the first time derivatives of the generalized coordinates [9]. The generalized speeds are defined using the identity matrix, simply, the generalized speeds are defined as $u_i = \dot{q}_i$ for i = 1, 2, 3, 4.

The non-holonomic constraints establish a relationship between the dependent and independent generalized speeds. By selecting the generalized speeds associated with longitudinal velocity and lean as the independent generalized speeds, u_s , the lateral velocity and yaw velocity can be expressed in terms of dependent variables, u_r . The linear relationship between independent u_s and dependent u_r generalized speeds is used to solve for the dependent speeds in terms of the independent speeds eliminating them from the equations of motion.

At this point, the time derivatives of the generalized coordinates can be written in terms of the generalized speeds, which can be reduced to only the independent generalized speeds using their linear relationship derived from the non-holonomic constraints.

Mass distribution

Each rigid body consists of a collection of particles within a defined volumetric boundary. For analysis, this distributed mass is conceptually concentrated at a single point known as the center of mass. The inertia of the bicycle then describes how this mass is distributed relative to the center of mass along each axis. An inertia tensor, represented as a matrix containing six unique inertia scalars, is used to define the moments and products of inertia [9].

In my simplified system, the principal axis align with the bicycle frames axis, $\hat{\mathbf{b}}_x$, $\hat{\mathbf{b}}_y$ and $\hat{\mathbf{b}}_z$; therefore, only the moments of inertia are present. In reality, this would not be the case: there is symmetry about the longitudinal axis of the bicycle, but the system is not symmetric in the lateral or vertical directions. For a more realistic bicycle, two products of inertia would be expected, corresponding to I_{yz} and I_{zy} . The products of inertia involving the longitudinal axis, such as I_{xy} and I_{xz} , would remain 0. The simplified inertia matrix is shown below.

$$I = \begin{bmatrix} I_1 & 0 & 0 \\ 0 & I_2 & 0 \\ 0 & 0 & I_3 \end{bmatrix}$$
 (2.11)

2.3. Equations of Motion

The Newton-Euler equations serve as the fundamental framework for multi-body dynamics. These equations encompass translational motion, governed by Newton's Second Law F=ma, and rotational motion, described by Euler's equation $M=I\dot{\omega}+\omega\times(I\omega)$. While they can be used to derive the equations of motion of a system, an alternative approach is Kane's method, which eliminates constraint forces and directly solves for the independent motion variables [9].

The equations of motion are derived from the generalized active forces, generalized inertial forces and inertia torques acting on each body. In Section 2.2, independent generalized speeds were expressed in terms of dependent speeds, generalized coordinates, and constants. This formulation will be used in the next Section 2.3 to determine the generalized active forces.

By defining dependent speeds in terms of independent speeds the bicycle can be defined using two generalized coordinates. Velocities and angular velocities will be projected onto each generalized speed by taking the partial derivatives. The number of generalized speeds was reduced therefore, partial velocities is reduced, consequently decreasing the number of force equations required to solve Kanes method.

Generalized Active Forces

The resultant forces acting on a system are determined by projecting each force onto the partial velocity at its point of application. The sum of these projections yields the total scalar force associated with each generalized speed. The resultant force considered here contains all contact and distance forces acting on the system [9].

Conservative forces are forces that depend only on the position of an object, not on the path it takes or when the force is applied. They do the same amount of work between two points, no matter how the object moves. In dynamics, only conservative forces are used to calculate generalized active forces because their effects can be described using potential energy.

In this model, the only generalized active force present is gravity, which acts at the center of mass. The partial velocities of the center of mass with respect to each independent generalized speed are computed and dotted with the gravitational force, which acts in the negative $\hat{\bf n}_z$ direction. This process results in a matrix containing two scalar values, representing the generalized active forces corresponding to the two independent generalized velocities.

$$F_r = \sum_{i=1}^{\nu} {}^N \bar{v}_r^{COM_i} \cdot \bar{R}_{gravity}$$
 (2.12)

Each entry is a scalar representing the force, because the only generalized active force on the system comes from gravity the resultants will be closely related to the potential energy. The active force matrix of the system is:

$$\mathbf{F}_r = \begin{bmatrix} 0\\ -mgh\sin(\theta) \end{bmatrix} \tag{2.13}$$

Generalized Inertia Forces

The generalized inertia force of a body contains the effects of mass distribution and accelerations projected onto each independent generalized speed. This accounts for both the translational and rotational motion of the system. By considering only the contributions to the independent generalized speeds, as determined in Section 2.2, the velocity constraints are inherently satisfied.

The generalized inertia force of a body can be further decomposed into force and torque components. The inertia force is a fictitious force that arises due to the acceleration of a mass and is given by:

$$R^* = m_i * a_i \tag{2.14}$$

In a multi-body system, an inertia force exists for each body and must be projected onto the relevant points of that body. In this study, a single rigid body with three points of interest is considered. Consequently, three inertia forces were computed, each corresponding to a specific point. These forces are then projected onto the independent generalized speeds and summed with the inertia torques, which are derived in this section.

The inertia torque component of the generalized inertia forces is then determined. The inertia torques arise from the angular acceleration of a rigid body. Although the model contains three frames, the bicycle is represented by a single rigid body; therefore, only one inertia torque is necessary.

The inertia torque is computed using the inertia tensor from Section 2.2, the angular velocity from Section 2.1 and angular acceleration. The angular acceleration is obtained by taking the time derivative of the angular velocity found in Section 2.1. These components are combined to yield the following expression for the system:

$$\mathbf{T}^* := -\left({}^{N}\boldsymbol{\alpha}^{B} \cdot \mathbf{I}^{B/COM} + {}^{N}\boldsymbol{\omega}^{B} \times \mathbf{I}^{B/COM} \cdot {}^{N}\boldsymbol{\omega}^{B}\right)$$
(2.15)

At this stage, the generalized inertia forces can be computed by projecting the inertia forces and inertia torques onto the independent partial velocities. Here, the index i denotes the partial velocity corresponding to each generalized coordinate. These projected forces are then summed and arranged into a matrix, representing the forces acting on each generalized coordinate.

$$F_r^* = {}^{N}\mathbf{v}_i^{\mathcal{P}_i} \cdot \mathbf{R}^* + {}^{N}\boldsymbol{\omega}_i^B \cdot \mathbf{T}^*$$
(2.16)

Due to the complexity of the resulting matrix, its full expression is omitted here. However, the corresponding linearized equations will be presented in Chapter ??.

Forming Kane's Equations

In the previous section, the generalized active forces F_r and the generalized inertia forces F_r^* were determined. The term F_r represents the translational forces, while F_r^* corresponds to the inertial terms. When combined, these equations yield the full set of dynamic differential equations governing the system.

By incorporating the kinematic differential equations that relate the generalized speeds to the generalized coordinates, the complete equations of motion can be generally written in implicit form as:

$$\bar{f}_k(\bar{u}_s, \dot{\bar{q}}, \bar{q}, t) = M_k \dot{\bar{q}} + \bar{g}_k = 0 \in \mathbb{R}^n$$
 (2.17)

$$\bar{f}_d(\dot{\bar{u}}_s, \bar{u}_s, \bar{q}, t) = M_d \dot{\bar{u}}_s + \bar{g}_d = 0 \in \mathbb{R}^p$$
 (2.18)

Where n is the number of generalized coordinates, and p is the number of independent speeds and m are non-holonomic constraints, p=n-m. results in a system of four first-order kinematic differential equations and two first-order dynamic differential equations describing the full motion of my system.

2.4. Slip

Tires at rest experience normal forces that create a contact patch with the ground. When a vehicle is moving in a straight-line motion, this contact patch shifts forwards with motion. Once the vehicle deviates from its straight-line trajectory, lateral forces generated by the tires influence the vehicle's path shifting the patch left or right [10].

To accurately model these dynamics, the equations of motion can no longer be constrained using non holonomic equations, such as those utilized in Section 2.2. Instead, a modified model must be developed to provide a more realistic representation of the bicycles dynamics, including slip.

What is slip

Before modeling a system that includes slip, it is essential to define and understand what slip is. To achieve this, it is necessary to closely examine the behavior of tires interacting with the ground. Tires behave like springs, deforming under external forces and returning to their original shape [10]. Their flexibility also causes a slight angle between the direction of travel and orientation.

As the direction of motion is altered through steering input, the tire does not instantaneously align with the new direction. Instead, there is a transition phase during which the tire undergoes deformation from the initial to the new direction. The contact patch of the tire on the ground experiences lateral deflection relative to the intended direction of travel. As the tire continues rolling forward, new contact points are established with progressively decreasing deformation until the tire aligns with the desired trajectory. This cyclic process of deflect, and relax dictates the actual path of the tire in a curve and is responsible for generating lateral force. The introduction of a lateral force alters the contact patch between the tire and the road surface, resulting in a slight change in the vehicle's direction [10].

The slip angle, denoted by α , quantifies the degree of deformation required to generate the necessary lateral force for cornering. During cornering, the slip angle increases, leading to a corresponding increase in lateral force. However, beyond approximately 6° of slip angle, the relationship between slip

angle and lateral force becomes nonlinear, and the tire begins to slide rather than deform. This transition marks the saturation of deformation, where further increases in slip angle result in nonlinear lateral force generation.

This phenomenon is illustrated in Figure 2.2 where the solid lines represent the slip simulated. As mentioned the relationship between slip and lateral force is linear until 6°, at that point the relationship becomes nonlinear, but can be modeled as a plateau. The tire can not produce more force than the maximum, therefore the lateral force generated beyond 6° is equal to the force generated at 6°.

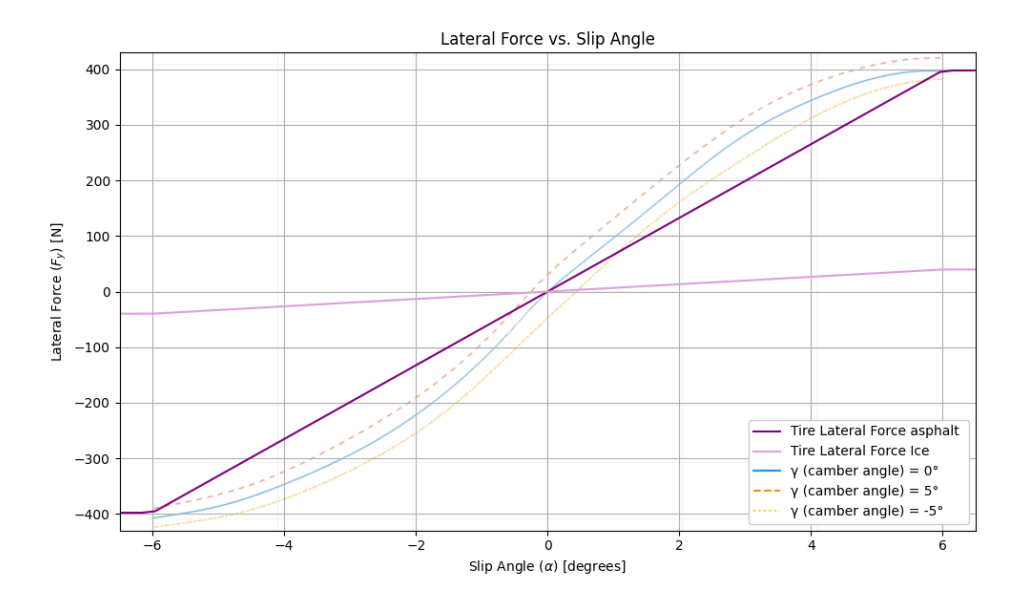


Figure 2.2: Comparison of measured bicycle tire data and linear approximation for lateral force versus slip angle

While more complex Pacejka models exhibit some overshoot and settling behavior beyond this threshold, the simplified linear model used in this study assumes that the force behaves in a linear manner.

Modeling slip

Slip angle is the angle between the direction the tire is pointing (heading) versus the direction of its velocity vector. Mathematically this is the ratio of lateral to longitudinal velocities at each contact point.

$$^{C}\alpha^{W_f} = \tan^{-1}\left(\frac{^{N}\mathbf{v}^{W_f}\cdot\hat{\mathbf{c}}_y}{^{N}\mathbf{v}^{W_f}\cdot\hat{\mathbf{c}}_x}\right)$$
 (2.19)

$${}^{A}\alpha^{W_{b}} = \tan^{-1}\left(\frac{{}^{N}\mathbf{v}^{W_{b}} \cdot \hat{\mathbf{a}}_{y}}{{}^{N}\mathbf{v}^{W_{b}} \cdot \hat{\mathbf{a}}_{x}}\right)$$
(2.20)

The velocity vector of the front wheel is aligned with the steer frame therefore, its components are expressed in terms of $\hat{\mathbf{c}}_x$ and $\hat{\mathbf{c}}_y$. The velocity of the rear wheel is aligned with the yaw frame, $\hat{\mathbf{a}}_x$ and $\hat{\mathbf{a}}_y$ are used to represent its components.

Lateral force refers to the force generated perpendicular to the direction of tire travel and is derived from the slip angle. Previously in this section, the concepts of linear and nonlinear slip regions were introduced. In this study, lateral tire forces will be calculated using the linear region, making them linearly proportional to slip by the coefficient of slip [13]. As mentioned, it is common to use a linear model of slip, relating lateral force F_y and slip angle α . The mathematical relationship between slip angle α and lateral force F_y is defined using a proportional constant, the cornering stiffness C_α .

$${}^{C}\mathbf{F}_{y}^{W_{f}} = -C_{\alpha}{}^{C}\boldsymbol{\alpha}^{W_{f}} \tag{2.21}$$

$${}^{A}\mathbf{F}_{y}^{W_{b}} = -C_{\alpha}{}^{A}\boldsymbol{\alpha}^{W_{b}} \tag{2.22}$$

While these relationships hold mathematically, it is important to understand the sign convention associated with each variable. When considering slip, this can be less straightforward. Figure 2.3 aims to clarify the direction of lateral force and slip angle, using the right-hand convention for positive angle. The blue arrows at each angle indicate how rotation is occurring.

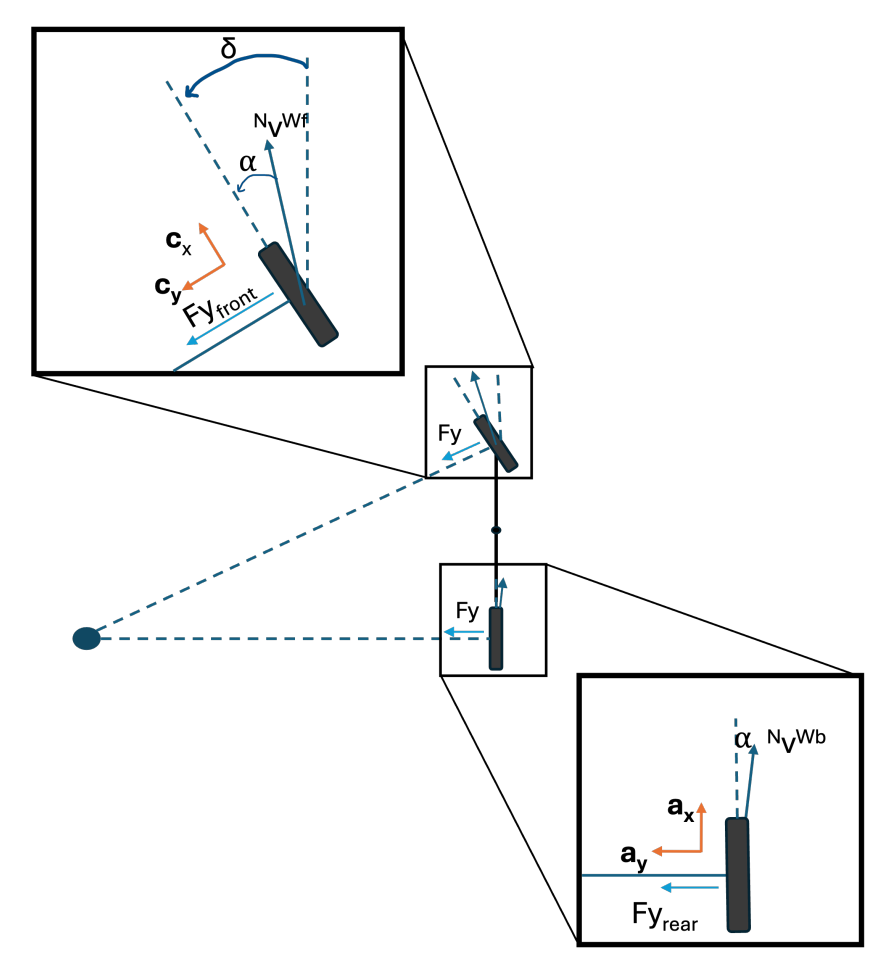


Figure 2.3: Detailed view of front and rear wheels highlighting the slip angle sign convention.

Figure 2.3 shows that the lateral force sign convention opposes that of slip angle, leading to the negative sign on the right side of Equations 2.21, and 2.22.

Cornering stiffness C_{α} linearly relates the slip angle α to lateral force F_y , and is the same for both tires. This assumption holds well within the range of -6°to 6°for tour/city bikes [14]. Outside of this range, the behavior can be simplified by assuming that the lateral force at the boundary reaches a maximum, and any slip angle exceeding this threshold will result in the same lateral force at the boundary. When a bicycle performs an abrupt evasive maneuver, the slip angle may fall into this region beyond -6°to 6°. Cornering stiffness varies based on tire type and size. Based on experimental bicycle data, the cornering stiffness of bicycle tires was determined to be 3600 N/rad within slip angle range -6°to 6°[14].

The lateral forces calculated using Equations (2.21) and (2.22) must still be integrated into the bicycles dynamics. The forces computed at each contact point are conservative forces, therefore they will be considered resultant forces. The lateral forces will appear as generalized active forces.

$$\mathbf{F}_r = \sum_{i=1}^{\nu} {^{N}\mathbf{v}_i^{COM_i} \cdot \mathbf{R}_{gravity}} + {^{N}\mathbf{v}_i^{W_{f_i}} \cdot {^{C}\mathbf{F}^{W_f}}} + {^{N}\mathbf{v}_i^{W_{b_i}} \cdot {^{A}\mathbf{F}^{W_b}}}$$
(2.23)

Equation 2.23 is used instead of Equation 2.12, where i represents partial velocities at each point. Summing these projections across all relevant particles yields the scalar force contributions associated with each generalized speed. These contributions, combined with the existing gravitational force, result in a vector of generalized forces expressed in terms of generalized speeds.

The generalized active forces for the slip model, which account for both lateral tire forces and gravity, are shown below:

$$\begin{bmatrix} C_{\alpha}{}^{C}\alpha^{W_{f}}\sin(\psi+\delta) + C_{\alpha}{}^{A}\alpha^{W_{b}}\sin(\psi) \\ -C_{\alpha}{}^{C}\alpha^{W_{f}}\cos(\psi+\delta) - C_{\alpha}{}^{A}\alpha^{W_{b}}\cos(\psi) \\ -C_{\alpha}{}^{C}\alpha^{W_{f}}L\cos(\delta) \\ ghm\sin(\theta) \end{bmatrix}$$
(2.24)

In contrast to the no-slip model, the slip model retains all four original generalized coordinates, resulting in a mass matrix M_d with entries corresponding to each of these degrees of freedom, as no constraints have been applied. The velocity related force vector g_d also have an entry corresponding to each generalized coordinate. These matrices are cumbersome and therefore will not be included here, however the linearized equations are presented in Chapter 3.

Adding ice

Previously, it was mentioned that slip will be modeled linearly. Slip angles beyond the range of -6°to 6°correspond to a maximum lateral force. The value of 3600 N/rad, calculated from experimental data, is based on riding on asphalt [14]. While the shape of the slip curve on ice is assumed to be similar, it exhibits a significantly lower slope and a much smaller maximum lateral force. This is expected as ice can not generate large amounts of lateral force even at large slip angles.

The coefficient of slip for a bicycle on dry asphalt has been measured and is available in the literature. However, studies involving bicycle tires on surfaces other than dry asphalt are limited. Fortunately, multiple studies of car tire behavior across various surfaces exist and can be used to proportionally estimate bicycle slip coefficients. Car tires have normalized coefficients of slip typically ranging between 0.8 and 1 on dry asphalt, and decreases to approximately 0.1 on ice [15], [16].

Assuming that the relative change in the coefficient of slip from dry asphalt to ice for cars is representative of the change for bicycles, a proportional approach can be applied. The measured bicycle coefficient of slip on dry asphalt is 3600, which is considered equivalent to a normalized value of 1 [14]. Using the same ratio observed in car tire data (1 to 0.1), the estimated coefficient of slip for a bicycle on ice is therefore calculated as:

$$\frac{\text{Bicycle coefficient on ice}}{\text{Bicycle coefficient on asphalt}} = \frac{\text{Car coefficient on ice (0.1)}}{\text{Car coefficient on asphalt (1.0)}}$$
(2.25)

This method assumes that the proportional reduction in slip behavior observed in car tires when transitioning from dry asphalt to ice is similarly applicable to bicycle tires.

To incorporate this change into the Python simulation, a simple if statement was implemented. This conditional logic temporarily altered the coefficient of slip for a specified time duration, allowing the simulation to account for changes in surface conditions.

$$C_{\alpha}^{W_f/W_b}(t) = \begin{cases} 360.0 & \text{if } 15 \leq t \leq 19.0 \text{ (ice)} \\ 3600.0 & \text{else (asphalt)} \end{cases}$$

This approach was chosen to enable the bicycle model to respond to variations in the slip coefficient without requiring trajectory-based switching. Section 4.3 extends this time-based slip change to simulate the presence of ice on the ground. For the current stage, modeling slip as a time-based event serves to verify that slip dynamics are correctly implemented in the system and provides a basis for testing the controllers.

Linearization

The equations of motion derived in the previous chapter are relatively simple compared to more complicated bicycle models. Despite their simplicity, these equations are long and exhibit non-linearities. The goal of this thesis is to design a stability controller for the bicycle; to achieve this, the equations must be linearized and expressed in state-space form.

Linearization is a powerful technique that approximates complex, non-linear systems by considering small deviations about a point of interest. Before linearization, an analysis of the equilibrium states of the system must be done to determine the best equilibrium for my purposes. The equilibrium point is selected based on the operating conditions of the bicycle, in my case fixed velocity forward riding to ensure that the linearized model accurately represents the system's behavior. By linearizing the equations of motion around the chosen equilibrium point, the system dynamics can be simplified, making it possible to analyze the system as if it were linear within a small range about that point. This process will produce similar results to the nonlinear dynamics in the vicinity of the equilibrium point. Linearization enables the analysis of local stability, simplifies controller design, and speeds up simulations [17].

Once the equations are linearized, they are expressed in state-space form, which provides a convenient framework for analyzing and designing controllers. The state-space representation allows for the examination of system properties such as controllability. The controllability of the system is assessed by calculating the controllability matrix and determining whether the state variables can be controlled by the available inputs. Additionally, the type of system will be determined by analyzing the eigenvalues of the system matrix, which provides insight into the system's stability characteristics.

3.1. Equilibrium

Equilibrium points are important because they represent positions in a system where, if undisturbed, the system remains unchanged. There are two classifications of equilibrium points: stable and unstable. A common approach to analyzing bicycle dynamics is to model it as an inverted pendulum on a cart, which offers useful insights into its equilibrium behavior. This serves as a foundational basis for analyzing the equilibrium positions of the system. An inverted pendulum on a cart is commonly used in the study of stability and feedback control [18]. Bicycle dynamics are slightly more complicated but conceptually similar.

Since the 1950s, inverted pendulums on carts have been used to analyze the open-loop stability of unstable systems. [18] These systems are conceptually simple to visualize but exhibit nonlinear dynamics with both stable and unstable equilibrium points. The stable equilibrium occurs when the pendulum hangs downward under the influence of gravity. This is a statically stable equilibrium, meaning that if disturbed, the system will return to its original position without external input. The unstable equilibrium, occurs when the pendulum is positioned upright, opposing gravity. This is a statically unstable equilibrium, meaning that after a disturbance, some form of motion or control is required to restore the system to the equilibrium position [19]. While the system naturally resides in the downward equilibrium, with appropriate control mechanisms, the mass can be moved to and maintained at the unstable upward

3.2. Taylor series

equilibrium [18].

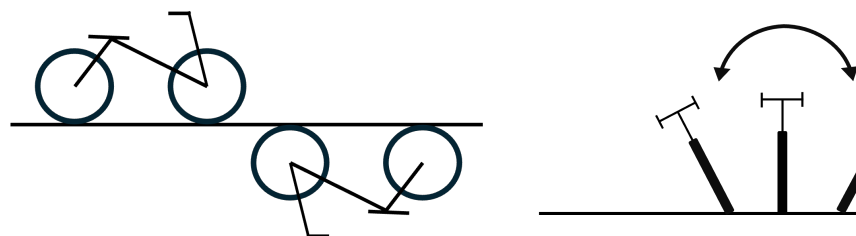


Figure 3.1: Bicycle in static equilibrium—upright and stationary on a flat surface

Figure 3.2: Bicycle in steady turn equilibrium,constant lean angle during circular motion

Similarly to the inverted pendulum, the bicycle exhibits the same equilibrium positions depicted in Figure 3.1. One equilibrium position is upright, which is dynamically unstable because any disturbance moves it away from balance. While this equilibrium can be restored, it requires dynamic intervention. The other equilibrium position is fully downward, which would be statically stable. In practice, the ground prevents this from occurring and the bicycle instead comes to rest on its side. The statically stable position is not of interest in this study, as it represents a static resting state rather than a controllable balance. Therefore, for the purposes of this study, only the upright, dynamically unstable position will be considered.

Unlike the inverted pendulum, which is a two-dimensional, two-degree-of-freedom system where the cart moves back and forth along a single axis, a bicycle moves freely in a plane. Therefore, an additional equilibrium condition must be considered. When turning at a constant radius of curvature, there exist specific values of velocity, steer, and lean that result in a stable circling motion [20]. This motion is subject to limitations on maximum lean and steer angles for a given velocity. If these three variables are balanced appropriately, several steady-turn configurations can be classified as conditional dynamic equilibrium.

My equations are linearized about a constant velocity with no lean, yaw or steer. This should result in linear equations that behave similarly to the nonlinear equations from approximately -30° to 30°. This is true at any velocity chosen, because at no lean, yaw and steer as long as there is a reasonable forward velocity the system will behave in a predictable way.

3.2. Taylor series

The Taylor series is a widely used method for approximating functions near a given point using polynomials. Computing the full Taylor series expansion is often unnecessary; however, using its first-order approximation, provides a linear first order representation of the equations of motion near an equilibrium point [17]:

$$\mathbf{f}(\mathbf{x}) \approx \mathbf{f}(\mathbf{x}_0) + \mathbf{J}(\mathbf{x}_0)(\mathbf{x} - \mathbf{x}_0),\tag{3.1}$$

The first term in Equation 3.1 refers to the nonlinear equation evaluated at the equilibrium conditions, which describe the system's dynamics at the equilibrium point. Typically, an equilibrium occurs when all variables are zero, resulting in the first term being zero. The second term contains the derivative at equilibrium point x_0 representing the instantaneous rate of change. These are evaluated at the equilibrium values with small perturbations around the equilibrium point. This term enables the system to be analyzed for stability and controlled effectively [17].

The no slip equations of motion, linearized about upright straight motion is:

$$\mathsf{EOM}_{\mathsf{no}\;\mathsf{slip}} = ghm\theta - \frac{vhm\dot{\delta}}{2} - \frac{v^2hm\delta}{L} + \left(-I_{xx} - h^2m\right)\ddot{\theta} \tag{3.2}$$

3.3. State-space

The linearized slip equations of motion about a constant velocity \boldsymbol{v} and straight line motion are shown below:

$$\begin{bmatrix}
 m\ddot{q}_{1} \\
 -\frac{C_{\alpha_{W_{f}}}L\dot{\psi}}{2v} + C_{\alpha_{W_{f}}}\delta + \frac{L}{2}m\ddot{\psi} - hm\ddot{\theta} + m\ddot{y} + \left(-\frac{C_{\alpha_{W_{b}}}}{v} - \frac{C_{\alpha_{W_{f}}}}{v}\right)(-v\sin(\psi) + \dot{y}) + (C_{\alpha_{W_{b}}} + C_{\alpha_{W_{f}}})\psi \\
 -\frac{C_{\alpha_{W_{f}}}L^{2}\dot{\psi}}{4v} - \frac{C_{\alpha_{W_{f}}}L\left(-v\sin(\psi) + \dot{y}\right)}{2v} + C_{\alpha_{W_{f}}}\frac{L}{2}\psi + C_{\alpha_{W_{f}}}\frac{L}{2}\delta - \frac{L}{2}hm\ddot{\theta} + \frac{L}{2}m\ddot{y} + \left(I_{3} + \frac{L^{2}}{4}m\right)\ddot{\psi} \\
 -\frac{L}{2}hm\ddot{\psi} + ghm\theta - hm\ddot{y} + \left(I_{1} + h^{2}m\right)\ddot{\theta}
\end{bmatrix}$$
(3.3)

These are listed in order of generalized coordinates, x, y, ψ, θ .

3.3. State-space

State space is mathematical framework used to model system dynamics describing a system using inputs, outputs and state variables. Transfer functions are an alternative way to consistently model bicycle dynamics but they can not handle inputs and coupled dynamics. I wanted to input a steer to influence the dynamics, making state space an ideal choice.

The state space solution extracts the second-order differential equation and reformulates it into a system of first-order differential equations. This thesis was concerned with the stability of the bicycle, particularly how changes in the steer angle, δ , influence the roll angle, θ , of the system. The steer rate was excluded from the slip model partly because it does not appear in the equations of motion, and partly because a rider can directly control the steer angle but cannot directly control the steer rate. I was not concerned with path following or trajectory at this point, so the state variable can be reduced to θ and $\dot{\theta}$.

By introducing ω as a variable the state representation can be rewritten in terms of first-order derivatives by defining ω as $\omega = \dot{\theta}$. This relationship was used in 3.4 and shows up in the first row of the A matrix. The system inputs are included in a separate vector denoted by u.

$$\dot{x} = \begin{bmatrix} \omega \\ \dot{\omega} \end{bmatrix}, \quad x = \begin{bmatrix} \theta \\ \omega \end{bmatrix}, \quad u = \begin{bmatrix} \delta \\ \dot{\delta} \end{bmatrix}$$
 (3.4)

The time derivative of the state vector is equal to the first-order derivatives of its components, effectively converting the system from a second-order differential equation into a system of two first-order equations. Now in first-order form, the state-space matrices are computed using 3.5. The A matrix characterizes the system's dynamics with respect to the state variables, x, while the B matrix describes how the system responds to the input variables, y [21].

$$A = \frac{\partial f}{\partial x}\Big|_{x_0, u_0}, \quad B = \frac{\partial f}{\partial u}\Big|_{x_0, u_0} \tag{3.5}$$

The model with no slip had one degree of freedom, therefore the state space matrix will be two by two. When this process is followed for the equations of motion of the no slip model the resulting A and B matrices are:

$$A = \begin{bmatrix} 0 & 1 \\ \frac{bghm}{I_1b + bh^2m} & 0 \end{bmatrix}, \quad B = \begin{bmatrix} 0 & 0 \\ -\frac{bhmv}{I_1b + bh^2m} & -\frac{ahmv}{I_1b + bh^2m} \end{bmatrix}$$
 (3.6)

Similarly, when the process is applied to the slip equations of motion, there are four degrees of freedom, resulting in an 8×8 A matrix. However, for stability analysis, it is not necessary to consider all eight states. The matrix can be reduced to focus on the key variables influencing stability: the roll angle θ and roll rate $\dot{\theta}$. This simplification retains the essential dynamics needed for stability assessment and simplifies the analysis.

3.4. Controllability 18

The bicycle's behavior is independent of its position in space or yaw orientation, allowing a controller to be designed using only roll θ and roll rate $\dot{\theta}$. The slip equations of motion do not involve the steer rate $\dot{\delta}$, the inputs for the slip model include only the steering angle itself, δ . Using these simplifications, the A and B matrices derived from the slip equations of motion are:

$$A = \begin{bmatrix} 0 & 1 \\ -\frac{ghm}{I_1} & 0 \end{bmatrix}, \quad B = \begin{bmatrix} 0 \\ -\frac{C_{\alpha}h}{I_1} \end{bmatrix}$$
 (3.7)

3.4. Controllability

State-space representation provides a mathematical model of how system inputs influence the internal states. The relationship between inputs and states is fundamental in determining controllability and determines whether a system can be driven to any desired state [19]. In this study, the goal was to steer a bicycle toward stable forward motion.

Evaluating controllability quantifies the extent to which system inputs influence the states. This was achieved by computing the controllability matrix, which was constructed using the A and B matrices. According to Kalman's Controllability Criterion, a linear system was controllable if and only if [19]:

$$\operatorname{rank} \begin{bmatrix} B & AB & A^2B & \dots & A^{n-1}B \end{bmatrix} = n \tag{3.8}$$

where n is the dimension of the state vector.

In both slip and the reduced no-slip model, the state matrix A is two by two. Consequently, the controllability matrix consists of the first two terms, and its rank must be two to ensure full controllability. In the case of slip the controllability matrix is full rank. The system is controllable, meaning the available inputs are sufficient to drive the system to any desired state. At this stage, if the system is determined to be controllable, various control methods can be evaluated and executed.



Figure 3.3: Block diagram of the uncontrolled bicycle, no feedback

The uncontrolled system in Figure 3.3 will be a building block for controller design in the next chapter.

3.5. System type

In Section 3.4, the system was determined controllable. However, before proceeding with controller design, it is important to examine one more property, the system type. System type directly affects the system's steady-state error response to standard input signals [22].

System type is defined by the number of integrators in the open-loop transfer function, which corresponds to the number of poles at the origin in the *s*-domain. A higher system type enables improved steady-state performance for higher-order input signals [22].

- Type 0 systems have no poles at the origin and thus no integrators in the open-loop transfer function. These systems exhibit a finite steady-state error in response to step inputs and infinite error for both ramp and parabolic inputs [22].
- Type 1 systems have one pole at the origin, corresponding to one integrator. They achieve zero steady-state error for step inputs, a finite error for ramp inputs, and infinite error for parabolic inputs [22].
- Type 2 systems have two poles at the origin, corresponding to two integrators. These systems
 exhibit zero steady-state error for both step and ramp inputs, and a finite error for parabolic inputs [22].

3.5. System type

Using the previously derived state-space model from Section 3.3, the transfer function is Equation 3.9:

$$\frac{-391.3}{s^2 + 92.77} \tag{3.9}$$

Applying this equation to the system yields a transfer function that indicates the system is type 2. This can be verified by checking the open-loop pole placement.

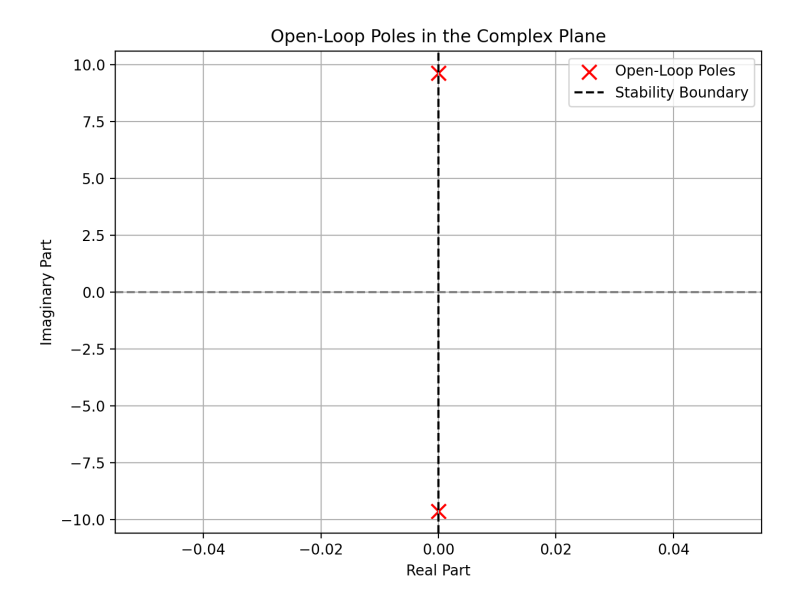


Figure 3.4: Slip, open loop poles

There are two open-loop poles, at 0.+9.63j, 0.-9.63j, both poles are at s=0. As a result, the system is type two and expected to track a step input with zero steady-state error. An additional integrator is not necessary, and if added could cause system instability.

4

Controllers

Bicycles present an intriguing case for control theory because they are typically underactuated systems. They possess more degrees of freedom than available control inputs [18]. This is shown in my model containing slip, with just steer we can control several variables. Conversely, when a no slip constraint is present the bicycle is not underactuated. Steering adjustments and forward velocity input are dynamically coupled, influencing the yaw and roll of the bicycle. The inherent instability of a bicycle at low speeds, combined with its self-stabilizing behavior at higher speeds, differentiates its control dynamics from those of other vehicles.

Beyond serving as an interesting case study in control theory, the system in question requires some form of control to maintain stability. In this chapter, the system will be simulated over time, both without a controller and with a simple proportional-derivative (PD) controller. This basic framework will then be extended to model a bicycle with a human rider.

A controller designed to handle the presence of an ice patch was developed and incorporated as an adaptive control strategy. This addition was motivated by the need to address abrupt, unexpected changes in road surface conditions that could otherwise lead to a crash. The controller acted as a stabilizing system, actively correcting deviations from equilibrium. Its primary objective is to intervene in situations where the rider alone would fail to maintain control, thereby ensuring stability across a broader range of scenarios.

Balancing a bicycle is conceptually similar to balancing an inverted pendulum on a cart. The point-mass model from Chapter 2 shows how the system dynamics were derived. Chapter 3 demonstrated how the nonlinear system can be approximated linearly around desired equilibrium points. This section takes the analysis further by stabilizing the bicycle using steering as the primary control input.

Linear Quadratic Regulators (LQR) and PD controllers both provide feedback based on the system's state, but they differ in design and performance. PD control provides a simple structure with proportional and derivative gains, but effective tuning requires understanding the system dynamics. It is easy to implement and often sufficient for basic stabilization tasks. However, it does not account for future behavior.

LQR, on the other hand, is an optimal control strategy that minimizes a predefined quadratic cost function, typically balancing state error and control effort. It requires a full state-space model of the system and computes the optimal feedback gain matrix by solving the algebraic Riccati equation. LQR is more computationally involved but considers the interactions between different state variables, which is important for coupled dynamics like in bicycles. Finally, LQR offers a systematic way to tune the controller by adjusting the weighting matrices in the cost function, whereas PD tuning typically relies on manual trial-and-error.

This chapter uses bicycle dynamics from Chapter 2 to simulate the system over time. This simulation will be used to establish what closed loop controllers are needed and most effective. The open loop

4.1. Simulating

linear dynamics from Chapter 3 will be the building block for closed loop feedback designed, then implemented into the nonlinear simulation.

4.1. Simulating

Simulating the system dynamics is a powerful tool for visualizing behavior under varying conditions. This involves solving the equations of motion, which must first be expressed in explicit first-order form. With specified initial states and inputs, the system is then numerically integrated over time.

To rewrite the equations in explicit form, the linear coefficients and remaining terms of the dynamic differential equations are separated. This yields two linear systems that can be solved for the system's velocities and accelerations.

The simulation is initialized with user prescribed inputs, and initial positions and velocities are defined. Realistic values for bicycle parameters used are shown in Table 2.1 [13]. Initial states were defined in Table 4.1. Roll angle and velocities were occasionally changed depending on what was being investigated. The no slip model used the same inputs but was reduced to include only the generalized coordinates, roll rate $\dot{\theta}$, and longitudinal velocity \dot{x} . It includes the first five entries in Table 4.1, along with roll rate $\dot{\theta}$. This simplification was possible because the remaining generalized speeds were written in terms of $\dot{\theta}$ and \dot{x} .

Description	Value	Unit
Position x	0.0	m
Position y	0.0	m
Yaw angle ψ	0.0	rad
Roll angle θ	10.0	deg
velocity \dot{x}	7.0	m/s
velocity \dot{y}	0.0	m/s
Yaw rate $\dot{\psi}$	0.0	rad/s
Roll rate $\dot{\theta}$	0.0	rad/s

Table 4.1: Initial conditions for state variables used in system simulation

Once the inputs and initial states are defined, the system can be passed to a numerical solver to simulate its response. The solver was configured to integrate over any defined time span, at any chosen frame rate. I decided to use 20 seconds because it was long enough to complete the majority of a circle. I chose a resolution of one thousand, so the simulation produced one thousand evenly spaced time points. I used a higher-order Runge-Kutta, specifically RK-45. I selected this controller because it adjusts time steps to balance accuracy and speed.

4.1. Simulating

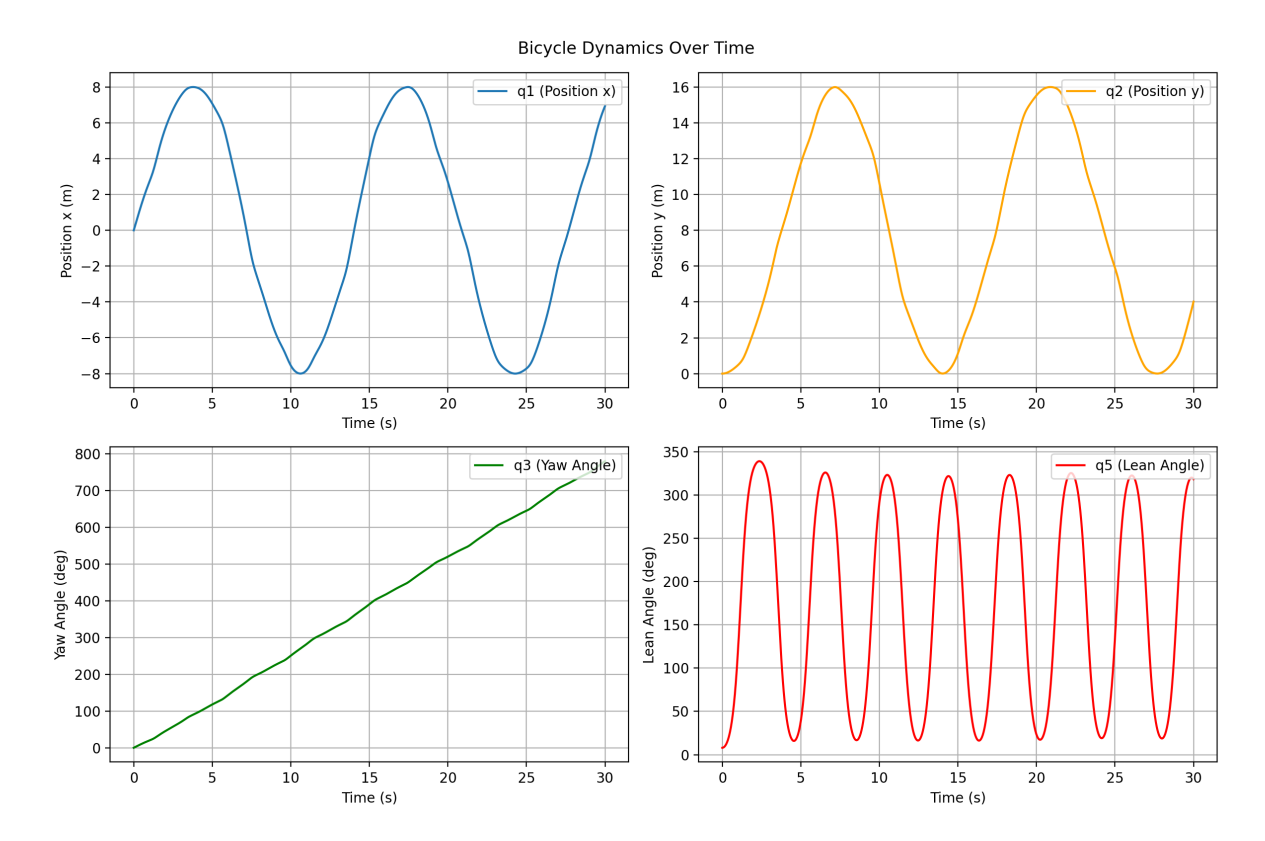


Figure 4.1: Time evolution of the generalized coordinates in the absence of feedback control

The initial conditions and vehicle constant parameters are used to solve the no-slip equations of motion without feedback control. The generalized coordinates are plotted over time, as shown in Figure 4.1. The x and y coordinates exhibit sinusoidal behavior, and the yaw angle ψ increases almost linearly, indicating that the bicycle is following a circular trajectory. The roll angle follows a sinusoidal pattern, rotating from 0° to 360° , suggesting that the center of mass is spinning about the bicycle's points of ground contact.

This data can be used to generate a moving three-dimensional animation of the system dynamics, offering a more intuitive visualization. However, while the motion reflects the mathematical solution of the uncontrolled system, it does not realistically represent actual bicycle behavior. To obtain a more meaningful and physically realistic assessment, the simulation must be constrained to stay within plausible bounds.

Roll Constraint

In the case of an uncontrolled bicycle, there is no active stabilization mechanism to prevent it from falling over, much like the behavior observed when a real bicycle is pushed and released without rider input. However, the simulation does not constrain the motion of the bicycle with respect to the ground plane. As a result, the numerical solution allows the roll angle to continue beyond the ground plane, causing the bicycle to unrealistically rotate below the ground seen in Figure 4.1.

To address this limitation, an event detection function was introduced into the system integration using events. This event function monitors the roll angle, θ , and triggers when it exceeds $\pm 90^{\circ}$. During integration, the solver continuously evaluates this condition, and terminates if the threshold is reached. By enforcing this constraint, the simulation more accurately reflects real-world physical behavior, allowing for a more realistic interpretation of the uncontrolled system dynamics and aiding in the validation of expected responses.

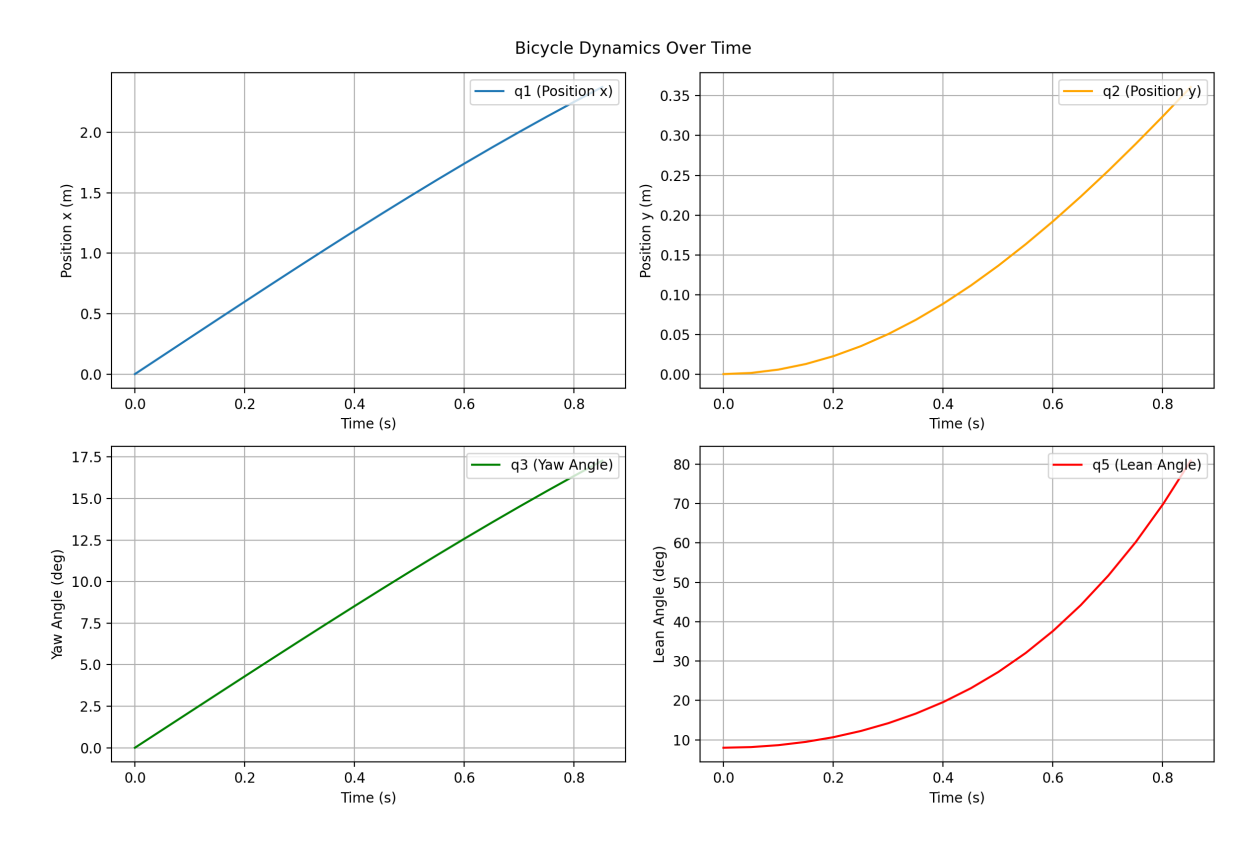


Figure 4.2: System without Feedback Control with a Roll Event

As seen in Figure 4.2, the roll angle θ begins at zero and rapidly falls toward the ground plane. In contrast to Figure 4.1, Figure 4.2 terminates the simulation at 90°, representing the point at which the bicycle would make contact with the ground and come to rest. To enable continued simulation beyond this point, a control input must be applied to the roll dynamics in order to maintain an upright configuration.

4.2. Proportional Derivative

The roll angle of a bicycle is inherently unstable without active control causing the bicycle will fall over. Proportional-Integral-Derivative (PID) control is one of the most widely used control strategies in industry [23], and it can be applied to a wide range of control problems, including steer-to-lean control. The proportional (P) term responds to the current error, the integral (I) term accounts for the accumulation of past errors, and the derivative (D) term predicts future error trends based on the current rate of change [23]. However, in the context of steering and leaning control, accumulating past error through the integral term is not necessary. The open loop control block is modified to contain the PD control law resulting in the closed loop dynamics shown in Figure 4.3.

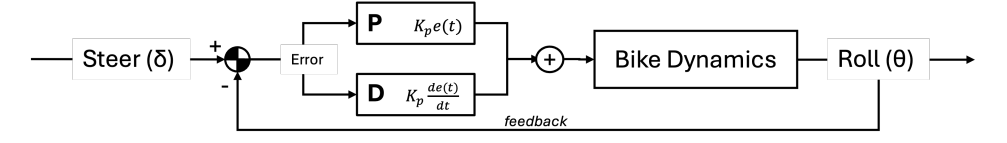


Figure 4.3: PD Control Block Diagram Emulating Rider Feedback

The error between the desired roll angle and the current roll angle can be addressed using a proportional gain. This gain determines how aggressively the controller responds to roll angle deviations, acting to minimize the difference between the actual and desired roll angles [23]. This control action aims to

maintain the roll angle, θ (Figure 4.1), close to zero for straight-line motion, or at an appropriate value for stable circular motion.

The second term in the controller addresses the roll rate error. Here, the same gain magnitude is applied but with a negative gain for roll rate. The negative sign is essential to introduce a damping effect, which reduces oscillations in θ around the desired value [23]. Damping the roll angle improves stability by suppressing oscillatory behavior, ensuring that the steering input not only reacts to the present error but also to the rate at which that error is evolving.

$$\delta_P(t) = K_p \cdot (\theta_{\text{desired}} - \theta) \tag{4.1}$$

$$\dot{\delta}_D(t) = -K_d \cdot \frac{d}{dt} (\dot{\theta}_{\text{desired}} - \dot{\theta}) \tag{4.2}$$

Where θ_{desired} is the desired roll angle, θ is the current roll angle, and $\dot{\theta}$ is the roll rate. Equation 4.1 and Equation 4.2 defines the relationship between steering and leaning. The PD controller with gains 3 stabilizes the roll angle by generating an appropriate steering input to counteract roll disturbances shown in Figure 4.4 . This approach is advantageous because it does not require system linearization or conversion to state-space form. However, PD control must be re-tuned under varying conditions such as changes in velocity or external forces like slip.

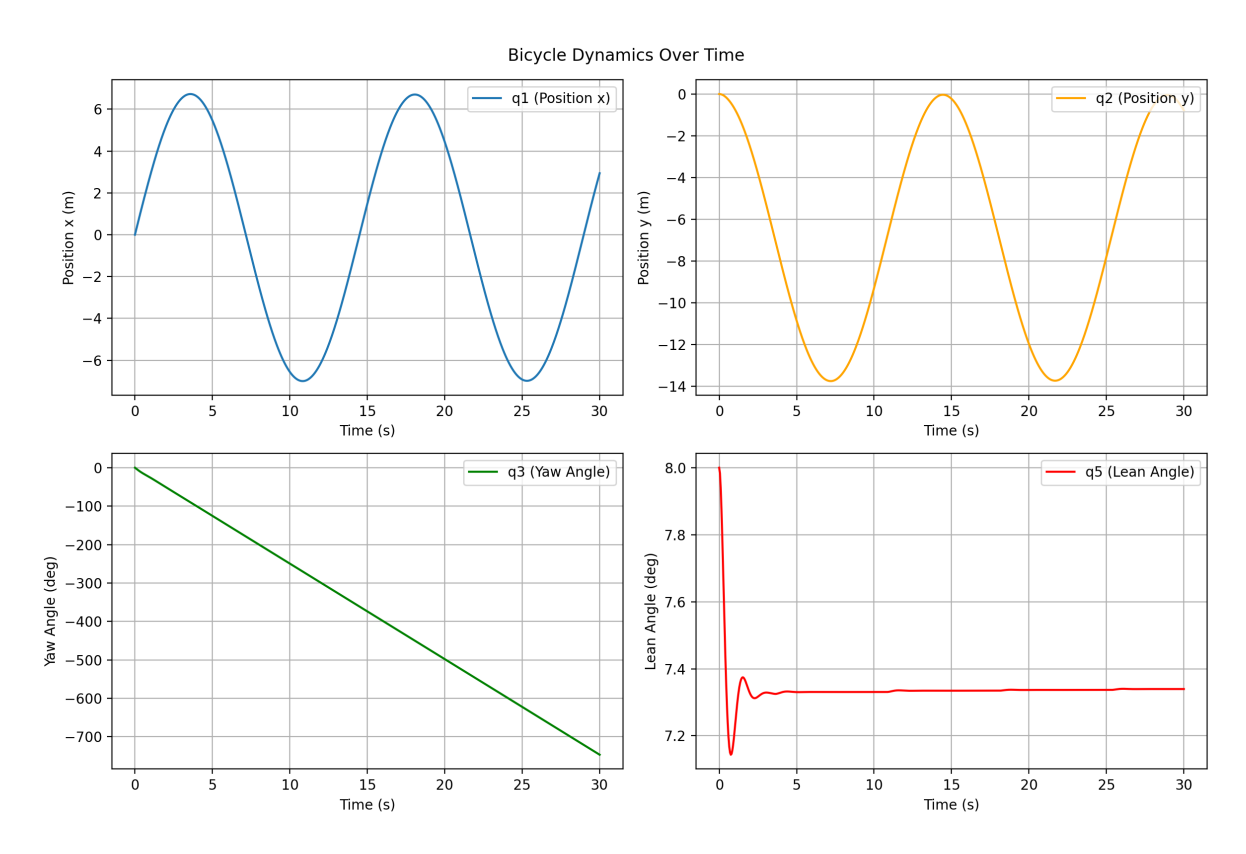


Figure 4.4: System response under PD control emulating rider behavior

A PD controller with gains set to 3 is used as a baseline, enabling the bicycle to ride in a straight line and perform turns with varying radii. This controller is considered equivalent to basic human control input. This will be used as the "rider" when looking into control over ice.

4.3. Linear Quadratic Regulators

Linear Quadratic Regulators (LQR) are a commonly used optimal control method that balance system response and control effort by defining a performance index [22]. The performance index is commonly known as the cost function, which mathematically represents the balance of input weights and state weights. In LQR design, this cost function is minimized to determine an optimal state feedback gain matrix K. By applying this feedback, the closed-loop system achieves stability through strategic placement of its poles in the complex plane [19].

The first step is creating weighting matrices for the states and control inputs, Q and R. These are symmetric, positive semi-definite weighting matrices that penalizes deviations from desired states or control input. The values along the diagonal of Q determine the relative importance of each state variable. The first entry corresponds to the importance of maintaining the desired roll θ , and the second entry maintains roll rate $\dot{\theta}$. Like Q, the entries in R define the relative importance of each input δ [19]. Changing the weighting in Q and R have a big effect on how the controller behaves. These matrices directly define the cost function J, which should be minimized to ensure small deviations in the state and minimal control effort.

$$J = \int_0^\infty \left(x^T Q x + u^T R u \right) dt \tag{4.3}$$

In Chapter 3 the bicycle dynamics were represented in state-space form. The open-loop poles of the system were plotted, and the system was identified as type 2. Using the equilibrium points defined in Chapter 3, the controller can regulate the system to maintain stability around the selected equilibrium state. To illustrate the closed-loop dynamics, the updated block diagram is shown in Figure 4.5.

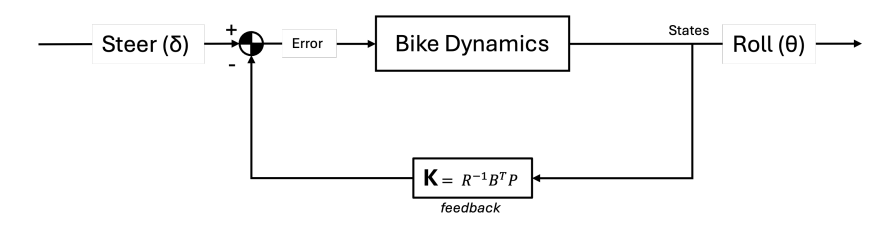


Figure 4.5: Block diagram showing LQR feedback

The closed-loop state-space representation of the system with LQR control is:

$$\dot{x} = (A - BK)x + Bu \tag{4.4}$$

To close the loop on the dynamics the optimal feedback gains K must be computed. The Riccati Equation must be solved using my bicycles A and B matrices from Chapter 3 and the weight matrices Q and R determined in the previous section.

$$A^{T}P + PA - PBR^{-1}B^{T}P + Q = 0 (4.5)$$

The result of calculating Equation 4.5 is matrix P. Matrix P is a symmetric, positive definite matrix that encapsulates the accumulated cost over time. Matrix P quantifies the cost of stability for my specific dynamics. It is crucial when calculating gains using Equation 4.6.

$$u = -K(x - x_{des}), \quad K = R^{-1}B^{T}P$$
 (4.6)

The gain matrix K takes the result of Riccati P and turns it into an actionable control. It is static, meaning it does not change dynamically with time. K is used in Equation 4.6 to close the dynamics loop resulting in a controlled system.

Now that the system is closed loop, the system stability must be analyzed. Eigenvalues play a critical role in LQR design, as they determine the stability and performance of the closed-loop system. Their location in the complex plane dictates the type of stability exhibited by the system. Calculating the gains K modifies the system dynamics from $\dot{x} = Ax + Bu$ to $\dot{x} = (A - BK)x$. The closed-loop system matrix is given by $A_{cl} = A - BK$ [19]. The eigenvalues of A_{cl} dictate the system's response over time and serve as a mathematical proof of stability.

For a system to be stable, the eigenvalues must have negative real parts; thus, they must all lie in the left-half of the complex plane [19]. When eigenvalues lie in the left half of the complex plane, the system states converge to equilibrium [19]. This represents a stable system, but there are two possible categories of stability. Marginal stability occurs when eigenvalues lie exactly on the imaginary axis, while asymptotic stability occurs when all eigenvalues have strictly negative real parts (Re < 0), meaning the system will return to equilibrium over time.

The LQR controller influences the eigenvalues through the selection of the weighting matrices Q and R. Higher values in Q shift eigenvalues further to the left, while increasing R moves the eigenvalues closer to the imaginary axis. If excessively large values of Q are chosen, the system may achieve stability but at the cost of high control effort. The key advantage of LQR lies in its ability to optimally balance eigenvalue placement and control effort, leading to an efficient and stable closed-loop system.

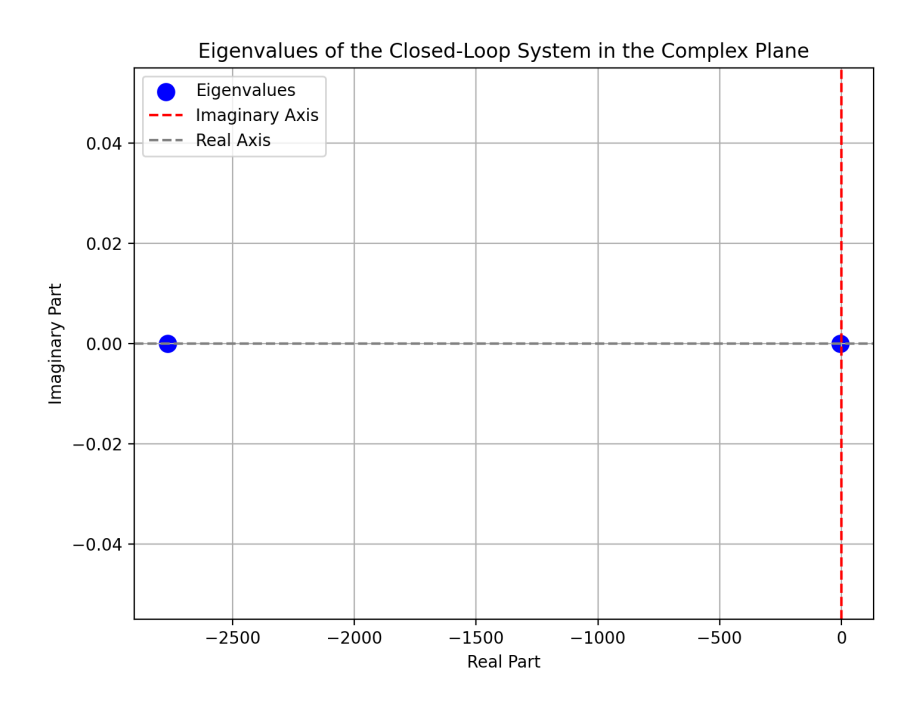


Figure 4.6: Closed-Loop System Eigenvalues Plotted in the Complex Plane

Figure 4.6 shows one eigenvalue clearly in the left plane and another closer to the imaginary line but still on the left side. My system has exponential decay and should not exhibit oscillation.

LQR no slip and slip

In the slip model, the system is described by two states: roll angle θ and roll rate $\dot{\theta}$. The control input consists of the steering angle δ . An LQR controller was designed by initially selecting identity matrices for the weighting matrices Q and R. These were modified logically based on system behavior: higher penalties were assigned to deviations in θ and $\dot{\theta}$, while changes in δ were penalized less. This prioritized keeping the state at the desired value with minimal oscillation.

Multiple weight configurations in the ${\it Q}$ and ${\it R}$ matrices produce stable and effective controllers. Changing the control weights had a noticeable effect on how quickly and accurately the system converged

to the target values. To analyze this effect, different control weights were applied at a forward velocity of four meters per second with a target lean angle of five degrees. These conditions were chosen because they represent a relatively low speed and a medium lean angle, making the system mildly challenging to control.

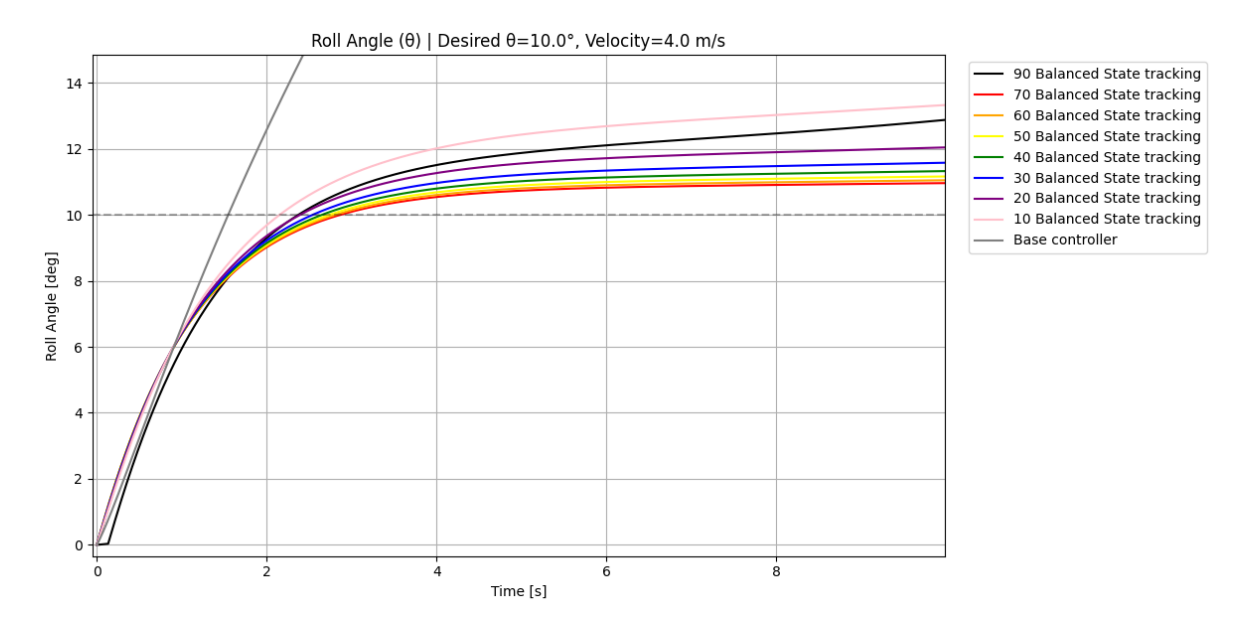


Figure 4.7: LQR increasing balanced weight on states

Figure 4.7 shows the effect of increasing the weights of roll and roll rate in matrix Q at equal intervals. A systematic guess and check approach was used. From the initial identity matrices, the weights related to roll θ and roll rate $\dot{\theta}$ were incrementally increased at the same rate. A graph with each set of weights was used to see how increasing the weights in matrix Q affected the system. The difference in roll deviation between control weights above fifty were found to be less than 0.1° , indicating a low gain in performance improvements at weights above 50. Beyond seventy the performance worsened, showing higher steady-state error than lower weights. I decided to select fifty as the weight for roll θ .

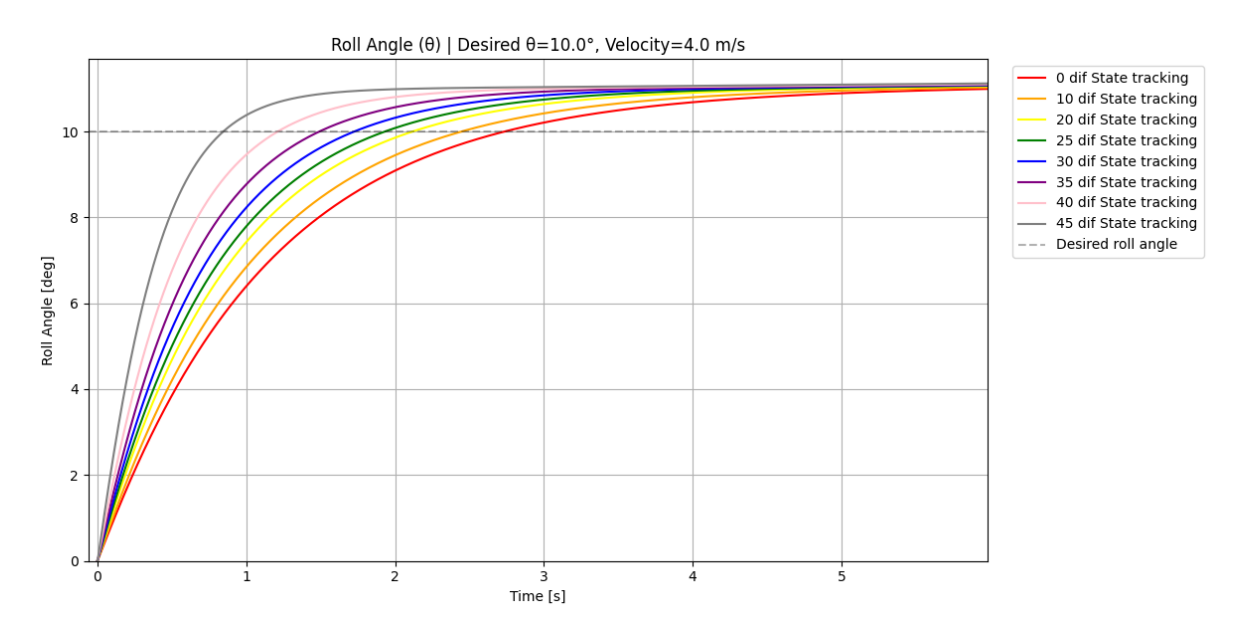


Figure 4.8: LQR different state weights

After selecting a roll weight of fifty as the baseline for further evaluation, the next parameter examined was the relative weighting between roll and roll rate. It is more critical that the roll converges to the desired value than roll rate so, the roll rate weight was decreased in intervals of five, from fifty down to one. Figure 4.8 shows the rise rate decreasing as the difference between the roll and roll rate weights increased. In other words, reducing the weight on roll rate led to faster convergence of to the desired theta. A weight value of five was selected for roll rate $\dot{\theta}$.

Based on the previous findings, the Q matrix weighted at fifty and five was evaluated with varying control input weights. Control weights increased from one to twenty five at regular intervals. This configuration was selected because maintaining the roll angle θ is considered more important than minimizing the steering effort; therefore, the steering input should be weighted lower.

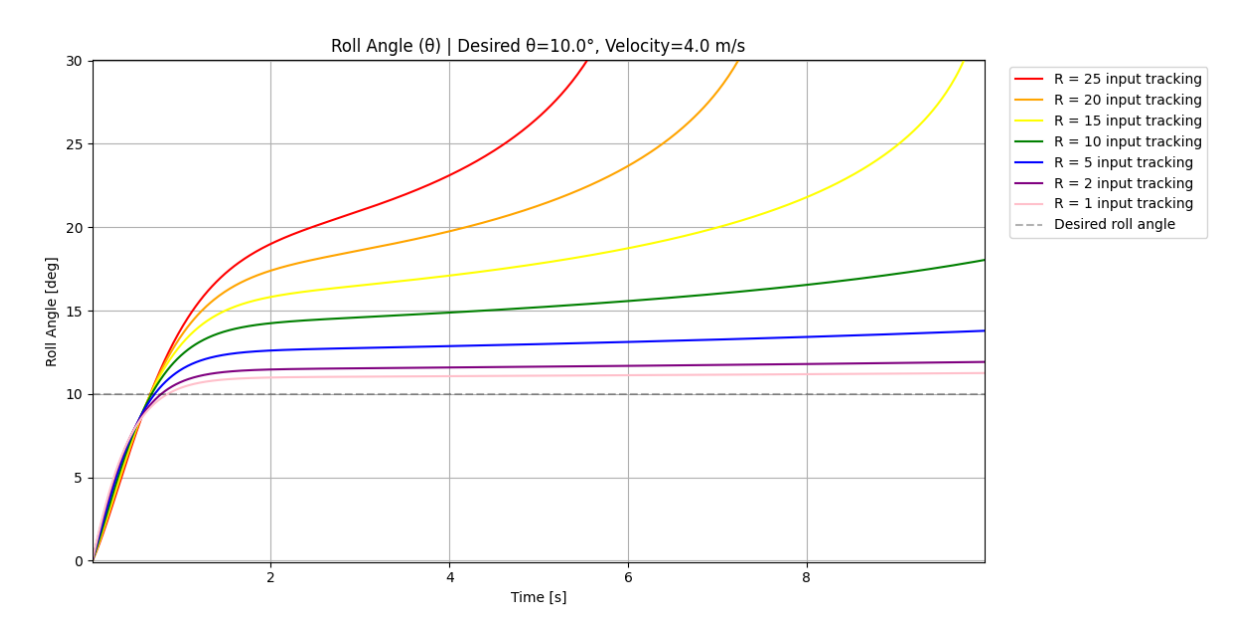


Figure 4.9: LQR different control input

Figure 4.9 showed as control input weight decreased, the steering input settled more quickly and exhibited less oscillation. Control input weights above five resulted in highly unrealistic steer angles. At a control input weight of one, the roll angle closely matched the desired value. As the control input weight increased, the steady-state roll angle deviated further from the target, reaching over 1° of steady-state error at a weight of twenty five. Based on these results, the optimal balance between reducing steering oscillations and maintaining the desired roll angle appears to be achieved with a control input weight of one. This setting provides sufficiently realistic steering inputs. The final controller weight configuration used is:

$$Q = \begin{bmatrix} 50 & 0 \\ 0 & 5 \end{bmatrix} \qquad \qquad R = \begin{bmatrix} 1 \end{bmatrix} \tag{4.7}$$

This weighting configuration resulted in a rapid convergence to the desired roll angle with minimal steady-state error. The same weighting scheme was used for both asphalt and ice conditions. Its performance was evaluated across a range of bicycle speeds and roll angles.

LQR ICE slip

Prior to testing controllers on ice, a slip detection method must be developed. In chapter 2, ice was modeled as a time-based event that triggers at time t=15 and ends at t=19. In this simplified scenario, the system was explicitly informed when ice was present. However, to create a more realistic model, ice was represented as a spatial region on the ground plane rather than a time interval. In this case, the system needed to detect when it was on an icy surface and autonomously trigger a control strategy.

To detect ice in simulation, a dictionary was created to track slip-related states and history in real time. A function was called that calculated the slip angles at each time step of the simulation. This function updated the velocities and slip coefficients at each time step. The resulting slip angle values were recorded and evaluated using a simple conditional logic structure and flag-based system to determine whether slip was occurring.

Initially, the detection logic ignores the first two seconds of simulation to allow the system to stabilize. After this period, it checked whether the slip angles exceeded the bounds of $\pm 6^{\circ}$. If they were within bounds, the system continued to the next time step and performed the same check. If a slip angle exceeded this threshold, a slip condition was detected and the corresponding flag was switched from False to True.

When the flag is set to false, PD gains of 3 were used to simulate human rider input and represent the minimal control needed to stabilize the system. These gains were stable in expected scenarios but are not sufficient to handle significant disturbances, such as slipping on ice. When the flag transitions to true, the system activated the ice controller by switching from the PD gains computed for normal riding to those computed for icy conditions. In this case, the PD gains were increased to 20. This control logic is visually represented in Figure 4.10.

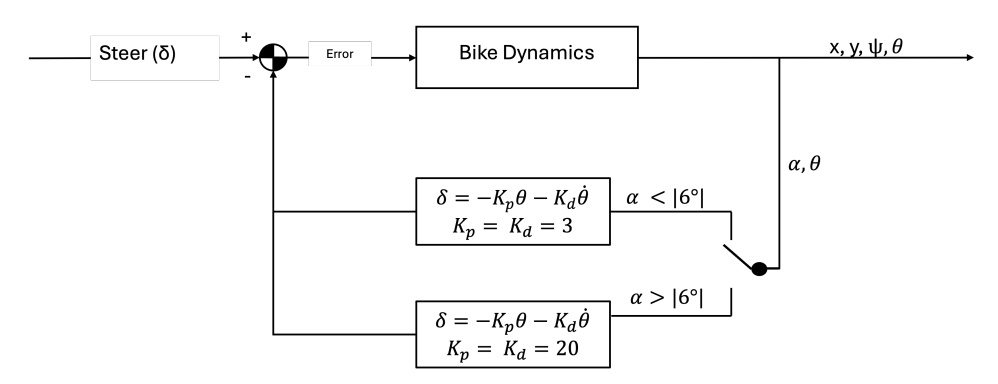


Figure 4.10: PD controller block diagram with ice-triggered gain switching

Similarly, when the LQR controller was tested the simulation started by using PD gains of 3 to simulate a normal rider. If the flag indicating ice was triggered the controller switched from PD gains 3 to the LQR controller calculated previously in this section. Figure 4.11 illustrates this control logic and the transition mechanism between PD and LQR control.

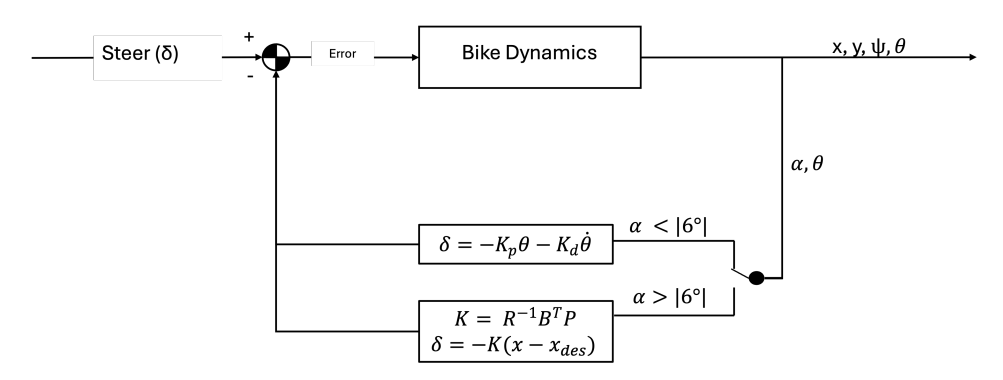


Figure 4.11: LQR controller block diagram with ice-triggered gain switching

Additionally, the current simulation time was recorded so the system knew when the slip event began. This enabled the controller to track and manage slip conditions dynamically based on surface properties during the simulation. A flowchart summarizing this process is provided in Figure 4.12.

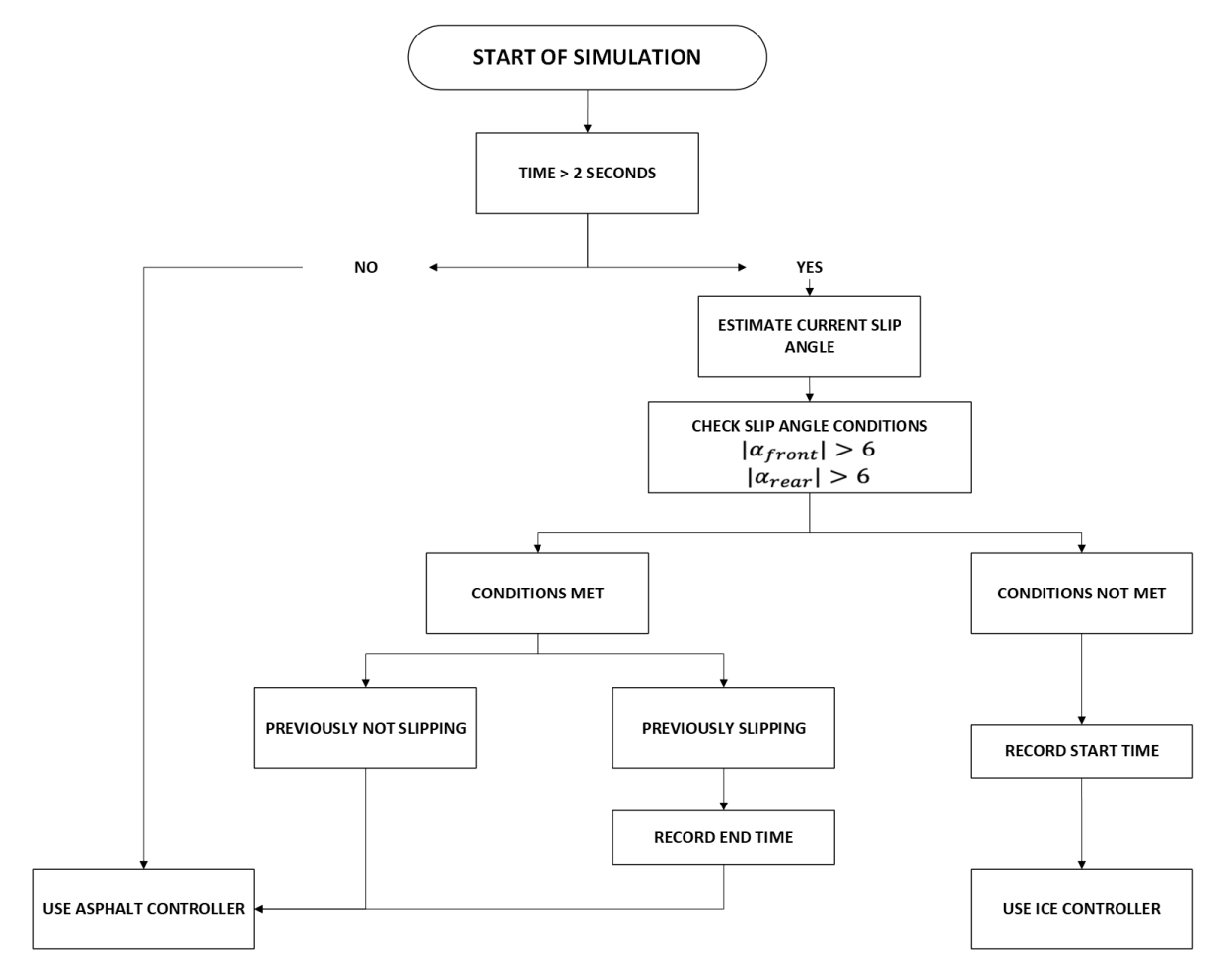


Figure 4.12: Flowchart of ice detection and controller switching logic based on simulation time and surface conditions

The controller showed that it detected ice at 15 to 19 seconds, ice was modeled on the ground plane instead of as a function of time. This was implemented using an if statement: if the time was between 15 and 19 seconds, the coefficient of slip was set to 0.1 times that of the rest of the simulation. To represent a patch of ice fixed in the ground frame N, this logic was updated to check the position coordinates. Specifically, if x is within a certain range and y is within a certain range, the coefficient of slip is set to 0.1 times the original coefficient.

$$C_{\alpha}^{W_f/W_b}(x,y) = \begin{cases} 360.0 & \text{if } \hat{\mathbf{n}}_x \in [x_{\min},x_{\max}] \text{ AND } \hat{\mathbf{n}}_y \in [y_{\min},y_{\max}] \text{ (Ice)} \\ 3600.0 & \text{otherwise (Asphalt)} \end{cases}$$

Bicycle dynamics including slip and ice were modeled and detected and the bicycle was equipped with either a PD controller or an LQR controller. The LQR weights were specifically tuned for this application. At this point the building blocks needed to evaluate the research question have been built. The next step is to evaluate the performance of these control methods in different conditions. The following chapter will examine how these controllers behave on both asphalt and ice in the hope of answering the main research question.

5

Results

This section presents the performance of controllers on bicycle model simulations. The models from Chapter 2 will be simulated and evaluated to ensure realistic dynamics. The linearized models from Chapter 3 were used to construct controllers in Chapter 4. The performance of a Proportional-Derivative (PD) controller and a Linear Quadratic Regulator (LQR) were evaluated on their ability to prevent the bicycle from falling. The simulations were conducted under two surface conditions: high-traction, asphalt, and a patch of low-traction, ice.

Several variables will be investigated including, A range of velocities within a normal riding range, as were various turn radii. The PD controller was tested at various gains to establish if any combinations successfully cross the ice patch. Finally, the results of the top performing PD and LQR were tested on an ice patch and presented. The results highlight each controller's ability to stabilize the bicycle and respond to sudden changes in traction

5.1. Models

The no-slip model, was designed to simulate basic bicycle dynamics while omitting slip and tire forces. In this model, the contact points were represented as skates to simplify the system and focus solely on the fundamental dynamics of the bicycle.

The model is built using four generalized coordinates and their four corresponding generalized speeds, along with constant parameters. A function that utilizes these states, with the equations of motion from Chapter 2, is used to solve for the accelerations and system dynamics.

The initial values used in the simulations below were listed in Table 4.1. Using these input parameters the equations of motion are calculated over time, the resulting trajectory was plotted in 5.1.

5.1. Models 32

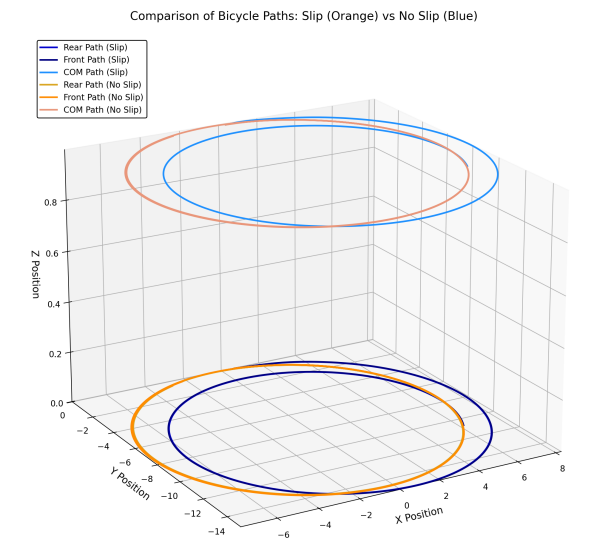


Figure 5.1: PD control at various velocities

Figure 5.1 illustrates the no-slip trajectory of the contact points and the bicycle's center of mass in orange. A basic Proportional-Derivative (PD) controller was implemented to maintain upright stability. This model omits slip and tire force dynamics, therefor the trajectory remains consistent throughout the simulation. The lack of variation in the turning radius reflects the absence of traction limitations.

Building upon the no-slip model, the slip iteration introduced lateral dynamics to incorporate a more realistic representation of bicycle behavior, shown in Figure 5.1 in blue. The contact point interactions were modeled using linear bicycle tire data, allowing for the simulation of lateral slip. This addition added a layer of complexity to the system, enabling a closer approximation to real-world dynamics. Figure 5.1 illustrates these realistic dynamics through the changing radius of turn with constant inputs.

Finally, the introduction of an icy surface into the model was expected to significantly alter the trajectory at the point where the bicycle encounters reduced traction. The impact of the ice patch is clearly illustrated below through the analysis of the bicycle's dynamic properties over the course of the simulation.

5.2. PD Controllers

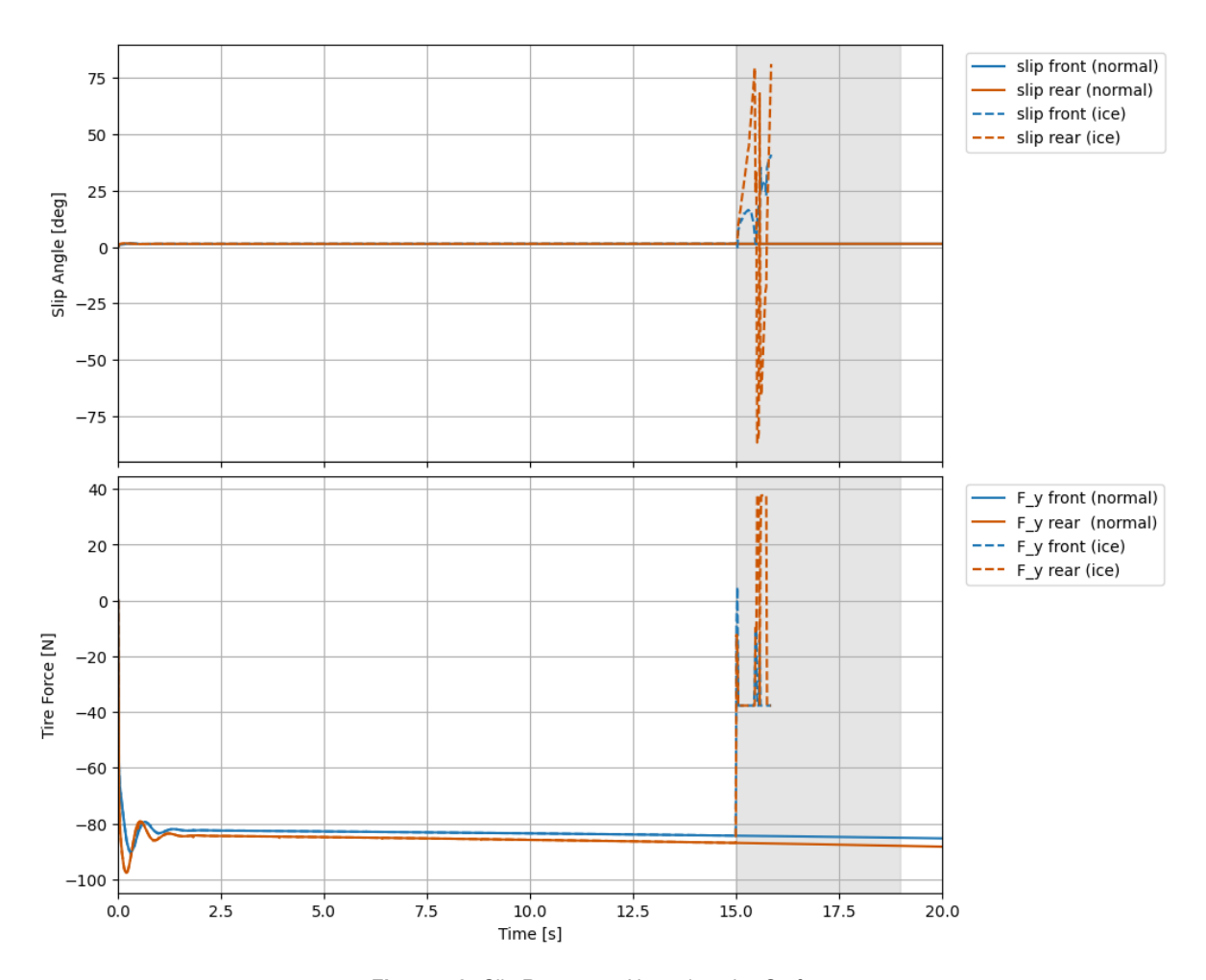


Figure 5.2: Slip Response: Normal vs. Icy Surface

Figure 5.2 demonstrates the significant impact of an ice patch on the bicycle's stability. When the front tire encounters the ice patch, indicated by the gray highlighted region, there is a sudden increase in the slip angle α as tire lateral grip. The lateral force F_y drops sharply, showing the tire's transition from a state of adhesion to sliding. This occurs because the ice surface does not have enough friction to maintain the necessary lateral forces for stability. The roll angle ϕ grows until it reaches 90°at approximately sixteen seconds, at which point the simulation terminates as the bicycle is assumed to have crashed.

In comparison, the solid lines representing riding on asphalt show stable slip angles and lateral forces, with the bicycle maintaining stability. The termination of the simulation at a roll angle of 90° corresponds to a complete loss of control, similar to what would occur in a real-world bicycle accident where the front wheel slides out. This behavior is consistent with theoretical tire models that predict a sudden reduction in lateral force when the slip angle exceeds a critical threshold on low-friction surfaces.

5.2. PD Controllers

Control weights

Different proportional-derivative (PD) control weights were tested under nominal conditions and in the presence of unexpected surface changes. It was observed that gains of 1 were insufficient to stabilize the bicycle. However, with gains increased to 3, the controller was able to stabilize the bicycle on asphalt. When the bicycle encountered a surface with a lower coefficient of friction, such as ice, a gain of 3 was no longer sufficient. Incremental increasing of the gains led to better and better results when hitting ice. Gains at 15 allowed the bicycle to remain upright while crossing a patch of ice, although this resulted in a large change in slip angle. Further increasing the gain from 15 did not significantly affect

5.2. PD Controllers 34

the system's behavior at a velocity of 4m/s.

When the same evaluation was performed at 7m/s, gains of 1 were again unable to control the system, while a gain of 3 stabilized the system on asphalt. At a gain of 15, the controller successfully allowed the bicycle to cross a patch of ice. At this higher speed, there was significantly more oscillation observed in most states. Increasing the gain to 20 reduced this oscillation significantly, leading to some damped oscillations before the system stabilized on ice. At gains of 30 and above, the oscillations reduced and stabilized within one second. For lower speeds, a gain of 15 was sufficient, but at higher speeds, gains between 20 and 30 provided enhanced stability.

Table 5.1 summarizes the performance of different proportional-derivative (PD) gains in stabilizing the bicycle on both asphalt and ice at speeds of 4 m/s and 7 m/s. The results highlight the effect of varying gain values on the system's stability under different conditions, including the challenges posed by lower friction surfaces like ice.

Gains	Stable or	1 4 m/s	Stable on 7 m/s		
Gailis	Asphalt	Ice	Asphalt	Ice	
1	×	×	✓	×	
3	✓	×	✓	×	
5	✓	×	✓	×	
10	✓	✓	✓	×	
15	✓	✓	✓	✓	
20	✓	✓	√	✓	
30	✓	✓	✓	✓	

Table 5.1: PD Gains and Stability on Asphalt and Ice Patch at 4 m/s and 7 m/s at 5° roll

Velocities

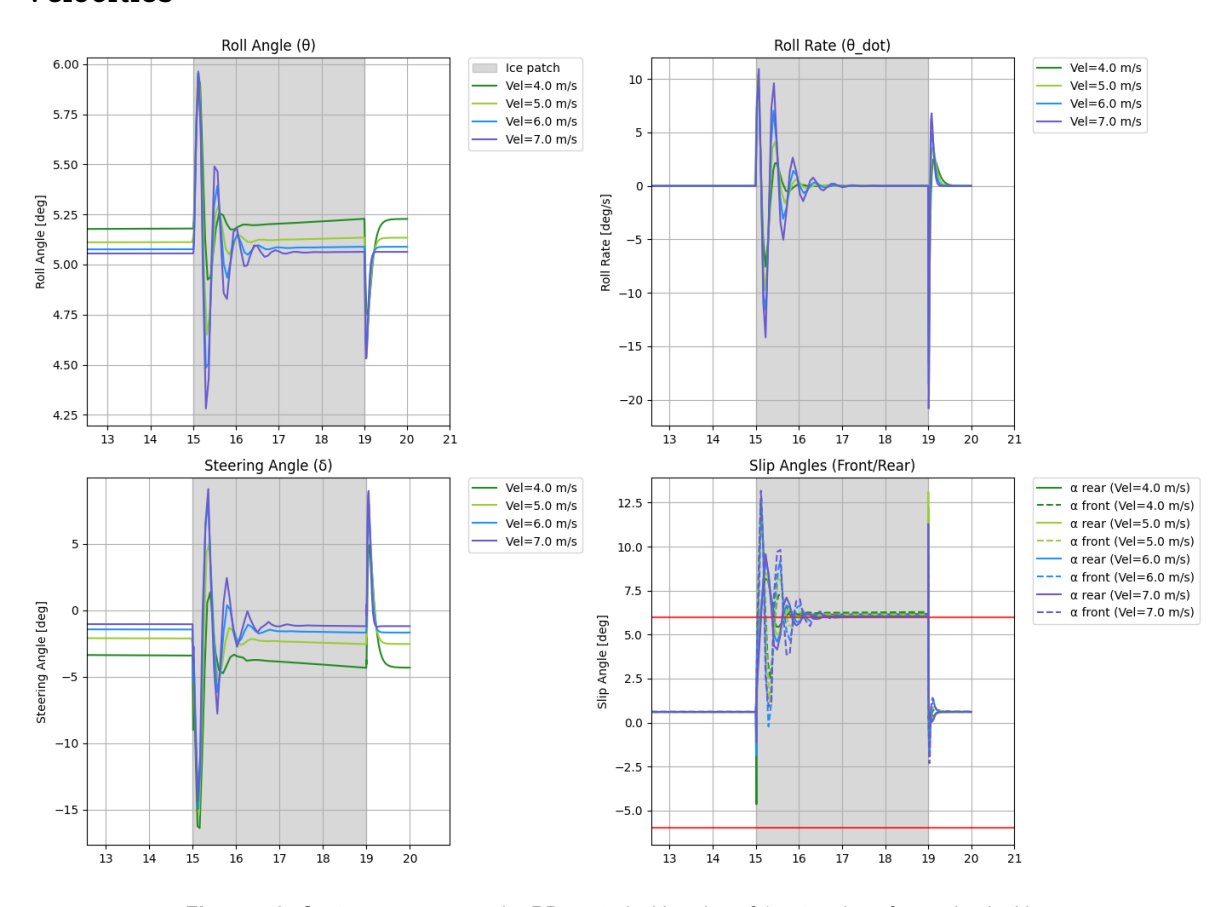


Figure 5.3: System response under PD control with gains of 15 at various forward velocities

The effect of forward velocity was evaluated using the PD gain that exhibited the most variation between 4 $\frac{m}{s}$ and 7 $\frac{m}{s}$. A gain value of 15 was selected for the PD controller and tested at bicycle speeds of 4, 5, 6, and 7 $\frac{m}{s}$, with an initial roll angle of 5° . As the velocity increased, the magnitude of roll oscillations upon encountering the ice patch also increased. Transitioning to ice and back to asphalt, the roll angle initially deviated from the desired value but stabilized after a few seconds on ice. At higher velocities, the system exhibited less aggressive oscillatory behavior in roll angle and roll rate responses. At speeds of 6 $\frac{m}{s}$ and above, roll oscillations were present throughout most of the ice patch, whereas lower velocities did not produce as much oscillation. Lower speeds also required more significant steering corrections to maintain balance. At 7 $\frac{m}{s}$, the rear slip angle oscillated between -2° and 17° , indicating a high likelihood of sliding. While these oscillations were reduced at higher gain values, they were not entirely eliminated across all tested velocities.

Target roll

When the gains were set to 15, the desired roll angle was varied from 0° to 15° in 2.5° intervals. The PD controller with a gain of 15 was able to handle roll angles less than 7.5° ; above that, the controller failed to stabilize the system across the ice patch. At 0° and 2.5° , the slip angle remained within the acceptable bound of $\pm 6^{\circ}$. At 5° , the slip angle slightly exceeded $\pm 6^{\circ}$, and at 7.5° , it reached 11° . This led to testing higher control gains to determine whether increased gains could better handle the ice patch at low roll angles and provide some level of stability at higher roll angles.

With a gain of 20, roll angles of 10° were stable enough to cross the ice patch, although they exhibited high slip angles and elevated lateral forces that would likely be difficult to achieve in a real-world scenario. Roll angles less than 10° crossed the ice patch with less oscillation compared to a gain of 15. Further increasing the controller gains to 30 reduced the slip angle on ice at a 5° roll to approximately 6° , and brought the slip at 7.5° under 10° . A roll angle of 12.5° was able to complete the ice patch but with extreme slip angle values, likely causing sliding.

Desired Roll (°)	Stable on 4 m/s		Stable on 7 m/s	
Desired Roll ()	Gain 15	Gain 20	Gain 15	Gain 20
0	✓	✓	✓	✓
2.5	✓	✓	✓	✓
5	✓	✓	✓	√
7.5	✓	✓	✓	√
10	×	✓	×	×
12.5	×	×	×	×
15	×	×	×	×

Table 5.2: PD stability ice patch at 4 m/s and 7 m/s at various roll angles

Table 5.2 summarizes the stability of the PD controller when subjected to increasing desired roll angles at 4 m/s and 7 m/s, using control gains of 15 and 20. The results indicate that gains of 15 are sufficient to maintain stability up to a roll angle of 7.5°, while gains of 20 extend this threshold to 10° under 4 m/s conditions. However, at higher speeds, even gain 20 is unable to maintain stability beyond 7.5°. This highlights the limitations of PD control for large roll commands, particularly on low-friction surfaces.

These results suggest that increasing the PD gains improves the controller's ability to handle the ice patch; however, to reliably maintain roll angles above 7.5° , a different control approach is likely required. The next section discusses the results of using Linear Quadratic Control in similar situations.

5.3. Linear Quadratic Regulator Control on Asphalt

Velocities

Using the weights defined in 4.7, the controller's performance was evaluated at various velocity intervals on asphalt and ice patches. The controller was tested at speeds of 4, 5, 6, and $7 \, \text{m/s}$ on asphalt [24].

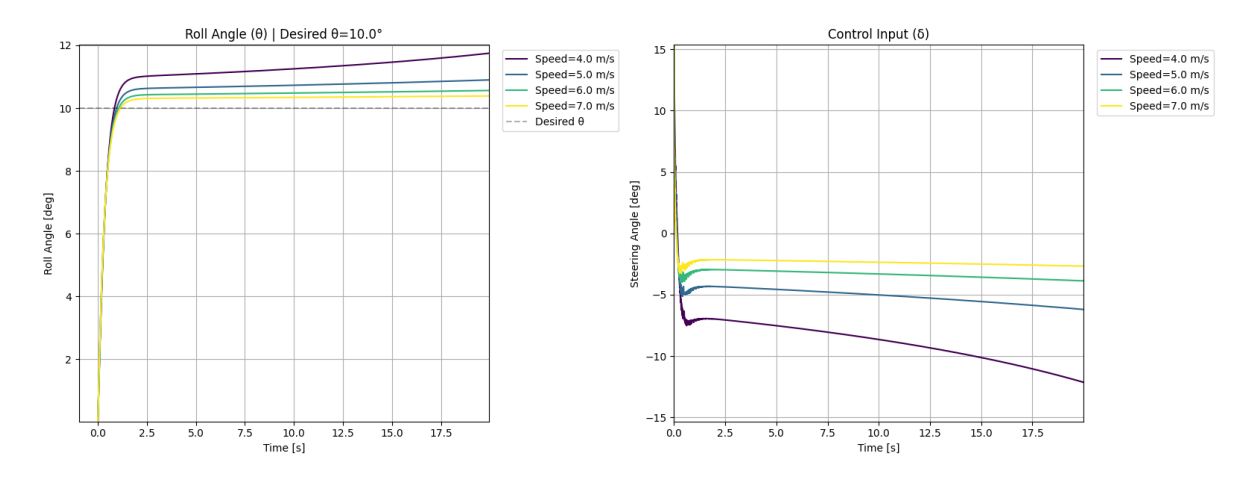


Figure 5.4: LQR asphalt performance across various speeds

The results indicated that at lower speeds, there is a greater steady-state error in roll; however, this error remains relatively small. At $4\,\mathrm{m/s}$, the roll deviation ranged from 1 to 2° , whereas at $7\,\mathrm{m/s}$, the error remained below 1° from the desired roll angle.

As shown in Figure 5.4 at higher speeds less steering input was required to achieve the same roll angle. The steering input for all evaluated speeds stabilized within approximately the same time frame. Ultimately, while minor deviations were observed due to changes in speed, the overall control performance remained relatively consistent and effective across the tested velocity range.

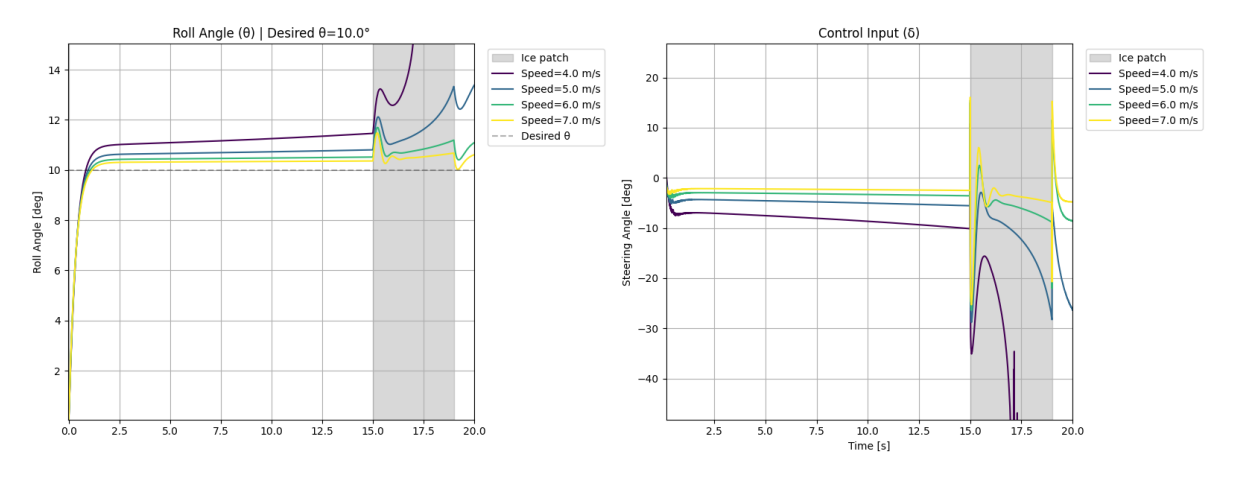


Figure 5.5: LQR ice patch performance across various speeds

The same controller was evaluated under the presence of an ice patch introduced between 15 and 19 seconds, across the range of speeds, 4 to $7 \mathrm{m/s}$. Figure 5.5 illustrates the change in roll response when the controller encounters the ice patch. The results indicate that the controller is unable to maintain the desired roll angle of 10° at $4 \mathrm{m/s}$ under these low-friction conditions.

Based on the previous results, further analysis was conducted to determine whether the controller could maintain sufficient stability across an ice patch when tracking a reduced roll angle of 5° over the full range of velocities.

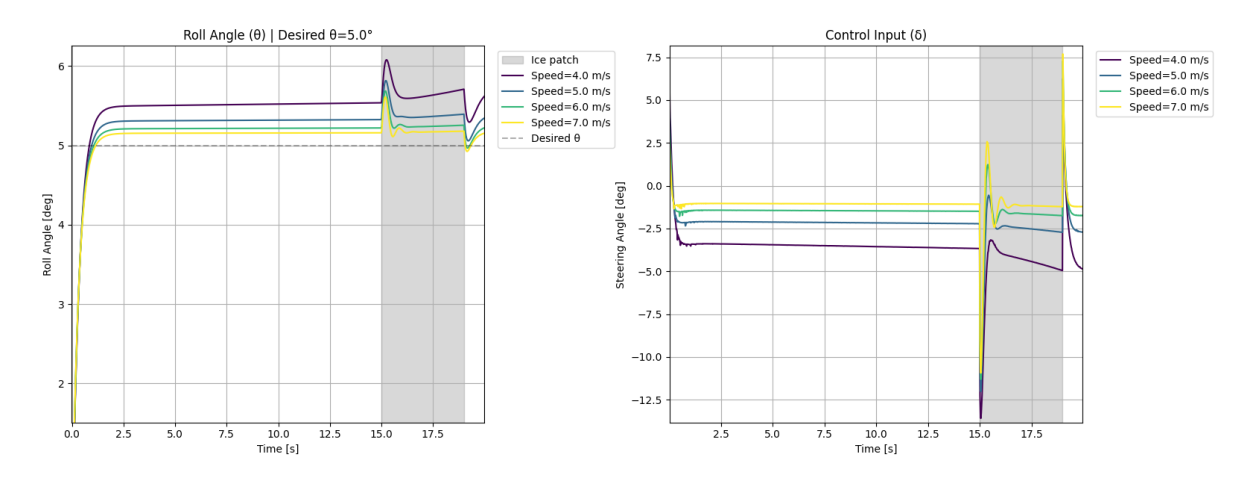


Figure 5.6: LQR ice patch performance across various speeds at 5 degree roll

Figure 5.6 demonstrates that the controller was able to maintain a roll angle of 5° across all tested speeds. The following section presents an investigation into the controller's performance over a range of desired roll angles.

Target roll

Similar to Section 5.3, the LQR controller is tested at roll angles ranging from 0° to 30° in 2.5° increments. This evaluation was conducted to assess the controller's ability to achieve the desired roll response up to the point of maximum normal riding, $30^\circ[25]$. The nonlinear dynamics model is expected to remain valid up to this roll angle. To evaluate controller performance within this limit, a range of desired roll angles were tested at $4\mathrm{m/s}$ and $7\mathrm{m/s}$, representing the lower and upper bounds of the velocity range, respectively.

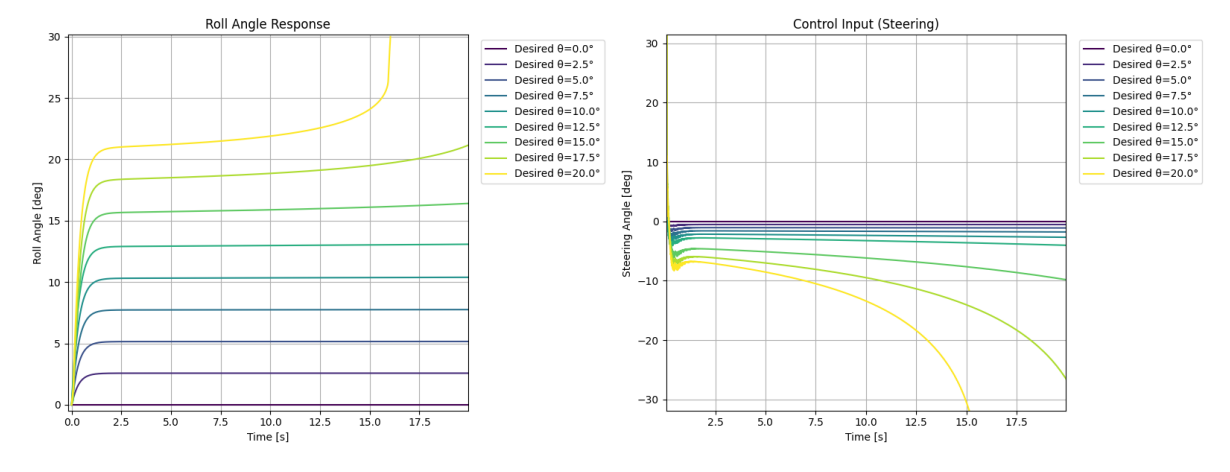


Figure 5.7: LQR performance across various roll angles at $7 \mathrm{m}/\mathrm{s}$

At $7 {\rm m/s}$ the controller performs reliably only up to approximately 15° . From 0° to 15° the controller stabilizes at the desired roll. Beginning at 17.5° , deviations from the desired roll response become apparent, with increasing severity at higher roll angles. By 25° , the deviation is significant enough to render the control response unrealistic, therefore Figure 5.7 will contain roll angles 0° to 20° . Similar behavior is observed in the roll rate response beyond 15° , where large spikes occur after the system reaches 0° , indicating instability at higher roll angles.

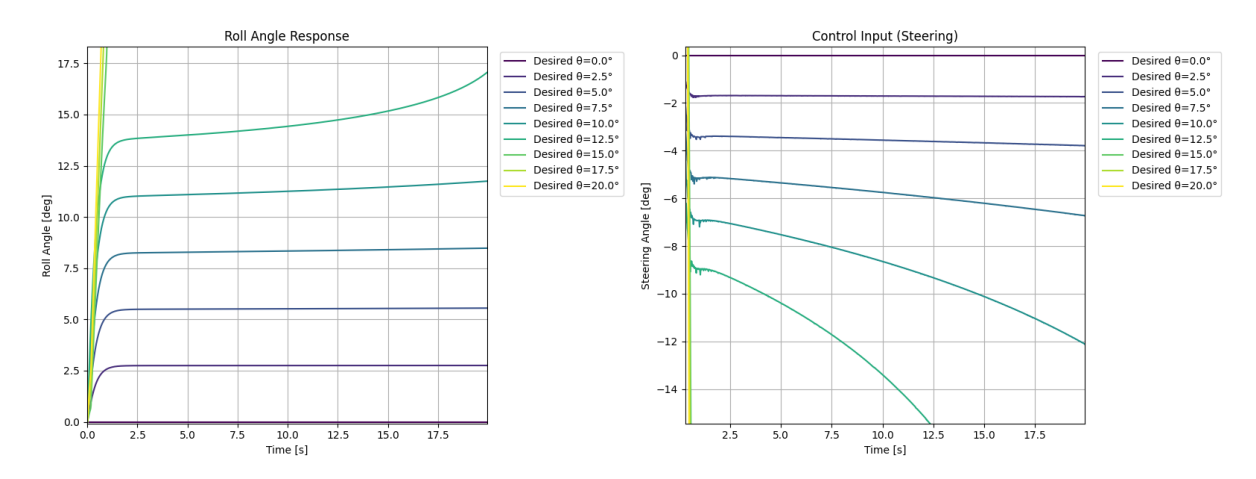


Figure 5.8: LQR performance across various roll angles at $4 \mathrm{m/s}$

At $4 \mathrm{m/s}$, the controller maintains reliable performance only up to approximately 12.5°. As shown in Figure 5.8, attempting to track roll angles beyond this threshold results in increasing roll deviation, eventually reaching the system's roll limit of 30° . These results indicate that, at lower speeds, the effective control limit is approximately 12.5° .

Unexpected surface variations, such as the introduction of ice, significantly affect the range of roll angles the bicycle system can stably maintain.

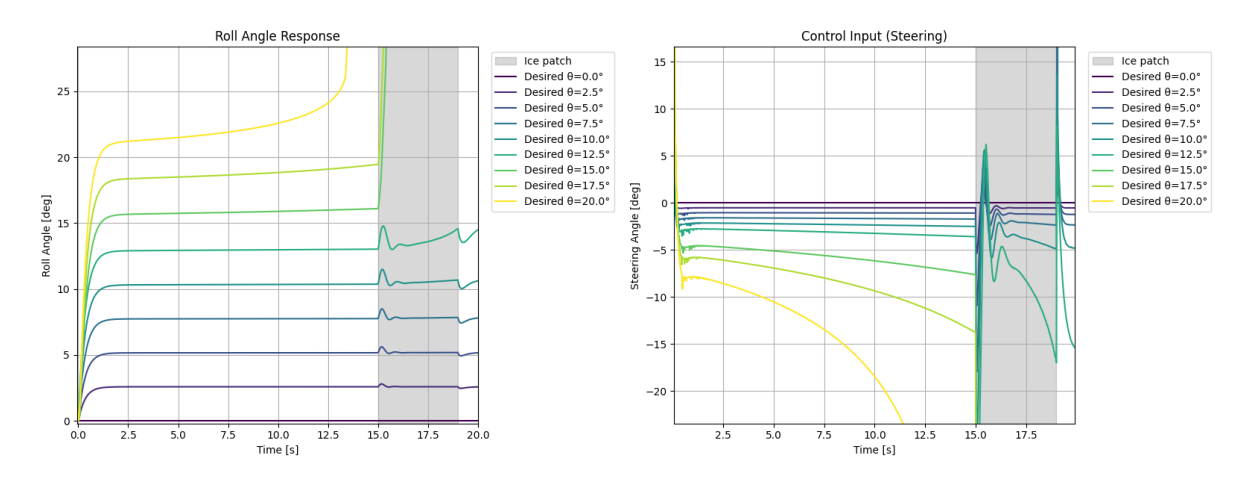


Figure 5.9: LQR ice patch performance across various roll angles at $7 \mathrm{m/s}$

Figure 5.10 shows at $7 \mathrm{m/s}$, the presence of ice causes instability at roll angles exceeding 12.5°, whereas under consistent asphalt conditions, the system remains stable up to approximately 17.5°.

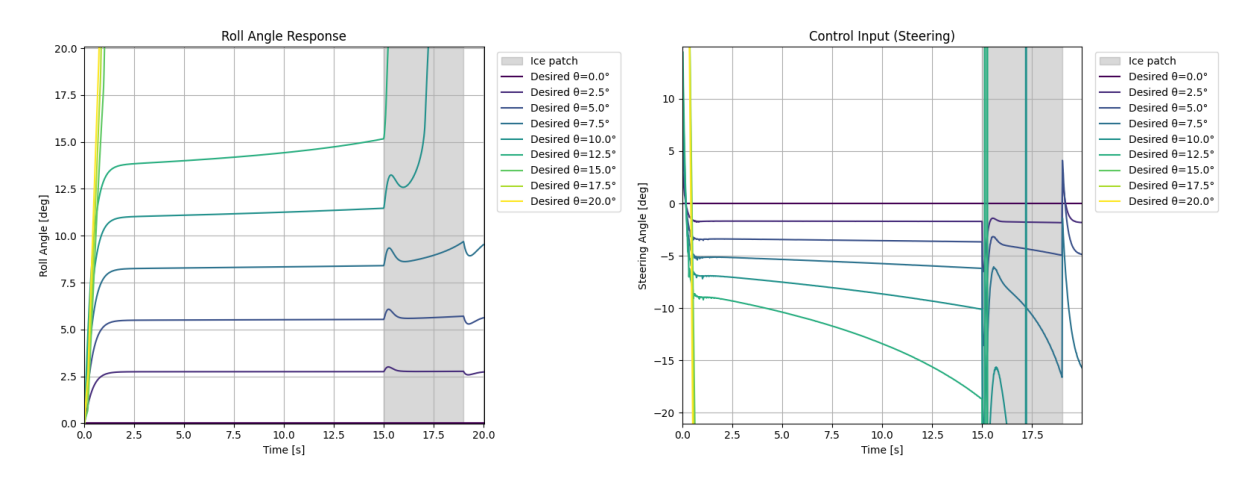


Figure 5.10: LQR ice patch performance across various roll angles at $4\mathrm{m}/\mathrm{s}$

When an ice patch was introduced, the range of roll angles that the controller can successfully maintain at $4\mathrm{m/s}$ is reduced. At a roll angle of 7.5° , the system remains sufficiently stable to complete the simulation. For roll angles exceeding this threshold, the system becomes unstable with loss of stability occurring on either the ice patch or the asphalt, depending on the specific roll angle.

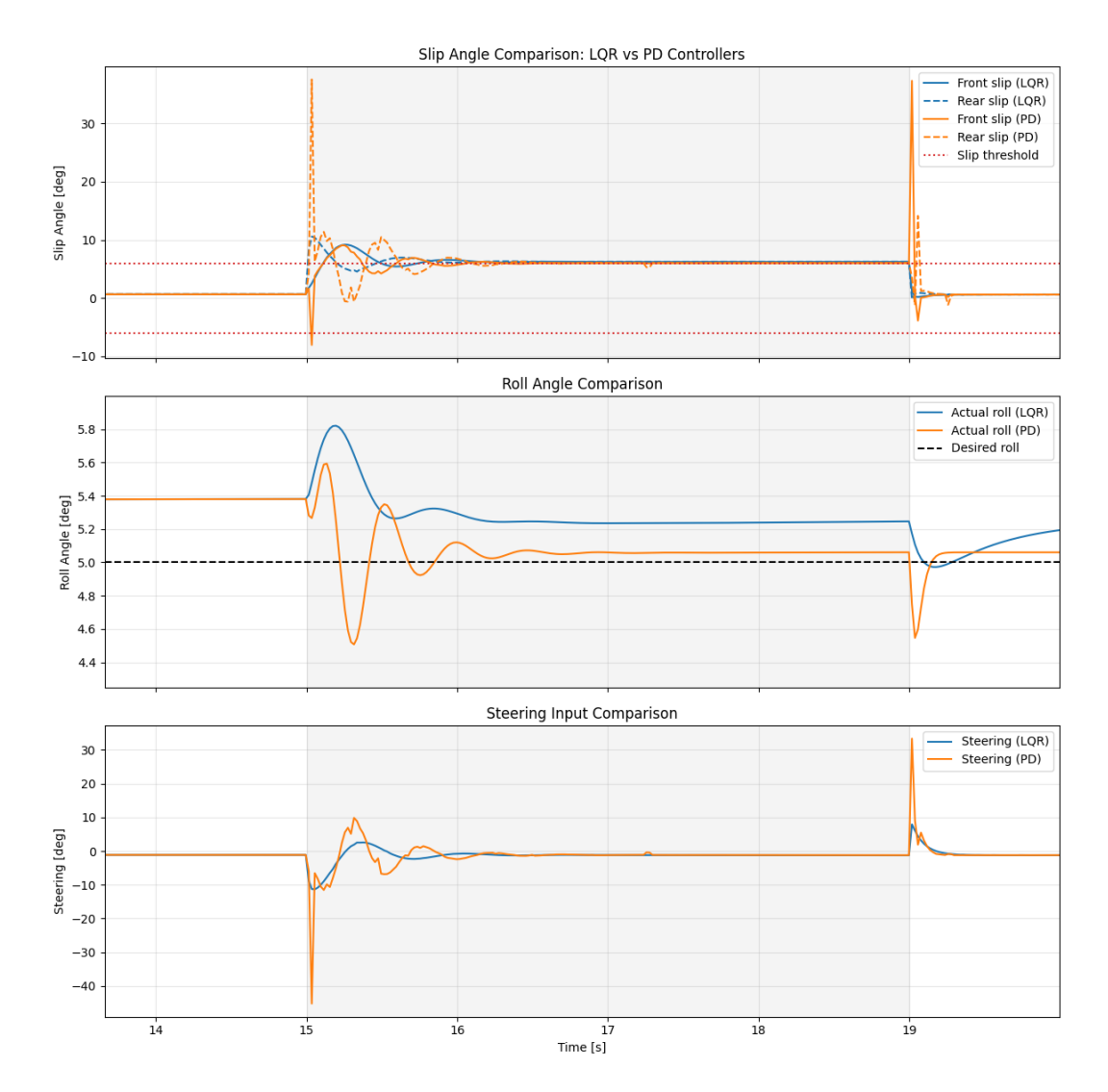


Figure 5.11: Comparison of PD and LQR on ice patch

The PD controller with gains of 3 performs well on asphalt and is used to mimic the bicycle rider's control input. However, when the PD controller with gains of 3 encounters ice, the bicycle falls over almost immediately. The PD control with gains 3 will be used initially to resemble a human rider, when ice is detected this will be changed to either a high gains PD or LQR controller. Figure 5.11 shows the effects of using either a PD controller with higher gains (20) or an LQR controller with weights defined in Section 4.7 to cross the ice patch.

The slip detector triggered the stronger control strategy, ultimately allowing the bicycle to complete the simulation and remain stable on ice. This was performed at a speed of 7 m/s and an initial roll angle of 5°. The LQR controller exhibited less oscillation in roll, steer, and slip angle after encountering the ice patch compared to the high-gain PD controller. However, the settling time was approximately the same for both controllers.

Overall, the controller demonstrated reliable performance across a range of roll angles and speeds under nominal conditions. However, its effectiveness was reduced in the presence of ice, particularly at lower speeds and higher roll angles. These limitations highlight the sensitivity of the system to surface friction. The following chapter discusses the implications of these results and explores potential improvements to enhance system stability under varying conditions.

6

Discussion

This chapter analyzes and interprets the findings presented in Chapter 5. The previous chapter detailed simulation results under various conditions, including no-slip, slip, and slipping on ice scenarios. It also presented the performance of the PD controller on asphalt, evaluated across different gain values, velocities, and turn radii, as well as the LQR controller's performance under varying velocities and turning radii.

In this chapter, these results are examined to assess whether the controllers are capable of stabilizing the bicycle, and if so, which controller performs most effectively. Particular attention is given to evaluating the potential of these control strategies to enhance stability when the bicycle encounters an ice patch.

While the simulations provide valuable information, this chapter also outlines directions for future work, including the real-world implementation of the simulated controllers. This includes exploring methods for detecting slip angle using sensors that can reasonably be integrated onto a bicycle.

6.1. Models

The first model simulated contained the no slip constraint. This model was intended to provide a base-line of the bicycle dynamics. The results in Figure 5.1 show the no slip model completing steady state circles and maintaining an upright center of mass. Modeling bicycle dynamics under the assumption of no slip provided a useful baseline for validating the simulation environment and confirming that fundamental bicycle behavior could be accurately modeled in Python.

The next model simulated contained lateral slip, this was intended to more closely align with reality. I expected the model to circle but with some lateral gain or loss. The overall motion should result in circling but with deviation. Figure 5.1 showed some deviation in the trajectory, leading me to conclude the model contains slip. Incorporating tire slip into the model revealed observable changes in the bicycle's trajectory, primarily due to lateral deviations caused by slipping. These differences highlight the importance of including tire dynamics for a more realistic representation of vehicle behavior.

When ice was incorporated into the model, I expected to see a sudden jolt in all generalized coordinates. Initially, I modeled the ice over a specific time period, from 15 to 19 seconds, so I could evaluate whether it had an effect on the dynamics. Figure 5.2 showed that the model with ice experienced an abrupt change in yaw, roll, slip angle, and lateral force at 15 seconds. The bicycle fell over shortly after 15 seconds, ending the simulation. The same variables were plotted without an ice patch in Figure 5.2 for comparison. This figure showed the parameters remaining relatively constant throughout the simulation and demonstrated that the simulation ran for the full 20-second duration. The differences between these graphs led me to conclude that modeling ice as a reduced coefficient of slip is a valid way to simulate "ice" in the model.

For the purposes of this study, modeling slip and ice were essential to accurately investigate how a bicycle behaves under challenging surface conditions. These are key components for evaluating the

potential for adaptive traction control strategies. Validating the model by starting with a no-slip case, then incorporating slip, and finally simulating slip on ice, systematically built a model suitable for control analysis.

6.2. PD performance

The PD controller was tested under various gains, operating velocities and turn radii. These results presented will be evaluated to determine if it is a viable controller for maintaining stability on ice.

The results of the PD controller showed variability in system stability depending on both control gains and surface conditions. When analyzing the controller's performance at different gain values, the results demonstrated that a gain of 3 or higher was sufficient to stabilize the system on asphalt at both 4 m/s and 7 m/s. Therefore, a gain of 3 was considered the minimum amount of control needed to keep the bicycle moving along the desired trajectory. This value is used as a baseline for control, as it represents the minimal input required to achieve stable performance on asphalt.

The controller's performance when encountering an ice patch revealed certain limitations. At 7 m/s, although the system remained upright with PD gains between 20 and 30, significant oscillations were observed. These oscillations suggest potential stability concerns at higher velocities, though the bicycle eventually regained balance. At 4 m/s, the system was unable to stabilize the bicycle on ice with gains below 15. From these results, it was concluded that a PD gain of 20 is sufficient to prevent the bicycle from falling when encountering an ice patch at any operating velocity. However, oscillations lasting approximately 2 seconds were still present, indicating only moderate stability. While the addition of a PD controller improved performance compared to having no control, the results suggest that alternative control strategies could have more stability.

Next the PD controller was evaluated based on turn radius, this was done by having the controller maintain different desired roll angles. The PD controller struggled with maintaining higher roll angles on ice, as evidenced by the increasing slip angle at roll angles greater than 7.5°. These findings suggest that while the PD controller was reasonably stable at low roll angles, but beyond 7.5°the controller fails to complete the ice patch. Performance on surfaces with higher traction is good up to 12.5°, but it was less effective at handling transitions to lower-traction surfaces.

Additionally, the results show that increased control gains improve system performance, but only up to a certain threshold. Beyond that, the system experiences instability or excessive oscillations, limiting the PD controller under extreme conditions. The PD controller is a possible solution for stable, moderate-speed operation on high-traction surfaces but lacks the robustness needed for extreme conditions, such as icy terrain and high roll angles. Later this section will explore how PD gains for ice will be used to enhance performance across varying surface conditions.

6.3. LQR performance

Now we have examined the abilities and limitations of PD control, LQR control will be evaluated at the same operating velocities and turn radii. The goal of this section is to determine the limitations and abilities of LQR control.

Bicycles are more stable at higher speeds, therefor it is expected that higher operating velocities would result in higher stability. The performance of the LQR controller at velocities 4 to 7 m/s on asphalt demonstrated a clear advantage in stabilizing the bicycle with small roll deviation. At 4 m/s, the LQR controller introduced a slight deviation of 1 to 2 degrees, while at higher speeds, the deviation reduced to less than 1 degree, suggesting better performance at higher velocities. Compared to PD the LQR controller showed more consistent results across varying speeds.

On asphalt, the LQR-controlled system was able to stabilize up to a roll angle of 17.5°, which is better than the performance achieved with PD control. Under icy surface conditions, the LQR controller demonstrated reduced effectiveness at lower operating speeds. At 4 m/s on ice, the system struggled to maintain a roll angle of 10°. At 7 m/s, the controller performed more effectively, maintaining stability up to a roll angle of 12.5° on ice. These results indicate that velocity and roll angle significantly influence the controller's ability to successfully cross an ice patch.

Although the LQR controller is expected to function across the full range of velocities, its performance on ice suggests it should be considered limited to a roll angle of 10°. This threshold is higher than that of the PD controller and is achieved with less oscillation across the ice patch. Overall, the LQR controller demonstrates better performance and a broader operable range compared to PD control. In the next section, the LQR controller will be evaluated as part of a hybrid control strategy to enable a direct performance comparison with PD control.

The LQR controller demonstrated clear strengths in managing the dynamic response to surface changes, with improved performance at higher speeds, which is consistent with the expected behavior of linear controllers. However, it was still limited in handling higher roll angles on ice, with stability breaking down around 12.5°at 4 m/s. While the LQR controller can handle moderate roll angles and is effective under controlled conditions, it is still prone to instability in extreme situations or when encountering unexpected changes like ice patches at high roll and low speeds.

6.4. Comparison of PD and LQR

When comparing the PD and LQR controllers, the LQR controller showed superior performance in stabilizing the bicycle at higher speeds, with less deviation from the desired roll angle and more consistent response. The PD controller, while effective at low speeds, became less stable under higher-speed conditions especially when dealing with ice patches. The LQR controller provided a smoother response and better control at both lower and higher speeds, despite the surface change. Both controllers displayed limitations under extreme roll angles or in low-traction conditions. The LQR controller exhibiting the best performance up to roll angles of approximately 15°at 7 m/s. Beyond 17.5°, the system became unstable.

The simulation model was able to detect slip using calculable variables derived from the bicycle states. By using velocity components and appropriate reference frames, slip could be calculated and evaluated against predefined boundaries. The method described in Chapter 2 successfully detected instances of slip both at expected times and scenarios where ice was simulated as a contact patch on the ground.

The initial control of the bicycle was assumed to be equivalent to a PD controller with gains of 3. These gains were sufficient for completing several maneuvers on asphalt but were ineffective on ice, reflecting the behavior of a cyclist unexpectedly encountering a low-friction surface. Adaptive control was implemented by detecting slip and increasing the PD gains to 20 in an effort to improve performance on ice. The same slip detection method was used to switch from a PD controller with gains of 3 to the LQR controller. These adaptive strategies were compared in Figure 5.11 to evaluate their relative performance in maintaining stability.

6.5. Research Outcome

Overall, the LQR controller exhibited less oscillation than the PD controller but had approximately the same settling time. For the purposes of developing a controller to prevent falling on ice, both approaches could be considered viable. Reduced oscillation leads to smoother and more predictable behavior, which is critical for maintaining rider balance and comfort during sudden changes in surface conditions. Figure 5.11 tested the controllers at 7 m/s maintaining a roll angle of 5°, when the roll angle is increased or the velocity is decreased the difference in controllers is amplified. LQR has a larger performance range than PD and has less oscillation making it the better choice of controller for maintaining stability across ice.

This study demonstrated that simulation-based methods were effective for designing and evaluating adaptive traction control systems for bicycles. By modeling slip dynamics and simulating different surface conditions, including ice, the system was able to detect slip events and respond accordingly. Testing both PD and LQR controllers in simulation allowed for a systematic comparison of their ability and limitations when maintaining stability with abrupt surface changes. These findings suggest that simulations provide a practical foundation for developing real-time control strategies aimed at reducing single cyclist crashes due to traction loss.

Implementing these controllers in simulation on an ice patch allowed for a direct performance comparison. While the PD controller with gains of 3 effectively mimics a cyclist on asphalt, it failed to success-

fully traverse the ice patch. This emphasizes the need for adaptive control strategies in variable terrain environments. Introducing a control aid triggered by slip detection enabled the bicycle to cross the icy surface. Increasing the PD gains to 20 offered improved performance on ice, allowing the system to remain upright; however, this came at the cost of increased oscillations in the roll and steer angles. In contrast, the LQR controller not only stabilized the bicycle but also exhibited smoother responses with reduced oscillatory behavior. The slip detection mechanism proved effective in identifying unstable conditions and triggering the stronger control strategy in time. Although both the high-gain PD and LQR controllers achieved similar settling times, the LQR offered better overall performance in terms of stability and control. These findings highlight the advantages of model-based control approaches like LQR in dynamically challenging scenarios, particularly when coupled with real-time slip detection.

The improved stability and reduced oscillations observed with the adaptive LQR controller are likely due to the fundamental design differences between LQR and PD control strategies. LQR minimizes a cost function that accounts for state error and control effort producing smoother, more balanced responses. PD control relies on error and its derivative, which can lead to oscillations, especially in nonlinear systems. Furthermore, the adaptive nature of the LQR in this study enabled the controller to adjust its gains in response to system changes, enhancing robustness and performance. These findings are consistent with those of [26], who reported better results when integrating LQR with PID control, than PID with PID. This suggests that LQR is advantageous in systems requiring stable control under variable conditions.

The benefits of adaptive LQR control have both theoretical and practical significance. From a theoretical perspective, the results support the idea that optimal control strategies provide better performance by accounting for the full dynamics of the system. This supports the use of model based approaches instead of simpler feedback methods in complex control scenarios, such as a bicycle encountering ice. The observed reduction in oscillatory behavior and the improved stability may contribute to increased safety for cyclists when facing unexpected changes in road surface conditions.

The aim of this thesis was to investigate how simulation-based methods can be used to design adaptive traction control systems for riding on normal and icy road surfaces to prevent single-cyclist crashes. Simulations, progressing from no-slip to slip, and finally to slip on ice, provided the foundation for testing controllers aimed at preventing falls on ice. A comparison of these controllers offered insights into which one yields the best performance on ice, making LQR the most suitable choice for fall prevention.

6.6. Limitation and Future work

While the results of both controllers suggest potential for stabilizing a bicycle, the performance under extreme conditions like ice patches or high-speed transitions could be further improved. Future work could explore more robust control strategies, such as model predictive control (MPC), to handle sudden variations in surface conditions. Additionally, further experimental validation, perhaps involving real-world testing on various surfaces, would be necessary to validate the control strategies.

A key challenge in transitioning from simulation to real-world implementation is the reliable measurement of slip. While the current model performs well in simulation, its effectiveness in practice depends on accurately detecting slip. The controller is designed to activate slip control when a slip angle outside the bounds of 6°occurs. In simulation, this slip angle is easily computed from known longitudinal and lateral velocity components, as described in Section 2.4. However, standard bicycles typically lack the necessary sensors to provide this information. That said, e-bikes and other bicycles can be equipped with compact sensors capable of measuring velocities or angular velocities, making real-world implementation feasible.

IMUs can be employed to measure longitudinal and lateral acceleration, as well as yaw rate [27]. Motor encoders can be used to calculate steering angles. Using this data, kinematic-based or vehicle-based models can estimate the slip angle. Using a simple bicycle model, IMU data and the steer encoder it should be possible to detect slip in real life. Unlike in simulation where everything is perfectly estimated, performing integration on sensor data with noise can cause drift over time, as does integrating accelerations to get velocity.

Further investigation into the costs, sensor size, and weight of the different methods should be con-

ducted to determine the most suitable option. These factors are important in lightweight, consumer grade bicycles. On the other hand, simplified setups using minimal sensors could reduce these burdens but may limit detection accuracy. Understanding these trade-offs is necessary to ensure slip detection is technically feasible and practical in real-world scenarios.

While the theoretical model and simulation results show promise, the real-world implementation introduces several challenges, particularly in sensor selection, noise handling, and computational robustness. Addressing these challenges through thoughtful design, filtering techniques, and sensor selection will be key to successfully translating this approach from simulation to practice.

abla

Conclusion

The aim of this thesis was to investigate *How surface conditions affect the dynamic stability of a bicycle and how can control strategies be used to stabilize the bicycle on normal and icy terrain to prevent single-cyclist crashes?* This objective was addressed by dividing the work into sub tasks, including the development of a bicycle model that incorporated slip and realistic dynamics when encountering an ice patch. The study then explored the use of different PD gains and LQR weights to prevent loss of control on ice, using a slip detection method.

The construction of a bicycle model without slip demonstrated that simplified bicycle dynamics could be effectively modeled in Python. A deeper understanding of slip and lateral forces enabled the inclusion of more realistic tire force modeling, transitioning the system from a no slip to a slip condition. Finally, varying the coefficient of friction over a specific time interval, and later linking it to a location in the ground frame, successfully simulated an ice patch. Observing the bicycle fall upon contacting the "ice" confirmed that the model was able to replicate the dynamics of a bicycle encountering a sudden loss of traction.

A basic PD controller was implemented to stabilize the system in upright motion, both in straight line travel and during steady turning. An investigation was then carried out into how increasing the PD gains affected system stability on asphalt and ice across a range of velocities and roll angles. The same test conditions were applied to an LQR controller, with different weight matrices tested through systematic trial and error to determine the most effective LQR configuration for traction control on ice.

The PD controller demonstrated stable roll control up to 8°across all speeds. At roll angles higher than 10°, stability was maintained only within the 5 to 7 m/s speed range. The performance at 4 m/s held a maximum stable roll angle of 7.5°, while at 7 m/s, 10°was maintained. The PD controller experienced a key limitation at higher speeds during surface transition: there was a momentary jump in steer control when going from ice to asphalt. This indicated that PD was better suited for applications with less than 8°roll at all speeds, and within 10°at speeds between 5 and 7 m/s.

The adaptive LQR controller demonstrated reduced oscillatory behavior and improved overall system stability compared to the adaptive PD controller. These results support the conclusion that lateral traction control was achieved through steering adjustments using relatively simple model based control strategies for bicycles.

The LQR controller maintained stability within defined speed and roll angle limits. It held up to 12.5°at 7 m/s and 7.5°at 4 m/s. The controller demonstrated better performance at higher speeds, which follows the same logic as when a human is controlling a bicycle. Across mid to high speed ranges (5 m/s to 7 m/s), it reliably sustained 10°. Over a broader operating velocity range, stability was maintained up to 8°. These results suggest that for applications requiring larger roll angles, velocity should be limited to speeds above 5 m/s. Unlike PD, LQR could maintain stability at 8°at all tested speeds.

Comparing PD and LQR controllers demonstrated that PD provided adequate stability for moderate roll angles, sustaining 7.5° across all speeds and up to 10° within a limited range (5 to 7 m/s). However, its

performance during transition phases was not as smooth as LQR. In contrast, LQR controllers delivered superior robustness, maintaining stability at larger roll angles up to 12.5° at 7 m/s and could sustain 8° across all speeds. The LQR controller exhibited smoother transitions from low to high traction and had settling times 1 second faster than PD, outperforming PD in adaptability and precision. While PD control remains a viable option for simpler, low-speed scenarios with conservative lean angles, LQR offers superior performance in applications like bicycles, where varying terrain demands greater maneuverability and adaptability.

This analysis was limited to simulation based testing under specific and predetermined conditions. As such, performance in real world scenarios may differ, and the slip detection method would require further development to be viable for practical applications. Future research could include implementation of the control schemes on physical hardware, refinement of the slip detection approach, or the development of more advanced and robust control techniques.

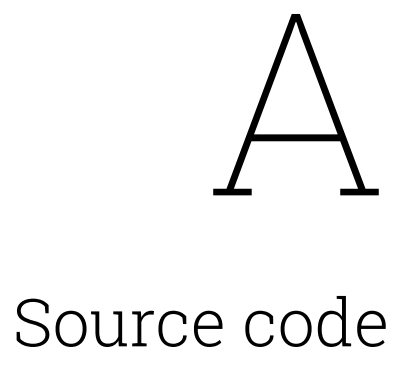
References

- [1] N. Clayton, *The Birth of the Bicycle*. Great Britain: Amberley Publishing Limited, 2016.
- [2] Euro NCAP, "Developments in car crash safety and comparisons between results from euro ncap tests and real-world crashes," European New Car Assessment Programme (Euro NCAP), Tech. Rep., 2020. [Online]. Available: https://cdn.euroncap.com/media/53186/developments-in-car-crash-safety-and-comparisons-between-results-from-euro-ncap-tests-and-real-world-crashes.pdf.
- [3] P. Schepers and K. Wolt, "Single bicycle crash types and characteristics," *Cycling Research International*, vol. 2, pp. 119–135, 2012, ISSN 2200-5366.
- [4] R. Utriainen, S. O'Hern, and M. Pöllänen, "Review on single-bicycle crashes in the recent scientific literature," *Transport review*, vol. 43, pp. 159–177, 2022, doi.org/10.1080/01441647.2022.2055674.
- [5] Statistics Netherlands, 684 road traffic deaths in 2023, Accessed: 2025-04-08, 2024. [Online]. Available: https://www.cbs.nl/en-gb/news/2024/15/684-road-traffic-deaths-in-2023/road-traffic-fatalities.
- [6] T. Frendo, "The classification and analysis of 300 cycling crashes that resulted in visits to hospital emergency departments in toronto and vancouver," Bachelor of Science (Honours) Thesis, University of British Columbia, Vancouver, Canada, 2010.
- [7] B. D. Geus, G. Vandenbulcke, L. Panis, et al., "A prospective cohort study on minor accidents involving commuter cyclists in belgium," *Accident Analysis Prevention*, vol. 45, pp. 683–693, Mar. 2012. DOI: 10.1016/j.aap.2011.09.045.
- [8] D. Karnopp, Vehicle Dynamics, Stability, and Control, 2nd. Springer, 2016. DOI: 10.1007/978-3-319-21296-4.
- [9] J. Moore. "Learn multibody dynamics." Accessed: 2025-04-23. (2024), [Online]. Available: https://moorepants.github.io/learn-multibody-dynamics/jupyter-python.html.
- [10] H. Pacejka, *Tyre and Vehicle Dynamics*, 3rd. Oxford: Butterworth-Heinemann, 2012, ISBN: 978-0-08-097016-5.
- [11] K. Åström and A. Lennartsson, "Bicycle dynamics and control: Adapted bicycles for education and research," *IEEE Control System Magazine*, 2005.
- [12] R. Rajamano, *Vehicle Dynamics and control*, 2nd ed. 233 Spring Street, New York, NY 10013, USA: Springer Science+Business Media, 2012.
- [13] B. Souh, "Influence of tire side forces on bicycle self-stability," *Journal of Mechanical Science and Technology*, vol. 29, no. 8, pp. 3131–3140, 2015.
- [14] G. Dell'Orto, "Bicycle tyre lateral characteristics and their effect on bicycle dynamics," Ph.D. dissertation, Delft University of Technology, Delft, Netherlands, 2025.
- [15] B. Coutermarsh and S. Shoop, "Tire slip-angle force measurements on winter surfaces," *Journal of Terramechanics*, vol. 46, pp. 157–163, 2009.
- [16] R. Rajesh, D. Piyabongkarn, J. Lew, K. Yi, and G. Phanomchoeng, "Tire-road friction-coefficient estimation," *IEEE Control Systems Magazine*, vol. 30, no. 4, pp. 54–69, 2012. DOI: 10.1109/MCS.2010.936931.
- [17] M. Henson and D. Seborg, *Nonlinear Process Control*, 1st ed. New Jersey, USA: Prentice Hall, 1997, ISBN: 9780136251798.
- [18] O. Boubaker, "The inverted pendulum: A fundamental benchmark in control theory and robotics," 2012 International Conference on Education and e-Learning Innovations, November, 2012. DOI: 10.1109/ICEELI.2012.6360606.

References 49

[19] R. W. II and D. Lawrence, *LINEAR STATE-SPACE CONTROL SYSTEMS*. Hoboken, New Jersey: John Wiley Sons, 2007.

- [20] D. Peterson and M. Hubbard, "General tteady turning if a benchmark bicycle model," ASME 2009 International Design Engineering Technical Conferences 7th International Conference on Multibody Systems, Nonlinear Dynamics, and Control, 2009.
- [21] D. J. N. Limebeer and M. Massaro, *Dynamics and Optimal Control of Road Vehicles*, 1st. Oxford, UK: Oxford University Press, 2018.
- [22] G. Franklin, J. Powell, and A. Emami-Naeini, *Feedback Control of dynamic systems*, 8th ed. 330 Hudson Street, NY, NY 10013: Pearson, 2020.
- [23] K. Åström and R. M. Murray, *Feedback Systems: An Introduction for Scientists and Engineers*, 3rd. Princeton University Press, 2020.
- [24] S. Selesnic and S. Kodsi, "Bicycling speeds: A literature review," *Accident Reconstruction Journal*, 2016.
- [25] B. Michini and S. Torrez, "Autonomous stability control of a moving bicycle," in *Proceedings of the [Name of the Conference]*, 2007. [Online]. Available: https://api.semanticscholar.org/CorpusID:165156499.
- [26] L. Prasad, B. Tyagi, and H. Gupta, "Optimal control of nonlinear inverted pendulum system using pid controller and lqr: Performance analysis without and with disturbance input," *International Journal of Automation and Computing*, vol. 11, no. 6, pp. 661–670, 2014, DOI: 10.1007/s11633-014-0818-1.
- [27] a. R. R. D. Piyabongkarn, J. Grogg, and J. Lew, "Development and experimental evaluation of a slip angle estimator for vehicle stability control," *IEEE TRANSACTIONS ON CONTROL SYSTEMS TECHNOLOGY*, vol. 17, no. 1, pp. 78–88, 2009.



The complete source code developed for this project is publicly available on GitHub at: https://github.com/mechmotum/bicycle-IcePatch



LQR and PD on ice

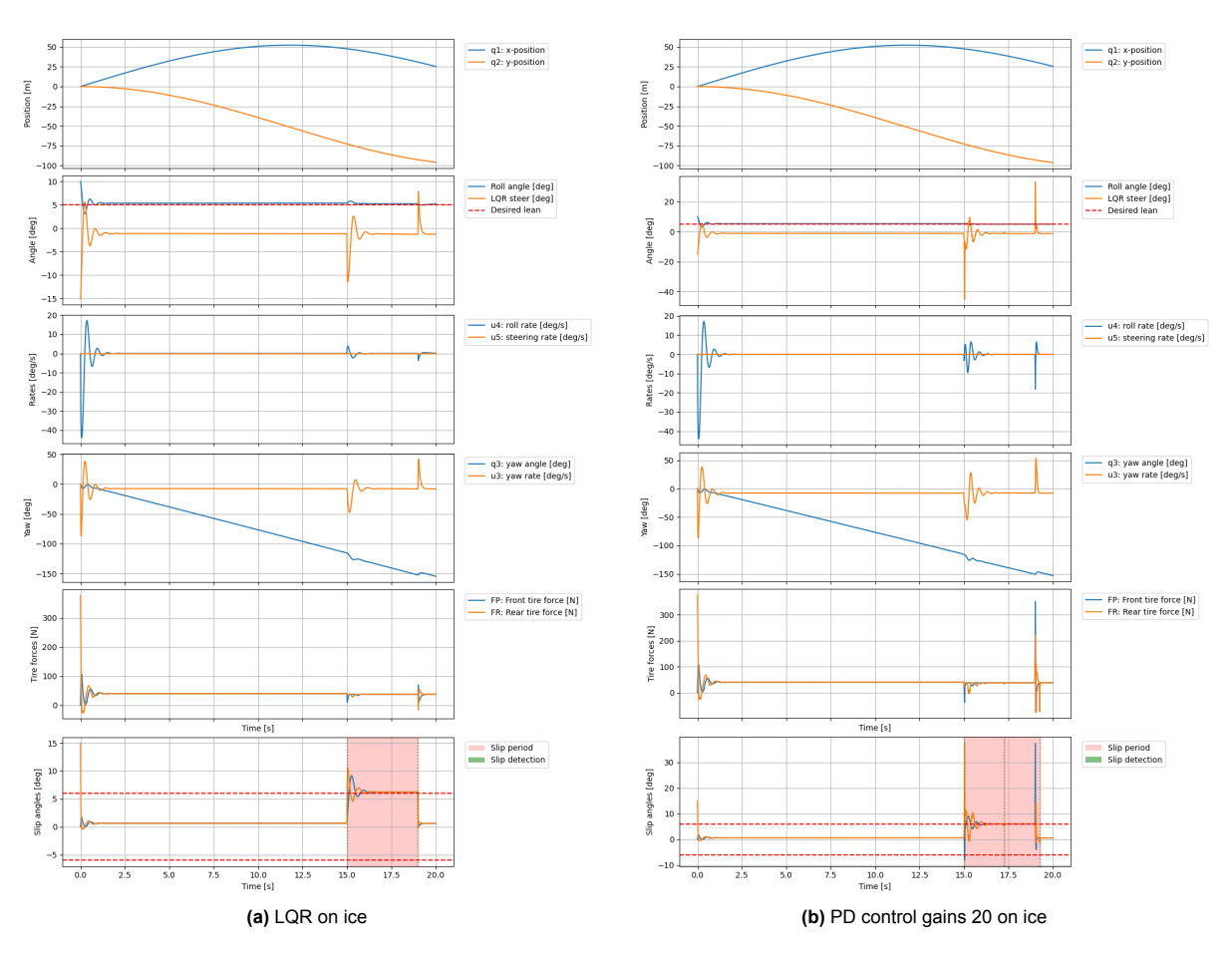


Figure B.1: Side-by-side LQR vs PD control of all variables

Figure B.1 contains all the variables looked at for the LQR versus PD controller on ice. This graph was simplified and put on the same plot to make a comparison in the results section.



Ice vs no ice

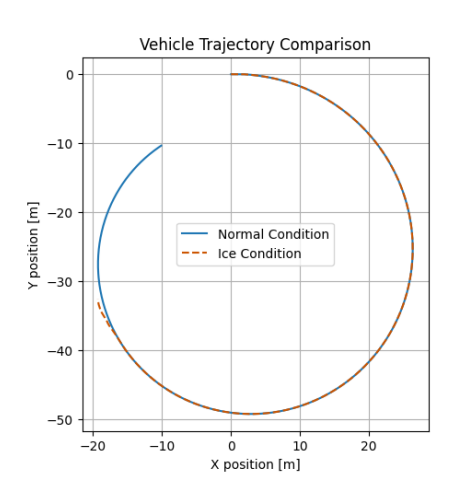
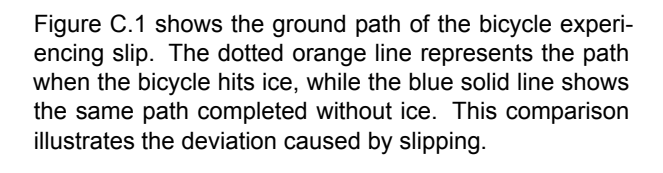


Figure C.1: Path of bike on ice and not



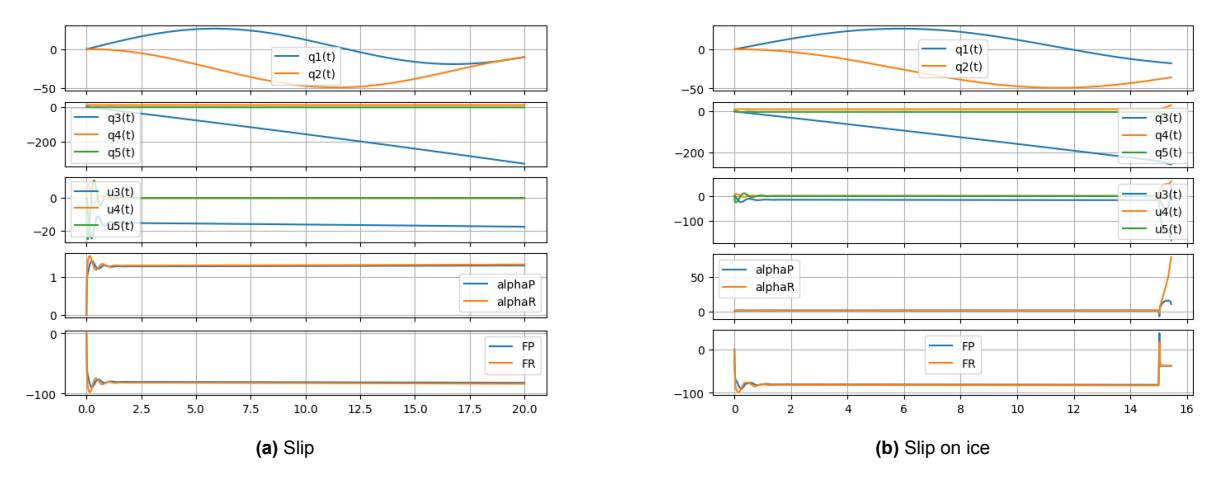


Figure C.2: Comparison of slip and slip on ice

Figure C.2 above shows all of the states of the bicycle when there is slip and slip on ice for a side by side comparison. The graphs in the paper focused in lateral force and slip angle but are the same as these.



PD graphs

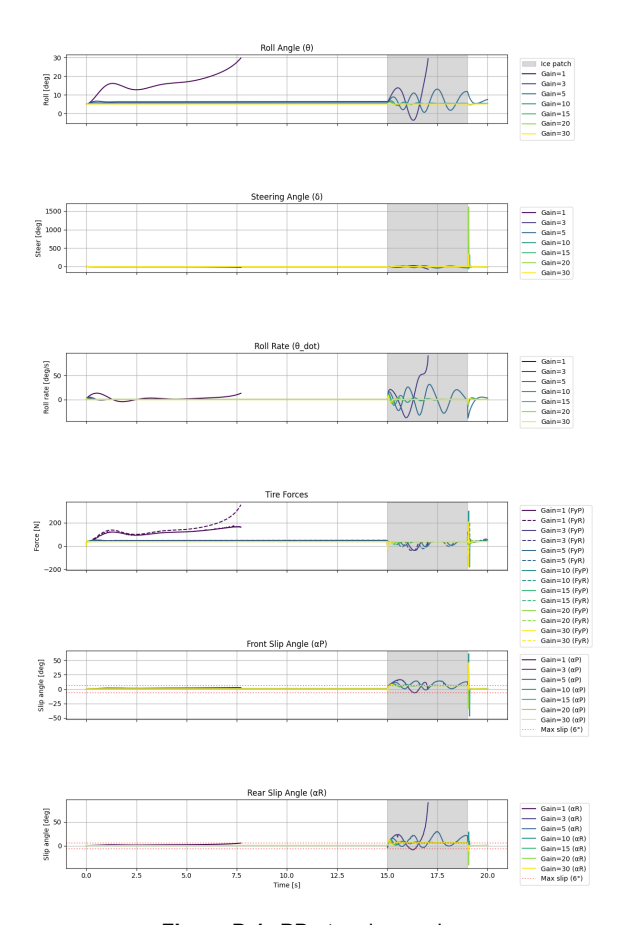


Figure D.1: PD at various gains

Figure D.1 shows the controller over several variables at many tested gains. This graph was used to determine which gains to use for simple riding and on ice.

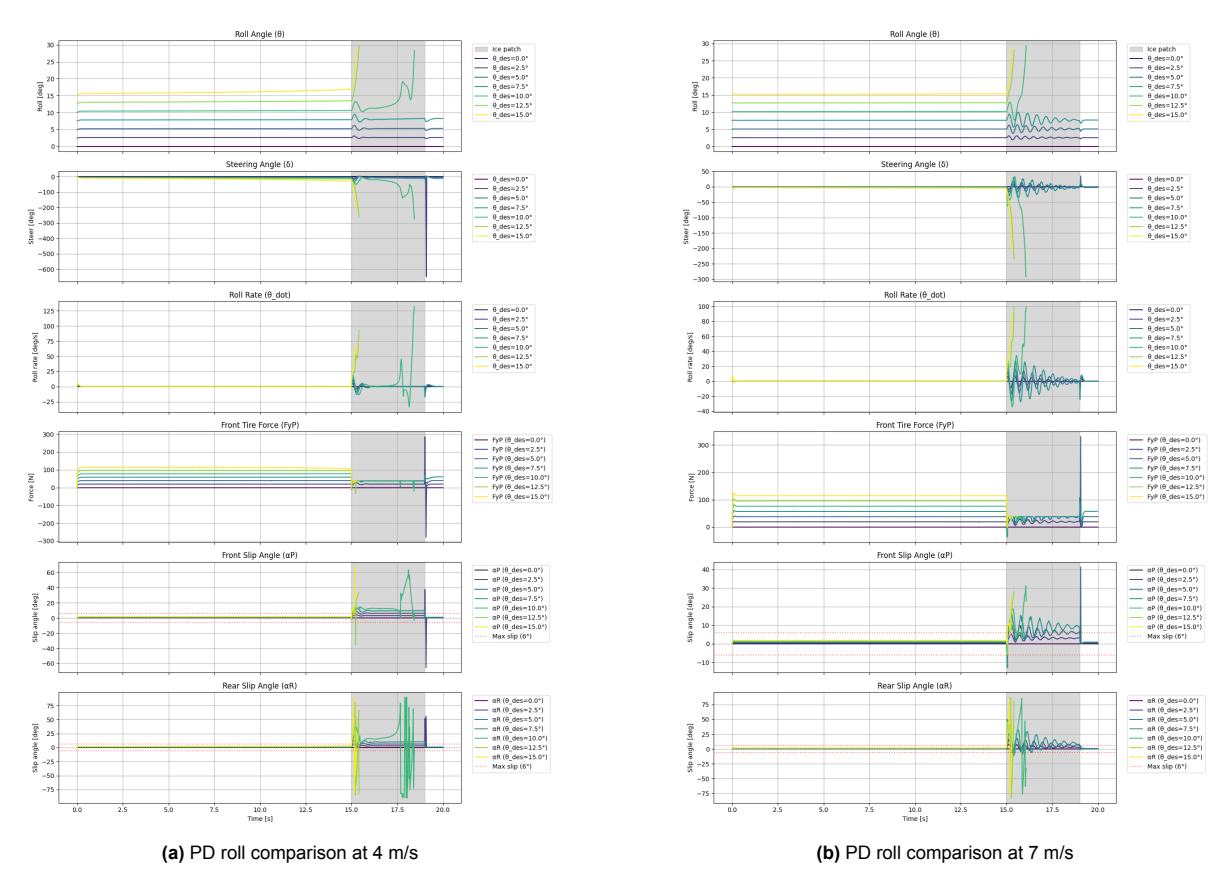


Figure D.2: Side-by-side PD roll angle comparison at 4 and 7 m/s

Figure D.2 shows all of the variables I plotted at various PD gains 15 at set speeds with desired roll angles. These were used in creating Table 5.1 and Table 5.2.

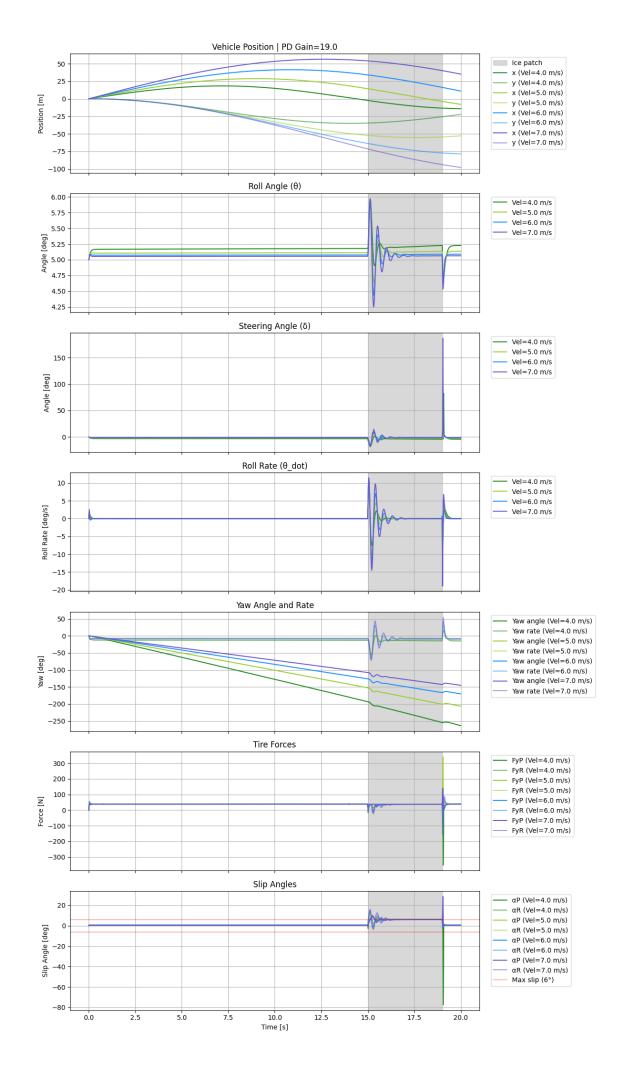
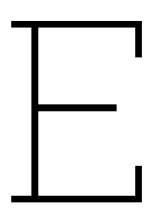


Figure D.3: PD at various speeds with all variables

This shows all variables plotted with PD gains 15, this report had a reduced version for clarity zoomed in on the ice patch.



LQR graphs

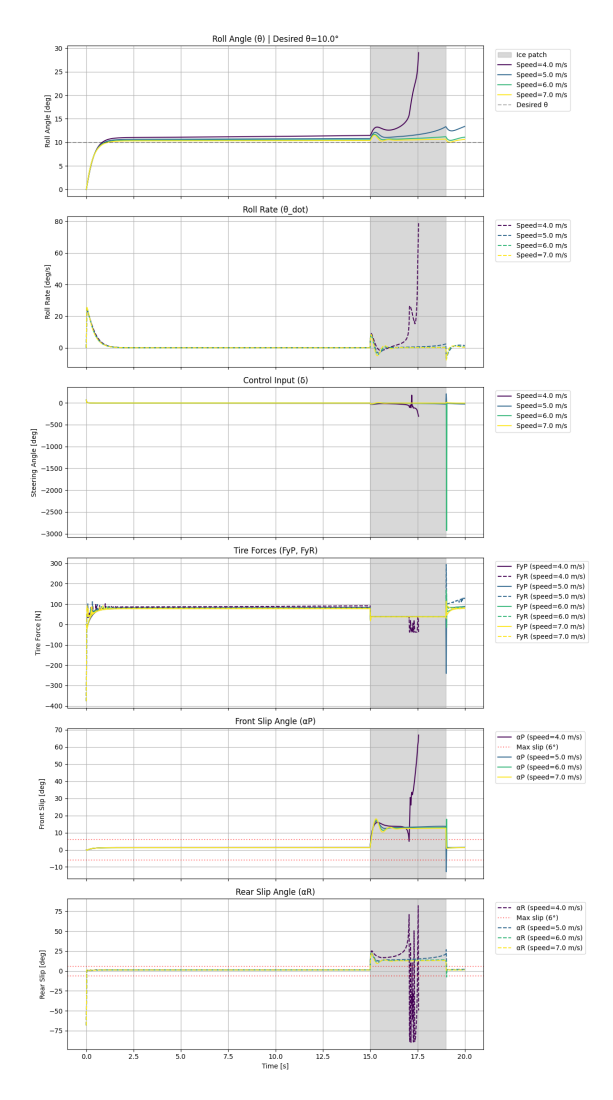


Figure E.1: LQR at various velocities with all variables

Figure E.1 plots all the variables initially plotted at a variety of velocities at 10 degrees roll. The roll and steer were extracted and presented in the Results section.

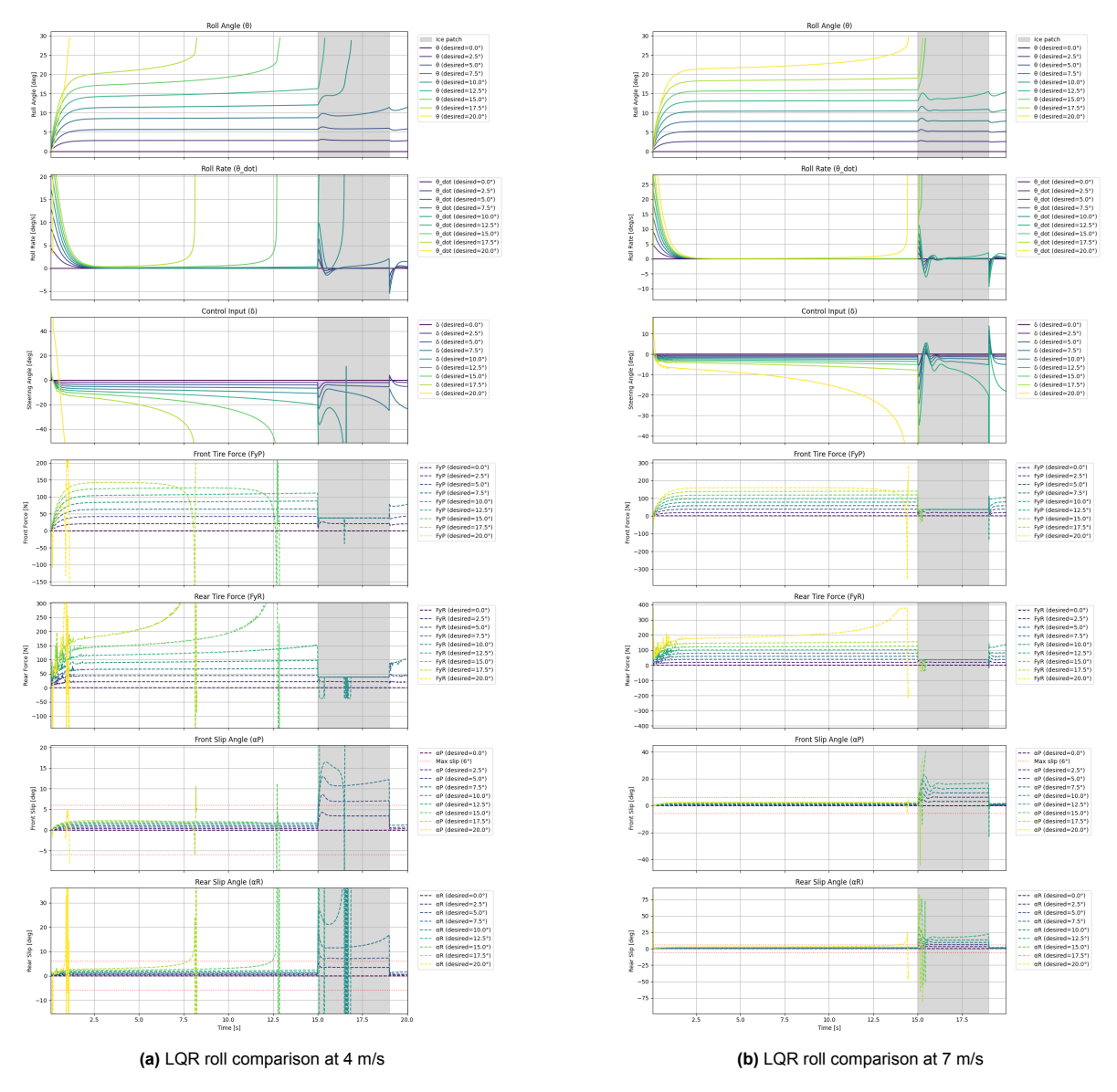


Figure E.2: Side-by-side LQR roll angle comparison at 4 and 7 m/s

Figure E.2 contains all variables plotted across several roll angles to assess if the LQR controller works for a variety of roll angles. 4ms and 7ms were tested because they are the operational bounds of typical biking. Most interesting variables were selected and plotted in the paper.

F

Literature Search

An examination of active safety features in response to common bicycle crash causes.

How could the integration of active safety features mitigates common causes of bicycle crashes, and what existing technologies from cars and motorcycles can be adapted or modified to enhance bicycle safety effectively?

Literature Review by Sara Youngblood May 10, 2024

Student number: 5773016

Supervisor: Dr. J. Moore, BMechE

Date: May 12, 2024



Abstract

Car safety has significantly increased while bicycle safety remains unchanged. Bicycle safety is a growing global concern, reducing common bicycle crashes is an opportunity to improve cyclists' well-being. The investigation into causes of bicycle crashes led to loss of control, skidding, and colliding with objects. Each could be reduced by the addition of an active safety features. Loss of control was reduced by the addition of ABS. Skidding could be reduced through traction control but requires some modifications. This paper explores active safety features such as Anti-lock braking, and traction control as proactive measured to mitigate cyclist risk. Inspiration from car and motorcycle safety technologies are used to study how existing systems could be adapted for bicycles. The research involved a comprehensive review of literature on bicycle crashes, active safety features of cars, and adaptations of these features for bicycles. It examines common causes of bicycle crashes focusing on avoidable instances, rider or environment based. It compares active safety features of cars and bicycles, as well as dynamic differences. Through comparison analysis the paper identifies technologies repurposed for bicycles, ABS, and gaps in those not yet implemented, traction control. The study explores innovative traction control systems, modified for bicycles, including the different dynamic inputs. The findings highlight potential integration of safety features to reduce crashes caused by skidding. Modifications of car active safety features to fit the dynamic needs of a bicycle to increase rider safety. The paper concludes by discussing autonomous bicycles and gaps in research for better skid control.

Table of Contents

1.	. Introduction	4
	1.1 Need for Study	4
	1.2 Research Method	
2.	Crash Investigation	<i>7</i>
	2.1 Underreporting	7
	2.2 Why single cyclist crashes	
	2.3 Results	8
3.	. Safety Features:	10
	3.1 Active vs Passive Features	10
	3.2 Anti-lock Braking systems	10
	3.3 Traction Control Systems	12
	3.3.1 Dynamics	12
	3.3.2 Slip Angle	
	3.3.3 Traction controllers	
	3.3 Hazard Detection	16
4.	Discussion	18
5.	Conclusion:	20
6	Sources	21

1. Introduction

1.1 Need for Study

Bikes were invented in 1817 and are one of the oldest forms of transportation. [1] Despite bicycles existing for a long time there is little modern research or technological advances. Bicycling is a low cost, environmentally friendly means of transportation. Cycling to and from work provides the greatest satisfaction among commuters This satisfaction is attributed to avoiding traffic or unexpected delay, experiencing sensory stimulation, euphoric feelings after exercise, and socialization. Exercising is known to improves mental and physical health, reducing future medical issues. [2] Cycling reduces pollution, wear on roadways and traffic. Despite these pros there are also risks when cycling.

A study in Finland found 30% of serious road injuries occur to cyclists. [3] Cars have been continuously monitored and improved as far as safety. A comparison of car models between 1980 and 2018 there was an 88% reduction in fatalities and 58% decrease in serious injury. The same decrease cannot be found when looking at bicycle data. Several studies have been conducted on cycling infrastructure. These studies include how to create a safe environment for cyclists and cars. [4] Despite having numerous studies focused on intersections, and car cyclist interaction there has not been much innovation on bicycles.

From 2019 to 2023 Statistics Netherlands CBS reported 32% of bicycle crashes were caused by falling. [5] Falling in this case meaning no other road users were involved. 47% of cyclists involved in bicycle falls said it was preventable if they had reacted differently or quicker. [6] This number is astonishingly high and could be reduced through better riding abilities and choices. I explored how incorporating safety features can improve accessibility and reduce bicycle crashes.

Improving bicycle safety involves multiple disciplines including, engineering, public health, transportation, human factors, and sociology. Investigating crash data gave an idea of what circumstances lead to a crash. Public health cost and concerns from bicycle crashes could be reduced through engineering solutions. Traumatic brain injuries were mostly caused by skidding or colliding with stationary objects. Recovery from these injuries is a lengthy costly process, avoiding these situations greatly improves rider experience. This research explored, how the integration of active safety features mitigates common causes of bicycle crashes, and what existing technologies from cars and motorcycles can be adapted or modified to enhance bicycle safety effectively? I investigated single bicycle crash causes, active safety features of cars, which of the features exist in bicycles or motorcycles, and what features could be further developed for bicycles.

1.2 Research Method

My investigation began by searching Scopus for "(car OR vehicle OR automobile) AND (crash OR accident OR collision) AND (causes OR source OR origin)" resulting in 21,976 documents, about half of them are recent, from 2015 to present. A similar search was done using "bicycle OR cycle OR 2-wheeler" in the place of car. 3,894 documents were found 5 times less than when searching cars. Yet cyclist account for just over 32% of serious road injury. [5] There are significantly less studies focused on bicycle crashes compared to cars. Less study availability makes it difficult to determine what safety features to add to bicycles.

Bicycles have a high center of gravity and relatively small wheelbase. They also have a much lower mass and inertia than motorized vehicles amplifying the importance of load transfers. [7] Due to the added weight and complexity of E-bikes, they will not be included in this study. The amplified load transfers demands fast dynamic action to establish control. [7] My starting point was to gain an understanding of what causes cyclists to crash, specifically single cyclist crashes.

Multi-vehicle crashes make up 51% of adult cycling crashes, however my focus prioritized features that can reduce individual risk. Hospital and police reports of 5000 crashes were used to categorize crashes faulting the bicycle, road, bicyclist, or other. The road included obstacles, climate conditions and infrastructure. In contrast the bicyclist included anything a bicycler did such as handling, loss of control, alcohol, speed etc. Categorization was done in this way to assess if the bicyclist or infrastructure was to blame for crashes. Reducing risk of the cyclist was found to be more effective than updating infrastructure in crash reduction. [8] This guided the research away from infrastructure updates, towards cyclist related causes. The objective is to find active safety feature that can be added to a bicycle to reduce common crashes. Infrastructure, interseactions and other road users will not be included.

I categorized single bicycle crashes of several studies in 3 main causes: loss of control, skidding or collision with objects. I established what causes the most crashes to determine if the modification of an active car safety feature could help. Loss of control was anything related to low/high speeds, braking issues, or obstacle avoidance. Collision was interaction with objects includes interaction with tram tracks, road signs, curbs, potholes, and cracks. Skidding was a change in traction caused by wet surfaces, ice, leaves, or different road surfaces.

After crashes were categorized, I investigated car safety features. I began my search by Googling "timeline of car safety features". I found an extensive timeline from the University of Iowa [9] including seatbelts, airbags, Anti-lock brake system (ABS), Electronic stability monitoring (Traction control), autonomous vehicles and more. I focused on the features that had a big impact on safety, that could potentially to be added to bicycles. Electronic cruise control, Lane assist, electronic tire pressure monitoring, forward collision warning, adaptive cruise control, backup cameras, and drowsiness alert will not be considered. The features not included are either too electro mechanically complex for consideration right now or would not reduce individual risk.

A search on Google scholar with the term "working principle" and "ABS or traction control or autonomous driving" and "car or bicycle or motorcycle" provided an understanding of working principles of each active safety feature. From the results the titles and abstracts were scanned, eliminating papers that did not discuss working principles or how the safety features are implemented in each vehicle. Elicit was also used asking questions to generate sources found in Table 1. Elicit is a source finding AI. It operates by the user typing in a query, then it provides a short paragraph summarizing the answer with citations as well as a list of several papers that could be related to the topic. From each search query, several papers that were irrelevant were generated. I focused my search on the papers that were accessible and had a title or abstract explaining my safety feature in cars/motorcycles or investigated safety features on non-electric bicycles. Accessible papers were papers that can be found in full text without additional subscriptions. I also searched for patents for traction control in cars to

better understand how it works. To get a more complete and visual understanding of traction control systems in motorcycles I searched "How traction control works in motorcycles" on YouTube, leading to a video that gave a mechanical in-depth description. From the sources generated by Elicit and google scholar a few others came from snowballing using their sources or citations.

Query:	Sources:
What robotic or automated traction control systems for lateral control for 2 wheeled vehicles such as bikes, motorcycles and scooters	Traction control systems for motorcycles (Pascal 2009) Improving lateral stability of a motorcycle via assistive control of a reaction wheel (Tanos 2014)
Current ABS systems for bicycles	An anti-lock braking system for bicycles (Corono 2018) Original Research Article Development of a bicycle anti-lock braking system prototype (Enzie 2014) Development of a bicycle anti-lock braking system prototype (Enzie 2014)
what has prevented the implementation of traction control to bicycles	Accident prevention in motorcycles with 3dimensional fuzzy logic traction control system (Surana 2020)
lateral control methods in bicycle traction control	Lateral Control of a Self-driving Bike (Wen 2022)

Table 1: A list of search query used in Elicit

The topic of road anomalies detection was more briefly searched on Google Scholar for a general understanding of how feasible the system would be. Using the search query "road hazard detection in cars" and "road hazard detection in motorcycles" I found many papers mostly detailing pedestrian and vehicle detection. I narrowed the papers based on title and abstract for those using more simple sensors, that processed in real time for non-vehicle hazards. My aim is to prevent single bicycle crashes therefor papers focused on vehicle/pedestrian detection were not in scope of my research. This led to a review on pothole detection methods. I investigated the sources from the review to gain a general understanding of methods used to detect non-moving hazards on the road. The study on pothole detection summarized 3 detection methods in depth providing a decent understanding of each method. I further researched topics such as YOLO, CNN, and neural networks as I read the review to fully understand the paper. I did not investigate further; it was clear from the papers in the review adding anomaly detection would be costly and inconvenient.

2. Crash Investigation

2.1 Underreporting

Car crashes are almost always reported to police or insurance regardless of severity, the same cannot be said for bicycle crashes. Bicyclists who crash with pedestrians, animals or road users do not report minor crashes. Typically, only major incidents requiring hospitalizations, or the police are reported. The difference between the number of crashes and reported crashes is due to a lack of obligation. [10] In Ireland more minor crashes are reported because it is required by law. Mandatory reporting ensures minor bicycle crashes are reported but does not fix under reporting of single-bicycle crashes. Even if it is mandatory, cyclists will not report falling on their bike if no one is around to witness. Single bicycle crash under reporting needs to be considered when investigating cycling accidents. Without a solution to under reporting, accurate crash data will never be available. A Belgian study found a population of 18-to-65 year old's who cycle as their main transportation to and from work. They asked the participants to recap their cycling experience each week, reporting any crashes or near misses. The prospective nature of this study shed light on the number of under reported cases. They concluded 5.9% of minor cycling accidents were reported. [6] A similar study gave a survey to cyclists across Ireland in 2018. They aimed to find contributing factors and compare collision characteristics with injuries. Their analysis concluded that 18% of serious injuries and 79% of minor injuries are unreported. [10] This study proves there are significantly more crashes than reported, especially in cases of minor injury. More prospective studies are needed to get tru crash statistics. When investigating crash causes in the following sections it was important to note, most statistics are the tip of the iceberg.

Most reports of bicycle crashes come from police, insurance, and hospitalization records. Data from these three places often overlaps but individually can't give the full picture. [8] Police and hospitals data had only a 14% overlap. [10] Studies typically send a survey to individuals selected from a data set asking for more information. Valuable information can come from this, but contains recall bias. Memories of an incident are usually different than what occurred. People unintentionally focus on the most sever aspects of their crashes blocking out other details. [8]

2.2 Why single cyclist crashes

Focusing on crashes caused by cyclists, I considered the difference between single and multivehicle collisions. Multi-vehicle crashes in my case will be a collision with any other road user, both motorized and not. Single-bicycle crashes will be any fall or collision caused by non-road users. Crash causes form survey data have been categorized into either multi or single vehicle crashes. They found 29% of crashes are single bicycle crashes cause by: colliding with obstacles, skidding on wet road, hitting a curb, or avoiding an obstacle. [10] Emergency room data over a 15-year span was collected and subdivided into 4 causes: traffic, falls, collisions and entrapment between bike and spokes. 51% percent of injuries were caused by falls, followed by colliding with a 4-wheeled vehicle. [11] The high number of single bicycle crashes affirms the decision to focus on active safety features as a means to reduce preventable crashes. A significant amount of single vehicle crashes can be examined for underlying cause to determine crash prevention solutions.

An important group of individuals not often studied is children. A study focused on the effectiveness of helmets provided some insight into children's causes of falls. 8000 children ages 0 to 17 hospital records divided the cause of crashes as: injured child, external factors, other/unknown. When the injured child caused a crash, responsibility was allocated to skill level, distraction or stunt performing. External factors included everything from infrastructure, road surface and maintenance to bicycle failure. Unlike adults, most injuries to children were due to single bicycle crashes, 84%. This percentage decreased with age, therefor. As children age, they become better at controlling their bicycles. Adding a control assist to children's bikes could have an even bigger effect on increasing safety and reducing crashes. [12] Children specifically will not be the focus of this research but should be considered as a population group that can benefit from the addition of active safety features.

2.3 Results

Crashes can similarly be categorized as collisions or falls. Collisions are considered a crash initiated when a cyclist encountering another object. The object can be part of the infrastructure, an organic object, other road vehicles and any forms of debris. Fall are crashes not initiated by the collision of the bicycle with an object. Falls can be initiated by collision avoidance, bicycle malfunction, wheel lodge, or behavior decisions. I combined falls and debris caused collisions giving 168 out of 300. [3] These are what I consider single bicycle crashes because they do not involve other road users. 23% of crashes were due to loss of control, 15% was due to collision with objects and skidding was not mentioned. [3]

Swedish traffic accident data acquisition (STRADA) provided insight into cycling crashes. Two studies using STRADA data were done, one in 2019 the other in 2022. In 2019, the data categorized single bicycle crashes into 5 subcategories: collision with stationary object, collision with temporary object, loss of control, road surface and other. I found 46% of single bicycle crashes were due to loss of control, 19% were skidding, 6% were caused by a loss of control. [14] The 2022 study using STRADA data sent a questionary to over 600 individuals involved in single-bicycle crashes. Crashes were first characterized in 3 different ways, the first was by rider data, then by specific cause, finally by injury sustained from the crash. The data sorted for specific cause had subcategories of cyclist behavior, road environment or another road user. Common crash causes were skidding at 34%, loss of control at 22% and colliding with an object at 26%. [13]

A Finnish study used 9000 cases from the Finnish workers Compensation Center data to organizes crash causes into 5 main groups: infrastructure, cyclist-related, bicycle malfunction, interaction with road users and other. Most crashes were caused by infrastructure. Infrastructure in previous cases focused on aspects of the road that do not change and are not related to the rider. In this case infrastructure included skidding on slippery roads, colliding with curbs, riding off the road and loss of control on uneven surface therefor it is in scope for my purposes. Road surface changes due to weather leading to slipping were categorized as slipping. Colliding with the curb was generalized into colliding with objects. Riding off the road and uneven surfaces were categorized as loss of control. Single-bicycle crashes represent 63% of crashes with injury but should also include the 16% of cyclist related and 5% of bicycle malfunctions. Cyclist-related encompasses braking mistakes, wheel lodge, (dis)mounting, foot slipping, and distraction all of which can cause single-bicycle crashes.

[15] Converting the percentages to my classification 47% were due to skidding, 9% colliding with objects and 10% loss of control. Figure 1 shows an overview of single cycle crash

causes fit to fall into loss of control, skidding or collisions. All cases not specified into the previously mentioned category are considered other/not specified. The figure shows the average percentages calculated from each crash study previously mentioned.

SINGLE BICYCLE CRASH CAUSES

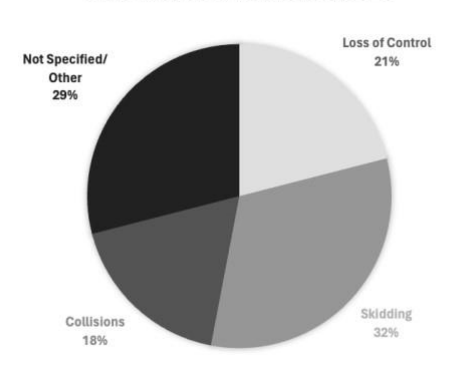


Figure 1: Single bicycle crashes: skidding, loss of control, collision, not specified.

Data from a Melbourne trauma centers led researchers to interviewing cyclist's post-crash. Based on event descriptions, the crashes were divided into single-bicycle and multi vehicle. Leading to a classification of 5 single bicycle crash types included: loss-of-control, interaction with tram tracks, struct object or pothole, bicycle mechanical issue and other. In both experienced and armature cyclists about half the crashes were single-bicycle crashes. Experience and skill only made a small impact when faced with unexpected changes in road friction, objects, or mechanical issues. [16] Cyclists were asked if preventable behavior/choices caused their crashes? 47% believe their crashes could have been preventive with more hazard awareness or better reflex. [13] Cyclists are not equipped to rapidly deal with these changes, this is where additional safety features can step in. Adding an active safety feature to pick up where cyclists lack reducing up to 32% of unnecessary crashes. Loss of control events were a large portion of crashes included sudden braking, skidding on wet/slippery surface, and losing control. [16] I calculated the average of each crash type from papers to get an overview of most common crash causes based on my classification. I found loss of control accounted for 21%, skidding was 32% and colliding with non-vehicles was 18% shown graphically in Figure 1. Focusing our active safety features reducing crashes in these scenarios should be the top priority. What robotic interventions can be used to pick up where people fail? The next section will investigate the safety measures added to vehicles that prevent crashes and improve safety. What active safety features were added to cars? Are they available for bicycles?

3. Safety Features:

3.1 Active vs Passive Features

Crash prevention was divided into two categories, passive and active measures. Both provide the user with increased safety. Passive measures are features that increase safety post crash, such as helmets, and seatbelts. Active measures aim to prevent crash causing events, such as braking, traction control or hazard warnings. Figure 2 shows an overview of safety features of bicycles versus cars. The chart shows bikes lack several safety features available in cars. A few crash studies focused on the effectiveness of helmets. Safety add on like helmets and protective clothing are useful passive safety measures for cyclists. Many countries do not have official laws requiring helmets, but helmets became widespread in the 1970's. Developing safety features typically starts with passive measures, they are easier to implement. Seat belts and airbags were added when car safety first became of concern in the 1950's. [17]

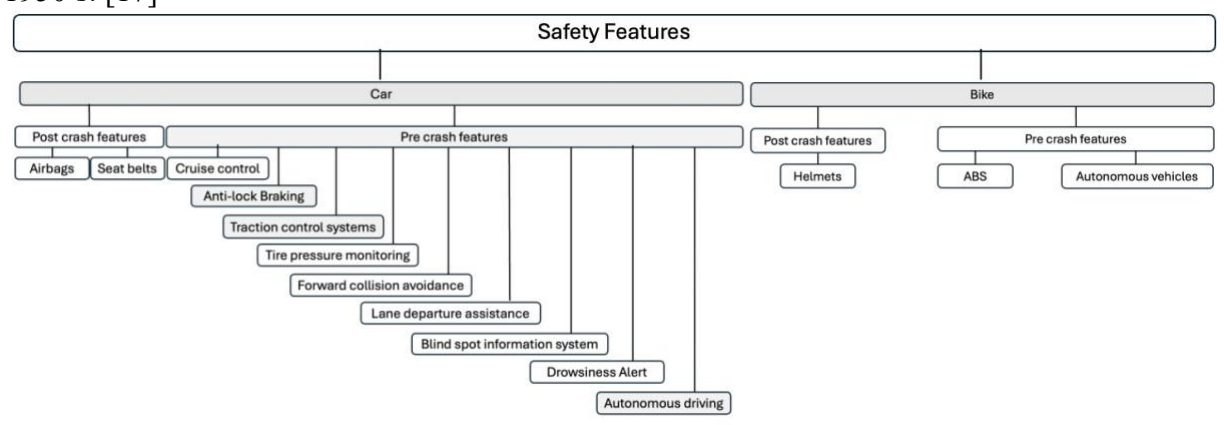


Figure 2: An overview of safety features

3.2 Anti-lock Braking systems

ABS were initially designed for trains in 1908, and soon modified for planes and cars. [18] By 1969 Ford modified the first ABS system for cars, leading to today's ABS systems. ABS prevents the wheels of a vehicle from locking during braking by releasing and reengaging repeatedly. This allowed the wheels to momentarily spin changing the direction of travel and traction. [19] Today ABS comes standard on all car models. [18] ABS has been widespread since 1984, why have not they been implemented on 2-wheeled vehicles? 4-wheel vehicles are stable when stopped, this is not the case with 2 wheelers. Bicycles are most stable when moving in a straight line at constant speed. Stability can also be found when traveling in a constant circle on smooth ground, or track standing. [20] The complexity involved in finding stable resting positions is likely partially to blame for the lack of active safety features. Adding sensors and electronics complicate bicycles significantly. Adding weight to bicycles changes the center of mass, dynamics, and equilibrium positions. Despite these difficulties ABS has become commercially available for bicycles.

Bicycle ABS actuates the hydraulic brakes. Hydraulic brakes are used in bicycles, motorcycles, and cars. When riders brake on a motorcycle, they trigger a piston adding pressure to the system. The added pressure engages the brakes decreasing velocity. There are two main components in this setup, hydraulics, and electronics. The hydraulics control the

brake fluid flow. The electronics transfer information from the controller to the hydraulics and vice versa. A control algorithm determines how much actuation should be applied for safe braking. [7] Before controlling braking behavior, the controller needs to be programed with decision making logic. This was done in several ways but always comes down to comparing theoretical speed, actual speed, and pressure on the brake lines.[7] A necessary sensor addition is used to measure wheel speed. This can be done through measuring polarity of magnetic tape, sensing holes, or sensors that double as induction generators. The simplest most common method is sensing holes. A sensor measures speed by counting how many holes pass in an amount of time. From the number of holes per unit of time rotational speed can be calculated show in Equation 1. Using rotational speed and a predetermined radius of rotation linear speed can be calculated shown in Equation 2.[21]

$$rotational\ speed = \underbrace{\frac{1\ turn}{to\ complete\ a\ rotation}}_{\ linear\ speed\ =\ rotational\ speed\ *\ radius\ of\ roation}_{\ Eq.\ 2}$$

$$Equation\ 1,2:\ used\ to\ relate\ sensor\ data\ to\ linear\ speed.[21]$$

Brake pressure must also be measured to get an idea of how hard the brakes are being pulled. This can be done by monitoring piston position, telling the system if the brakes are deployed. [7] Finally, a comparison can be made between how much pressure a rider applies to the brake levers and brake pad pressure. [19] Combining wheel velocity and pressure on the brakes lets us calculate expected vs real deceleration values. Different wheel deceleration controllers are used in decision making but the general process of ABS follows the flow depicted in figure 3. The wheel deceleration (n) controller affects the front wheel speed. The actuator position (x_{ref}) lets the system know how much braking is occurring. Different controllers are used in the place of wheel deceleration with varying complexities.

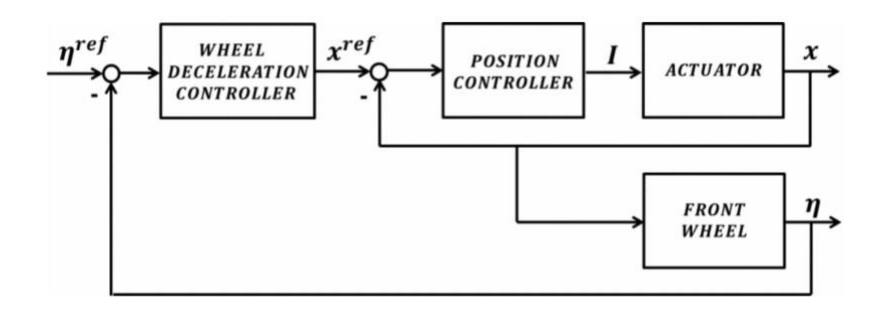


Figure 3: general ABS block scheme [7]

Difference in wheel speed is used with one of three controllers determining system behavior. Three methods of control were compared: Bang-Bang, Second Order Sliding Mode, and Proportional Integral controllers. Bang-Bang deals with non-linearities, the Second order Sliding Mode deals with limitations and Proportional Integral amplifies desirable features of the control law. Proportional integral controllers provided the most comfortable ride and were most accurate. [7] After the controller detected wheel lock a valve is actuated reducing or increasing the brake pressure. This application and removal of pressure prevents locking

but still slows the bicycle relatively quickly. [22] There is adequate research on ABS systems for bicycles. Research led to a few commercially available options, mostly targeted to Ebikes. Shimano and Blubrake, Outbraker and Bosch produce commercially available bicycle ABS. ABS is a viable active safety feature bicyclists can use to increase riding safety. Research showed a significant amount of single bicycle crashes are caused by loss of control, many of which can be eliminated with ABS. Bosch claims their ABS for bicycles has prevented almost 30% of bicycle accidents. [23]

3.3 Traction Control Systems

Patented in 1992, traction control built upon ABS reacting to wheel speed discrepancies. Using the same wheel speed sensors as in ABS, wheel speeds are measured and sent to a controller. If the controller detects slip it will try to correct by reducing torque from the engine by applying the brakes. [24] Traction control has significantly increased vehicle safety and control on wet surfaces, cornering, gravel. 11% of multivehicle and 52% of single vehicle car crashes were reduces thanks to adding traction control and ABS.[25] Unlike 4wheeled vehicles, we can not only look at wheel speeds when executing traction control bicycles. In a corner 2-wheeled vehicles balance the centripetal and friction forces. If there is too little friction between the wheel and the ground, a skid will occur.

3.3.1 Dynamics

To accurately control bicycles, wheel speeds, roll angle, steer angle, frictional and centripetal force need to be continuously monitored and compared. More complex and costly control functions are needed. [26] 4-wheel vs 2-wheel vehicles have very different dynamics and stability points. Cars are stable at zero velocity thanks to their wheelbase and multiple points of ground contact. Turning the front wheels steers the car and the back end follows with negligible lean. [27] Conversely, bicycles are stable at constant velocity, increasing with speed. Bicycles in a turn rely on both steer and lean angle to complete a turn. The higher the speed the more important it is to balance lean and steer angle. [27] The complexity of bicycles leaves many variables to control. Luckily bicycles are underactuated, meaning one variable can control multiple degrees of freedom. This is demonstrated by Huang, who used a steer and torque motor to self-stabilize a bike in a circular and track-stand motion. [20] Controlling the front wheels' steer angles and rear wheels' torque, most degrees of freedom were eliminated. Controlling wheel steer and torque allowing for basic maneuvering in realworld testing.

There are many simplified models used in bicycle simulation. The most simplified is a 2 degree of freedom system. The two factors of focus are lean and turn angle. These variables give a general idea of where the bicycle is in 3D space. [20] This approach models a bicycle as a pendulum neglecting complex uncertainties of the real-world. One of the most common bicycle dynamics models is the Whipple Model shown in figure 4. The Whipple model breaks the bike into four ridged bodies: front or rear frames, and front or rear wheels.

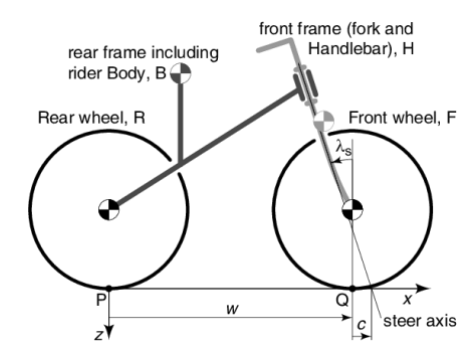


Figure 4: Whipple bicycle model from [28]

The system can be controlled by setting forward velocity, lean angle, and turn radius. These three variables were investigated in a simulation by Sangduck who created a dynamic control algorithm. When the system is dominated by lean, circling in a constant size can be considered a stability point. [29] Forward motion with no lean angle is considered another stability position. The goal when recovering from a skid is to return to a safe state. Either circling or travel in a straight line can be the post skid goal. A traction control system in a bicycle should have the end goal of returning to one of the two safe positions. Simulating a realistic bicycle turn related lean angle to angular velocity, steer angle and center of mass. The goal was to establish a maximum lean angle relationship to controllable variables. When the maximum lean angle is exceeded, traction control logic can be initiated. Exceeding the maximum lean angle most likely will cause the system to skid. The resulting relationship is equation 3.

Equation 3: relation between velocity and lean angle [20]

3.3.2 Slip Angle

It is important to understand curving and slip angle before looking further into traction controllers. The front wheel is closer to the center than the rear wheel when curving. The rear wheel must spin faster to cover the same ground. When motorcycles skid, the rear wheel moves faster, and farther from the center resulting in sliding out. [27] Motorcycle traction control aims to reduce torque on the rear wheel, balancing speed with the front. Control logic calculates the difference in wheel speeds related to turn radius. The difference is compared to a maximum safe lean angle. [20] The maximum angle also must consider the ratio between tire tilt and coefficient of friction. The coefficient of friction between the road and tire changes with road surface and can be unpredictable. The maximum lean angle is proportional to the coefficient of friction. The greater your friction, the more you can lean before skidding. The critical angle therefor also changes with friction.

The final aspect of dynamics to consider is slip. Turning the handlebars points the wheel in the direction of desired travel instead of current travel. Slip refers to the deformation of tires on the ground from the central axis shown in figure 5. Friction causes this deformation. The tire grips the ground resulting in a change of direction. Tire deformation can compensate for small amounts of sip but is not enough to overcome larger lean angles or sharp turns. Lateral slip can be controlled by finding balance between roll angle and coefficient of tire friction.

[30] Unfortunately, the coefficient of friction is dependent on everchanging road surface. Tactile paving, metal train rails and ice patches are examples of changing road surfaces often encountered by cyclists. Any one of these changes' friction, and rider control. The friction can be estimated in real time of cars by comparing front and rear wheel speeds. If the speeds are similar, it is assumed friction is adequate. Large discrepancies in wheel speed indicate insufficient friction. For bicycles, difference in fiction also involves lean angle, and tire contact.

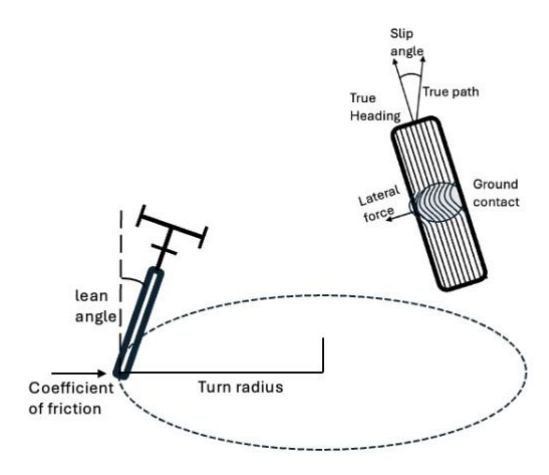


Figure 5: a visual representation of slip, and lean angle vs turn radius

Forces between the road and tires propel vehicles forward. Torque of wheels overcomes frictional forces generating forward movement. Vehicles also experience longitudinal slip, the difference in spin of the driven and nondriven wheel. [31] Unfortunately, a lot of nonlinearity and uncertainty also comes from these forces. Some uncertainties come from different road surfaces, and tires. Bicycles have several different tire types each with different traction, coefficients of friction and contact patches. To control the difference between front and rear wheels traction control was invented. Car traction control works by applying a brake to the slipping wheel and applying power to the other.[31] The aim is to balance the speeds, so the wheels rotate at the same rate, hopefully generating velocity in the desired direction.

Motorized vehicles have the advantage of rapid, controllable torque generated by inverters lacking in standard bicycles.[32] Traction controllers use a closed loop controller to relate slip, driver input and vehicle state.[31] Figure 6 shows a simplified traction control structure.

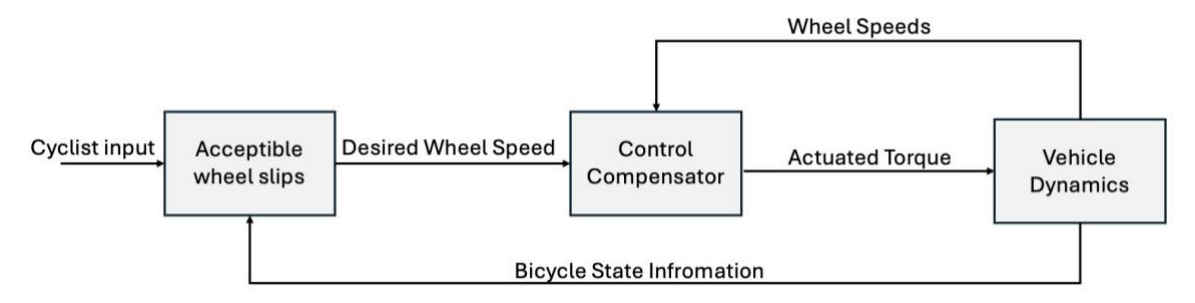


Figure 6:Traction control system structure for bicycles based on traction controllers of cars

Bicycles cannot copy the exact architecture of car traction control but similar principles can be used. Forward velocity, turn radius, lean angle and acceleration need to be measured to determine slip. Most road vehicles experience variability in friction with changing weather

and road conditions. Controlling the torque of each wheel is important when controlling slip. In cars it is easy to control the torque on the wheels by controlling the throttle, spark advance, and transmission. [31] In bicycles your energy comes from the rider. An additional motor on the drive wheel could be controlled electronically. Traction control was introduced commercially in motorcycles for MotoGP, a motorcycle racing event. Yamaha and Ducati measured wheel speeds and controlled the torque of each wheel. They measured wheel speed, roll angle, engine RPM and energy into the system. [32] Similar variables can be used for a bicycle traction controller, if torque motors are added to each wheel.

3.3.3 Traction controllers

Control in variable operating conditions required a closed loop a linear quadratic controller followed with a cascading PI controller is the best option. Linear Quadratic regulators (LQR) are based on control law combining gain and the state vector. They try to find stability at minimal cost, balancing performance, and control. LQR controllers are not the best when dealing with uncertainty and nonlinearity, therefore PI controllers are also needed. [33] Adding the PI component allows you to react quickly in many environments. The cascading PI controllers were used to nest an output as the setpoint to the next. The cascade method allowed them to prioritize multiple objectives with one main objective. In the case of bicycles lateral control and balance can both be optimized. [34] Finally if you add tuning you can adjust to reduce delay in actuating the controls. Controlling traction in bicycles and motorcycles can be slightly more complicated than cars because they are not stable at zero velocity. The control laws balancing slip, steer angle and velocity used in cars cannot be reused. [31] Motorcycle traction control continuously measured wheel speeds. The difference between the wheels was compared to a preset threshold value. If the threshold was exceeded the controller cut the energy into one of the wheels reducing the difference. [32] This is a very simplified preliminary model focused on longitudinal slip. The simple controller was built only considering longitudinal slip. Today's motorcycle traction control also considers the vehicles angles, using fuzzy logic and machine learning models encorperating control for lateral slip.

Attempts to create traction control for bicycles started with Lab VIEW simulations controlling steer angle and wheel torque to prevent slip. A simple controller was created to keep bank angle under a determined maximum safe angle. [35] Simple controllers are effective in simulation but not so much in reality. Reality adds a lot of external factors and variable road conditions. Fuzzy logic and machine learning models can provide a more robust controller. Fuzzy logic is typically a combination of If/Then statements based on set assumptions. Incorporating learning allows he system to adapt based on riders' behavior and preference. [36] Traction control from motorcycles could provide a useful template for bicycles but is protected by intellectual property of each manufacturer.

Unlike cars, specific details of the traction controllers in motorcycles is hard to find. Traction control is available in motorcycles, but there has been little research published on what control algorithms are used. Motorcycle traction control inputs sensor data into a controller, if necessary, it will change power to the drive wheel. The slotted rim measurements used for ABS can be reused to get wheel speed data. The wheel speed data is needed for traction control but unlike cars other variables must also be incorporated. Calculating slip for motorcycles is more complicated than for cars. In curves, motorcycle wheels experience

different diameters of contact with the road whereas cars have a consistent amount of ground contact. Most systems use inertial measurement units (IMU) to get more data than just wheel speed.[37] IMU's output data from gyroscopes and accelerometers. They can measure linear acceleration, angular velocity changes, yaw, pitch, and roll shown in figure 7. [38] Data from IMU's is input to a control algorithm and checked against acceptable slip values. When activated the traction control system adds power to the drive wheel evening out the wheel speeds. Motorcycles includeing changeable thresholds based on road surfaces.[37] For example, riders can set a hard-to-reach level of intervention for drifting on gravel. An easier to reach threshold may be desired on wet pavement.

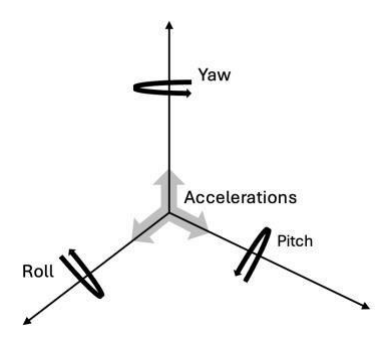


Figure 7: Accelerations and gyroscopic measurements from IMU's

LQR and PI controllers have been researched for use in bicycles in simulation and real-world scenarios. Studies agreed roll angle and lateral dynamics can be controlled through steering and wheel torque. Various controllers were found to determine when to actuate the steer angle and wheel torque. [39] A robust LQR method was developed to account for uncertainties. Simulation showed the controller could deal with a 2 degree of freedom bicycle model. The simplified version of a bicycle is not a true representation but proved stability can be achieved. To account for more complex, uncertain situations addition of an integral term was done eliminating gyroscopic drift. [40] This method worked better than the previously but has not been tested outside of simulation, nor on 4 degrees of freedom. It showed, similarly to cars LQR and PI controls can be modified from traction control of cars and implemented on bicycles. A major modification will be factoring more variables, such as yaw, pitch, and roll.

One study used only PID controllers without LQR. The objective was to move the bike forwards/backwards and execute small angle turns. They created a controller to compensate for the changes in center of mass when the bike is not stabile. The offset was supposed to relate the steer angle to the center of gravity, triggering the corresponding gyroscopic motion. [41] The method was not robust and required recalibrations for all changes in load. If the user changed the controller would not know how to handle the different weight. They use of gyroscopes to correct when tilt angle was too large. The gyroscopes used in this study were cumbersome and impractical. In the end, the study was a good exploration into PID control but lacks practical implementation in real-world bicycle traction control.

3.3 Hazard Detection

Although car safety increased with the addition of passive safety features, active features had a big impact on safety. ABS and traction control were not enough, cars incorporated vision sensors to detect hazards before they were encountered. Blind spot detection, back-up

camera, lane departure and Auto-emergency braking were added in the 2000's. [42] Cars have integrated vision systems used to detect lanes, road anomalies, and environmental hazards. These can be detected by robotic or human action through data acquisition, data preprocessing, data extraction and classification. People acquire information about our environment by looking, then processing what we saw for hazards. Finally, we classify hazards based on perceived risk. After determining risk factors and appropriate course of action is found. Using technology, the method is similar but falls into 3 detection categories: vision-based, vibration-based, and 3D reconstruction. [45]

Vision based systems take images or video as input to assess the presence of anomalies through image processing and deep learning. Simply put they take a still image and give a confidence score to anomalies, prioritizing more sever hazards. [43][44] Vibration based methods measure anomalies using acceleration sensors on a vehicle. [45] 3D reconstruction uses stereovision or deep learning to predict the shape and volume of anomalies. Stereovision refers to the ability to perceive depths and three-dimensional structures. [45] Vision and 3D reconstruction are more useful in detecting future anomalies while vibration detects current hazards as riders hit them. For bicycles, vision and 3D reconstruction would be more useful in detecting hazards. Riders have more time to correct their action if they are informed before they encounter hazards. Vision and 3D reconstruction are not reliable when detecting minor road surface differences, especially in poor light. [45] All methods require costly computing, requiring the addition of heavy hardware not practical for bicycles. Until more compact vision systems are available bicycles will need to react retroactively.

Vision systems success eventually led to the newest safety feature, autonomous driving. Cutting the driver out completely, and letting controllers make most driving decisions. Autonomous vehicles remove the human as a contributing factor. The first autonomous bike was created to test cars' ability to react to cyclists. [34] Prior to these cars were tested using stationary bicycles. Dynamic bikes test the cars' ability to recognize and react similarly to real-world scenarios but remain safe for cyclists. The autonomous bike doesn't directly increase bike safety, but improves car detection of cyclists.

Autonomous bikes, like traction control, had 2 control outputs. They controlled movements through steer, and wheel torque. The method was entirely theoretical but constructed similarly to controllers in cars. They simulated cascade LQR and PD controllers on a bicycle to self-drive following a curving path. The cascade method used in bicycles allowed them to prioritize both lateral control and stability. [34] A Riccati equation solved in real time was also used to self-drive a bicycle along a curving path. [46] The variable gain LQR showed decent results, as did the cascade effect. Combining a feedback loop with a cascade LQR+PD controller could be an interesting next step in generating a safe self-driving bicycle. There remains a gap in research with the controller architecture. The real-world testing has been done in a controlled environment, on consistent road surfaces. In the real-world riders encounter various surfaces and conditions on a day-to-day basis. Controllers developed to deal with diverse road conditions need to be developed and tested.

4. Discussion

Passive and active safety features of 4-wheel vehicles have been a focus of researchers and industry. The same cannot be said for bicycles. Cyclists crash for a variety of reasons, the most single cyclist crashes are caused by skidding, 32% followed by loss of control 21% and collisions with objects 18%. Many crashes caused by loss of control and lateral skidding can be reduced with the addition of ABS. Lateral skid and loss of control due to friction changes can be reduced with the addition of traction control. Colliding with objects could be reduced with hazard warning systems. Car safety features modified for bicycles has the potential to reduce up to 32% of crashes, making the effort well worth it.

ABS have become commercially available for cars, motorcycles, and bicycles. While it is widespread in cars, it is not common on non-electric bicycles. Bosch claims adding their ABS reduced single cyclist accidents by one third. ABS is a main reducer of longitudinal slip and loss of control. Much of the remaining loss of control and skidding issues could be reduced through the addition of traction control. ABS is commercially available and typically measured wheel speed using slotted rims. The same data from the slotted rims can be compared to determine slip. Calculations could be used to correlate slip, steer angle, and velocity in a curve on normal surfaces. This should be real-world tested and characterized.

Motorcycles have traction control, especially for lateral slip but creating a control system capable of dealing with a lot of uncertainty is difficult. Several controllers used predetermined thresholds or linear controllers prevent slipping. Many of the explored controllers work in simulation but have not in real-world complex scenarios. The dynamic complexity of 2-wheel versus 4-wheel stability makes it impossible to copy paste safety features from vehicle to vehicle. Bicycles are underactuated allowing them to be controlled through fewer output that input variables. When trying to implement traction controller, as with motorcycles, bicycles can be almost entirely controlled by steer and toque. Cars measure a loss of traction by comparing wheel speeds. Two wheeled vehicles require modifications must be made including input variables to the control algorithm, thresholds, and output. Many of the missing variables can be measured using IMUs. With the correct variables a controller could be created using knowledge of dynamics. Calculating the slip threshold at which to initiate traction control could reduce the number of single cycle crashes. Cars use LQR and PID controllers to deal with uncertainties and non-linearities in real-world settings. While it may be more difficult to implement the same controller for a bicycles similar principle should be explored. Using a robust controller equipped to deal with uncertainties in a real-world environment is the next crucial step in traction control. Modifying controllers used in cars' to include more input variables should be explored.

Running control in simulation usually uses a simplified dynamic model and lacks the everchanging variables of the real world. The most technologically advanced self-driving bikes can execute curves but lack robustness. The addition of ABS, traction control, and collision avoidance technologies have increased car safety significantly. Increasing the robustness and handling of uncertainty is an important next step in bicycle safety. The remaining single cyclist crashes, collision with objects, could be reduced using detection

systems. Vision systems could be used with autonomous driving to adapt to different road surfaces. Major concerns are the weight, size, and complexity. Vision systems notifying riders of hazards in real time could reduce collisions with unnoticed hazards but with a working control system could also react to the hazards. Further research should relate slip to steer and velocity, create a control algorithm based on dynamics and test it in varying conditions. Improving bicycle safety relies on research creating a robust traction controller capable of reducing lateral slip.

5. Conclusion:

Bicycling is an environmentally friendly, social, active mode of transportation. Car safety continues to increase, while bicycle safety remains the same. Active safety features from cars can be modified to reduce crashes in bicycles. Reduction of common single cycle crashes has the potential to reduce up to 32% of crashes. Focus on reducing crashes caused by skidding, loss of control and skidding can be modeled from car and motorcycle features. ABS, now commercially available in bicycles had the potential to reduce crashes by 30%. Modifying a traction control system can further reduce single cyclist crashes. Controller setup can mimic the one used in cars but should include more sensors data. The dynamic differences between cars and bicycles complicated traction control. Autonomous driving is possible in cars, motorcycles and bicycles, therefor complete control of dynamics is possible. Further research into bicycle traction control systems is needed prior to add it to bicycles. Integrating more safety features on bicycles can enhance rider experiences and make bicycling more accessible.

6. Sources:

- [1] N. Clayton, *The Birth of the Bicycle*. Amberley Publishing Limited, 2016.
- [2] K. Wild and A. Woodward, "Why are cyclists the happiest commuters? Health, pleasure and the e-bike," *Journal of Transport & Health*, vol. 14, p. 100569, Sep. 2019, doi: 10.1016/j.jth.2019.05.008.
- [3] T. Frendo, "The Classification and Analysis of 300 Cycling Crashes that Resulted in Visits to Hospital Emergency Departments in Toronto and Vancouver." Accessed: Mar. 04, 2024. [Online]. Available: https://open.library.ubc.ca/soa/cIRcle/collections/undergraduateresearch/52966/items/1.0053589
- [4] S. Handy, B. Wee, and M. Kroesen, "Promoting Cycling for Transport: Research Needs and Challenges," *Transport Reviews*, vol. 34, Feb. 2014, doi: 10.1080/01441647.2013.860204.
- [5] S. Netherlands, "684 road traffic deaths in 2023," Statistics Netherlands. Accessed: May 09, 2024. [Online]. Available: https://www.cbs.nl/en-gb/news/2024/15/684-roadtraffic-deaths-in-2023
- [6] B. de Geus *et al.*, "A prospective cohort study on minor accidents involving commuter cyclists in Belgium," *Accident Analysis & Prevention*, vol. 45, pp. 683–693, Mar. 2012, doi: 10.1016/j.aap.2011.09.045.
- [7] M. Corno, L. D'Avico, and S. M. Savaresi, "An Anti-Lock Braking System for Bicycles," in 2018 IEEE Conference on Control Technology and Applications (CCTA), Aug. 2018, pp. 834–839. doi: 10.1109/CCTA.2018.8511615.
- [8] M. Møller, K. H. Janstrup, and N. Pilegaard, "Improving knowledge of cyclist crashes based on hospital data including crash descriptions from open text fields," *Journal of Safety Research*, vol. 76, pp. 36–43, Feb. 2021, doi: 10.1016/j.jsr.2020.11.004.
- [9] "Timeline of Vehicle Safety Technology Through The Years," Gilbert & Baugh Ford Blog. Accessed: May 09, 2024. [Online]. Available:

 https://www.gilbertbaughford.com/blogs/2815/gilbert-baugh-ford-blog/timeline-ofvehicle-safety-technology-through-the-years/
- [10] K. Gildea and C. Simms, "Characteristics of cyclist collisions in Ireland: Analysis of a self-reported survey," *Accident Analysis & Prevention*, vol. 151, p. 105948, Mar. 2021, doi: 10.1016/j.aap.2020.105948.
- [11] A. C. Scholten, S. Polinder, M. J. M. Panneman, E. F. van Beeck, and J. A. Haagsma, "Incidence and costs of bicycle-related traumatic brain injuries in the Netherlands," *Accident Analysis & Prevention*, vol. 81, pp. 51–60, Aug. 2015, doi: 10.1016/j.aap.2015.04.022.
- [12] A. Axelsson and H. Stigson, "Characteristics of bicycle crashes among children and the effect of bicycle helmets," *Traffic Injury Prevention*, vol. 20, no. sup3, pp. 21–26, Dec. 2019, doi: 10.1080/15389588.2019.1694666.
- [13] B. Algurén and M. Rizzi, "In-depth understanding of single bicycle crashes in Sweden Crash characteristics, injury types and health outcomes differentiated by gender and age-groups," *Journal of Transport and Health*, vol. 24, 2022, doi: 10.1016/j.jth.2021.101320.

- [14] M. Ohlin, B. Algurén, and A. Lie, "Analysis of bicycle crashes in Sweden involving injuries with high risk of health loss," *Traffic Injury Prevention*, vol. 20, no. 6, pp. 613–618, Aug. 2019, doi: 10.1080/15389588.2019.1614567.
- [15] R. Utriainen, "Characteristics of Commuters' Single-Bicycle Crashes in Insurance Data," *Safety*, vol. 6, no. 1, Art. no. 1, Mar. 2020, doi: 10.3390/safety6010013.
- [16] B. Beck, "Crash characteristics of on-road single-bicycle crashes: an underrecognised problem," May 2022, doi: 10.26180/19807744.v1.
- [17] R. Nayak, R. Padhye, K. Sinnappoo, L. Arnold, and B. K. Behera, "Airbags," *Textile Progress*, vol. 45, no. 4, pp. 209–301, Dec. 2013, doi: 10.1080/00405167.2013.859435.
- [18] M. Schinkel and K. Hunt, "Anti-lock braking control using a sliding mode like approach," in *Proceedings of the 2002 American Control Conference (IEEE Cat. No.CH37301)*, Anchorage, AK, USA: IEEE, 2002, pp. 2386–2391 vol.3. doi: 10.1109/ACC.2002.1023999.
- [19] K. Enisz, I. Szalay, K. Nagy, G. Kohlrusz, D. Fodor, and R. Jakab, "Development of a bicycle anti-lock braking system prototype," *IJAET*, vol. 3, no. 3, p. 111, Dec. 2014, doi: 10.18245/ijaet.96943.
- [20] Y. Huang, Q. Liao, L. Guo, and S. Wei, "Balanced Motions Realization for a Mechanical Regulators Free and Front-Wheel Drive Bicycle Robot Under Zero Forward Speed," *International Journal of Advanced Robotic Systems*, vol. 10, no. 8, p. 317, Aug. 2013, doi: 10.5772/56701.
- [21] "Equations of motion," *Wikipedia*. Mar. 29, 2024. Accessed: May 09, 2024. [Online]. Available: https://en.wikipedia.org/w/index.php?title=Equations_of_motion&oldid=1216091588
- [22] D. A. Rawicz and M. Sjoerdsma, "Bicycle Anti-lock Braking System".
- [23] "ABS," SHIMANO BIKE-EU. Accessed: Apr. 22, 2024. [Online]. Available: https://bike.shimano.com/en-EU/technologies/component/details/steps/abs.html
- [24] G. Naito, "Traction control system for four-wheel drive vehicle" U.S. Patent 5 168 955, Dec, 8, 1992
- [25] G. Bahouth, "Real World Crash Evaluation of Vehicle Stability Control (VSC) Technology," *Annu Proc Assoc Adv Automot Med*, vol. 49, pp. 19–34, 2005.
- [26] M. A. Kumar, S. A. Kannan, A. S. Kumar, and S. Kumaravel, "Simulation of Corner Skidding Control System," *IJAERS*, vol. 4, no. 3, pp. 120–125, 2017, doi: 10.22161/ijaers.4.3.18.
- [27] C. Pascal, D. Camillo, and M. Conti, "Traction Control System for Motorcycles," *EURASIP Journal on Embedded Systems*, vol. 2009, Jan. 2009, doi: 10.1155/2009/161373.
- [28] A. Schwab, J. Kooijman, and J. Nieuwendijk, "On the Design of a Recumbent Bicycle With a Perspective on Handling Qualities," presented at the Proceedings of the ASME Design Engineering Technical Conference, Aug. 2012. doi: 10.1115/DETC2012-70391.
- [29] Sangduck Lee and Woonchul Ham, "Self stabilizing strategy in tracking control of unmanned electric bicycle with mass balance," in *IEEE/RSJ International Conference on Intelligent Robots and System*, Lausanne, Switzerland: IEEE, 2002, pp. 2200–2205. doi: 10.1109/IRDS.2002.1041594.

- [30] B. Ciechanowski, "Bicycle Bartosz Ciechanowski." Accessed: Mar. 27, 2024. [Online]. Available: https://ciechanow.ski/bicycle/
- [31] D. Hrovat, M Fodor, Ford Motor Company "Automotive Engine-based traction control", *The impact of Control Technology,vol.* 2 2014, https://ieeecss.org/sites/ieeecss/files/2019-06/IoCT2-SS-Hrovat-1.pdf
- [32] C. Pascal, D. Camillo, and M. Conti, "Traction Control System for Motorcycles," *EURASIP Journal on Embedded Systems*, vol. 2009, Jan. 2009, doi: 10.1155/2009/161373.
- [33] D. A. Bravo M., C. F. Rengifo R., and J. F. Diaz O., "Comparative Analysis between Computed Torque Control, LQR Control and PID Control for a Robotic Bicycle," in 2019 IEEE 4th Colombian Conference on Automatic Control (CCAC), Medellín, Colombia: IEEE, Oct. 2019, pp. 1–6. doi: 10.1109/CCAC.2019.8920870.
- [34] G. Wen and J. Sjöberg, "Lateral Control of a Self-driving Bike," in *2022 IEEE International Conference on Vehicular Electronics and Safety (ICVES)*, Nov. 2022, pp. 1–6. doi: 10.1109/ICVES56941.2022.9986548.
- [35] J. Yi, D. Song, A. Levandowski, and S. Jayasuriya, *Trajectory tracking and balance stabilization control of autonomous motorcycle*, vol. 2006. 2006, p. 2589. doi: 10.1109/ROBOT.2006.1642091.
- [36] A. Surana, J. Jeffs, and T. Dinh, "Accident prevention in motorcycles with 3 dimensional fuzzy logic traction control system," in 2020 8th International Conference on Control, Mechatronics and Automation (ICCMA), Nov. 2020, pp. 156–161. doi: 10.1109/ICCMA51325.2020.9301500.
- [37] "PowerDrift Simplified | Traction Control Explained YouTube." Accessed: May 09, 2024. [Online]. Available: https://www.youtube.com/watch?v=LLnq66BzUwY&ab_channel=PowerDrift
- [38] L. Hayward, "Inertial Measurement Unit (IMU) an introduction," Advanced Navigation. Accessed: May 08, 2024. [Online]. Available:

 https://www.advancednavigation.com/tech-articles/inertial-measurement-unit-imu-anintroduction/
- [39] A. Tanos, T. Steffen, and G. Mavros, "Improving lateral stability of a motorcycle via assistive control of a reaction wheel," in 2014 UKACC International Conference on Control (CONTROL), Jul. 2014, pp. 80–85. doi: 10.1109/CONTROL.2014.6915119.
- [40] A. Owczarkowski and D. Horla, "Robust LQR and LQI control with actuator failure of a 2DOF unmanned bicycle robot stabilized by an inertial wheel," *International Journal of Applied Mathematics and Computer Science*, vol. 26, no. 2, pp. 325–334, Jun. 2016.
- [41] Y.L. POM "Design and Development of a self-balancing bicycle using control moment gyro" *National University of Singapore, Department of Mechanical Engineering*, 2012
- [42] R. Bogenrieder, M. Fehring, and R. Bachmann, "PRE-SAFE® IN REAR-END COLLISION SITUATIONS".
- [43] R. Cheng, "A survey: Comparison between Convolutional Neural Network and YOLO in image identification," *J. Phys.: Conf. Ser.*, vol. 1453, no. 1, p. 012139, Jan. 2020, doi: 10.1088/1742-6596/1453/1/012139.
- [44] Y.-M. Kim, Y.-G. Kim, S.-Y. Son, S.-Y. Lim, B.-Y. Choi, and D.-H. Choi, "Review of Recent Automated Pothole-Detection Methods," *Applied Sciences*, vol. 12, p. 5320, May 2022, doi: 10.3390/app12115320.

- [45] L. Suong and K. Jangwoo, "Detection of Potholes Using a Deep Convolutional Neural Network," *JUCS Journal of Universal Computer Science*, vol. 24, no. 9, Art. no. 9, Sep. 2018, doi: 10.3217/jucs-024-09-1244.
- [46] Y. Kim, H. Kim, and J. Lee, "Stable control of the bicycle robot on a curved path by using a reaction wheel," *J Mech Sci Technol*, vol. 29, no. 5, pp. 2219–2226, May 2015, doi: 10.1007/s12206-015-0442-1.

Declaration of Generative AI and AI-assisted technologies in the writing process. During the preparation of this work, the author utilized ChatGPT to enhance English grammar and the paper structure. After using this tool, the author reviewed and edited the content as needed and takes full responsibility for the content of the publication.